

Synthesis,
Characterization, and
Reactivity of “Reverse
Pyridine” Bis(phosphinite)
Pincer Complexes

Thesis by
Nicholas Adam Swisher

In Partial Fulfillment of the Requirements for
the degree of
Doctor of Philosophy

CALIFORNIA INSTITUTE OF TECHNOLOGY
Pasadena, California

2019
(Defended January 25, 2019)

© 2019

Nicholas Adam Swisher

ORCID: 0000-0002-5320-407X

ACKNOWLEDGEMENTS

I would like to thank my advisor, Bob Grubbs for providing the opportunity to conduct the research described in this thesis. Harry Gray, Dennis Dougherty, and Jonas Peters are also thanked for their guidance as members of my advisory committee.

The person who helped me the most in graduate school was Mike Haibach. My thanks to him for his patience and willingness to discuss anything and everything. Tzu-Pin Lin also provided inspiration with his overwhelming scientific excellence. Alexey Fedorov is also thanked for making the critical initial discovery for the “silane project.”

In the lab, I was also fortunate to be surrounded by Brendan Quigley, Chris Marotta, Myles Herbert, Zainab al-Saihati, Pablo Guzman, John Hartung Jr., Benjamin Ragnar Sveinbjörnsson, Juneyoung Lee, Benjamin Suslick, Hoyong Chung, Victoria Piunova, Shane Mangold, Allegra Liberman-Martin, Chris Daeffler, Matthew van Wingerden, Keith Keitz, Nanditha Nair, Patrick Montgomery, Raymond Weitekamp, Bill Morandi, Choonwoo Lee, and Garret Miyake. Around campus Andrew Wang, Paul Walton, Matt Lehman, Guy Edouard, Seth Arnold, and Greg Miller helped provide a lot of fun. Thanks to Meaghan Deegan, Marcus Drover, Angela Shiau, Wesley Kramer, and Dinesh Aluthge with experimental assistance from other groups.

In the department, many thanks go to Elisa Brink and Steve Gould for always insuring a smooth purchasing experience. Special thanks go to Elisa for being so fun to hang out with and providing a knowing perspective on life. Joe Drew manned the stockroom. David VanderVelde kept the NMR facility running incredibly smoothly. Rick Gerhart expertly fixed a lot of broken glass. Michael Takase and Larry Hennling obtained some crystal structures and elemental analyses. Naseem Torian and Mona Shahgholi helped collect mass

spectrometry data. Scott Virgil provided a helping hand with troubleshooting more than once. Jeff Groseth repaired many damaged electronic goods.

I would be remiss if I failed to mention the staff and patrons of T. Boyle's Tavern, a welcoming place where everyone knew my name and was glad I came. Thanks to Rudy, Matt, Merc, Scott, Patrick, Cliff, Tanya, Mason, Rich and Troy for maintaining such a great establishment. Jordan Wright, Lauren McNally, Daniel Duffy Clauser, Elliot Maude, Dave, Gary, Vernon, and Irish Phil were all great people to talk to and simply be around. Special thanks go to Dustin Vander Haar and Winnie Borzage for their friendship during the difficult times.

Most of all I wish to express my gratitude to my family. Their love and support throughout the years of my chemistry education have been immense and unwavering. Thanks to Mom and Dad for always being understanding of the demands of my extended time away from home. Every time I came home for a break from California or received a visit in Pasadena was truly rejuvenating. I hope we can explore Colorado and other great places together soon! My brother Joe provided refuge in the Bay Area during Thanksgivings and a friendly ear who understood the perils of academia. Thanks also to Casey and the Passmores for providing such a welcoming escape from Los Angeles. Young Lucas Andrew's growth provides hope for the future.

To my family, who I love

ABSTRACT

In the first portion of the thesis, the synthesis, characterization, and reactivity of “reverse pyridine” bis(phosphinite) pincer complexes are described. The synthesis of a precursor ligand and the formation of a nitrogen-coordinated borane-adduct are detailed, as well as factors affecting the metalation of the two new ligands. Structural and spectroscopic characterization of the resulting metal complexes are explored as a function of borane Lewis acid coordination to the ligand backbone. Modification of complex reactivity by Lewis acid binding is further discussed.

In the second portion of the thesis, an unusual cleavage of strong carbon-oxygen bonds with silanes mediated by alkoxide bases is discussed. Furthermore, an unusual C-H silylation was discovered in the course of optimizing the C-O reduction. Factors affecting the unusual selectivities observed in these reactions are explored, and initial results towards cleavage of carbon-sulfur bonds are presented.

PUBLISHED CONTENT AND CONTRIBUTIONS

Fedorov, A. ; Toutov, A.A. ; Swisher, N.A. ; Grubbs, R.H “Lewis-base silane activation: from reductive cleavage of aryl ethers to selective *ortho*-silylation” *Chem. Sci.* **2013**, 4, 1640-1645. doi: 10.1039/C3SC22256J.

A.F. initially discovered the reported reactivity. N.A.S. helped identify unexpected side products, optimize the reaction selectivity, prepare and evaluate additional substrates, and co-wrote the manuscript with A.F. and A.A.T.

TABLE OF CONTENTS

Acknowledgements.....	iii
Dedication.....	v
Abstract	vi
Published Content and Contributions.....	vii
Table of Contents.....	viii
List of Figures.....	x
List of Tables.....	xi
List of Schemes.....	xii
List of Abbreviations.....	xiii
 Chapter 1: Introduction to Pincer Complexes and C-X Bond Cleavage	1
Pincer Complexes.....	2
Proposed Pincer Research.....	12
C-X Cleavage	12
References	13
 Chapter 2: Synthesis, Characterization and Reactivity of “Reverse Pyridine” POCOP Pincer Complexes	16
Abstract.....	17
Introduction, Ligand Synthesis and Metalation.....	18
Structural Characterization.....	31
UV-Visible Spectroscopy	35
Electrochemistry.....	38
Nickel hydride reactivity	38
Iridium pincer reactivity.....	46
Conclusion.....	47
Experimental Details	49
X-ray structural data.....	63
References	67
 Chapter 3: Alkoxide-mediated C-X Bond Cleavage with Silanes	70
Abstract.....	71
Introduction	72
Results and Discussion.....	74

Experimental	83
References	91

LIST OF FIGURES

<i>Number</i>	<i>Page</i>
1. Figure 1.1. Variety of late transition metal pincer complexes	4
2. Figure 1.2. Structure of SCS Ni pincer in lactate racemase	7
3. Figure 1.3. Previously reported reverse pyridine pincer complexes...10	
4. Figure 2.1. Coordination polymers containing pincer ligands	24
5. Figure 2.2. UV-Vis spectrum of POCOP Ni complex	17
6. Figure 2.3. UV-Vis spectrum of pyrPOCOP Ni complex.....	37
7. Figure 2.4. UV-Vis of BCF-pyrPOCOP Ni complex.....	38
8. Figure 2.5. CV of POCOP Ni complex	39
9. Figure 2.6. CV of reverse pyridine POCOP Ni complex	40
10. Figure 2.7. CV of BCF reverse pyridie POCOP Ni complex	40
11. Figure 2.8. Known pincer nickel hydrides	43
12. Figure 2.8. CO ₂ insertion rates of known nickel hydrides	44

LIST OF TABLES

<i>Number</i>	<i>Page</i>
1. Table 2.1. Attempted metalation of 2.1 with Ir precursors.....	22
2. Table 2.2. Attempted metalation of 2.1 with Rh precursors	25
3. Table 2.3. Attempted metalation of 2.1 with Pd and Ni precursors	26
4. Table 2.4. Attempted metalation of 2.1 with Ni precursors	27
5. Table 2.5. Structural parameters of POCOP Ir complexes.....	32
6. Table 2.6. Structural parameters of POCOP Ir complexes.....	32
7. Table 2.7. Structural parameters of POCOP Ni complexes	34
8. Table 3.1. Optimization of dibenzofuran reduction.....	76
9. Table 3.2. Reduction of diaryl ethers.....	78
10. Table 3.3. ICP-MS analysis of reagents.....	87
11. Table 3.4. Additional dibenzofuran reduction optimization	88

LIST OF SCHEMES

<i>Number</i>	<i>Page</i>
1. Scheme 1.1. Shaw's synthesis of PCP pincer complexes.....	2
2. Scheme 1.2. NCN pincer complexes for the Kharasch addition	3
3. Scheme 1.3. Alkane transfer dehydrogenation by pincer complexes....	4
4. Scheme 1.4. Lactate racemization by LarA	8
5. Scheme 1.5. Alcohol dehydrogenation by an SCS nickel pincer	9
6. Scheme 1.6. Milstein's reverse pyridine PCP pincer complexes	11
7. Scheme 1.7. C-O cleavage with nickel and hydrogen	12
8. Scheme 2.1. Reverse pyridine POCOP ligand synthesis	18
9. Scheme 2.2. Lewis acid coordination to reverse pyridine POCOP	19
10. Scheme 2.3. Effect of remote Lewis acid binding by Bergman	20
11. Scheme 2.4. POCOP metalation with $[\text{Rh}(\text{CO})_2\text{Cl}]_2$	28
12. Scheme 2.5. Reverse pyridine POCOP metalation with Ni and Ir	31
13. Scheme 2.6. DMAP-mediated $\text{B}(\text{C}_6\text{F}_5)_3$ removal	34
14. Scheme 2.7. Pincer nickel hydride syntheses	42
15. Scheme 2.8. CO_2 insertion by pincer nickel hydride	45
16. Scheme 2.9. Attempted catalysis with iridium complexes	47
17. Scheme 3.1. Structure of lignin with C-O bonds highlighted	73
18. Scheme 3.2. Cleavage of aryl alkyl ethers	80
19. Scheme 3.3. Reduction of lignin model substrates	82
20. Scheme 3.4. Reduction of dibenzothiophene	84

LIST OF ABBREVIATIONS

atm	atmosphere
BCF	tris(pentafluorophenyl)borane
br	broad
cat.	Catalyst
COA	cyclooctane
COD	1,5-cyclooctadiene
COE	cyclooctene
CV	cyclic voltammogram
DBU	1,8-diazabicyclo[5.4.0]undec-7-ene
DCM	dichloromethane
DFT	density functional theory
DMAP	4-(N,N-dimethylamino)pyridine
DME	1,2-dimethoxyethane
DMSO	dimethylsulfoxide
EtOAc	ethyl acetate
eq	equation
equiv	equivalents
E°	reduction potential
FAB	fast atom bombardment
Fc/Fc⁺	ferrocene/ferrocenium couple

Fc⁺/Fc⁺	decamethylferrocene/decamethylferrocenium couple
FID	flame ionization detector
g	gram
GC	gas chromatography
GC/MS	gas chromatography/mass spectrometry
HDS	hydrodesulfurization
HRMS	high resolution mass spectrometry
Hz	Hertz
iPr	isopropyl
IR	infrared
kcal	kilocalorie
LarA	lactate racemase
mg	milligram
MLCT	metal-to-ligand-charge-transfer
mmol	millimole
MS	mass spectrometry
NHC	N-heterocyclic carbene
NMR	nuclear magnetic resonance
ORTEP	Oak Ridge Thermal Ellipsoid Plot
PCET	proton-coupled electron transfer
ppm	parts per million
TBA	2,2-dimethylbutane

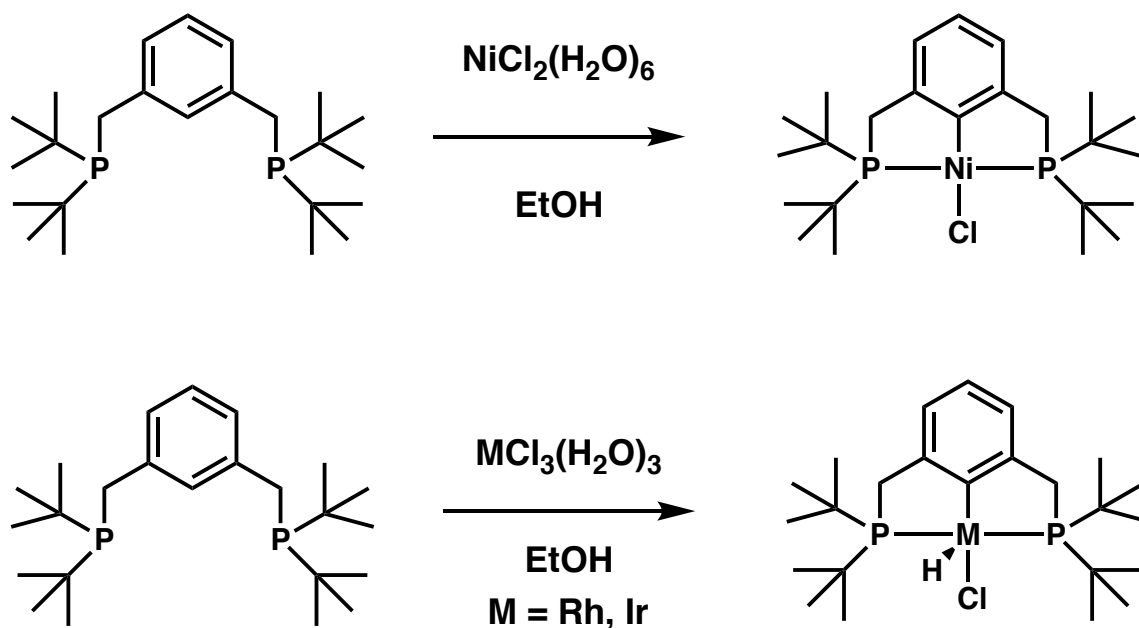
TBE	<i>tert</i> -butyl ethylene
tBu	<i>tert</i> -butyl
TEMPO	2,2,6,6-tetramethylpiperidine-N-oxide
THF	tetrahydrofuran
TON	turnover number
rt	room temperature
UV	ultraviolet
XRD	X-ray diffraction

Chapter 1

Introduction to Pincer Complexes and C-X Bond Cleavage

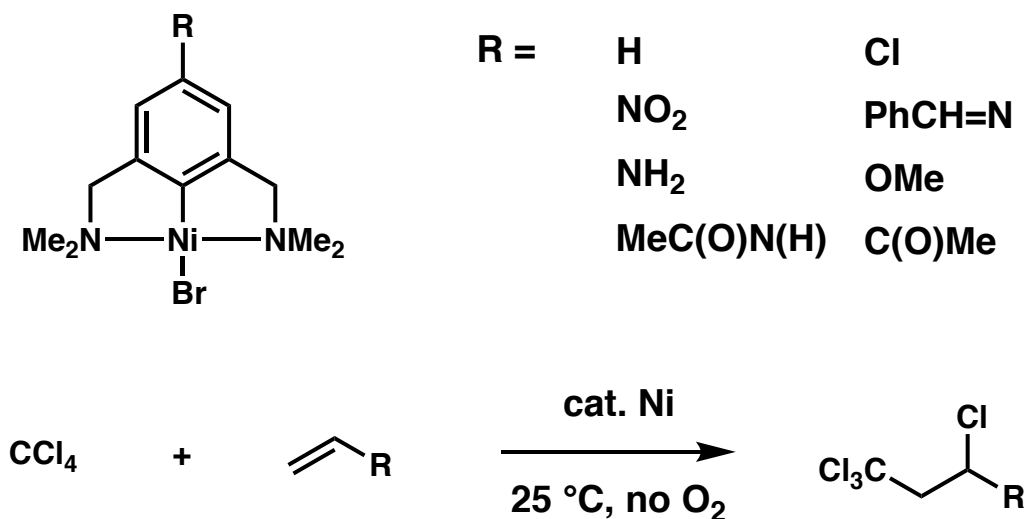
Pincer Complexes

Pincer ligands are commonly defined as tridentate, meridionally coordinating ligands and have been studied extensively as ancillary ligands for organometallic complexes since their initial synthesis more than forty years ago.¹ Shaw's seminal report on the cyclometalation of 1,3-bis(di-*tert*-butylphosphinomethyl)benzene would inspire the development of future late transition metal pincer complexes via the same synthetic approach.² The orthometalation of this PCP ligand with nickel, rhodium, and iridium precursors as shown in **Scheme 1.1** is illustrative of this synthetic strategy. Cyclometalation, or metallacycle formation via C-H or C-R bond activation, was discovered in the 1960s and has been explored across the d-block of transition metals and with multiple promoting donor atoms, especially phosphines.³



Scheme 1.1. Shaw's original synthesis of PCP pincer ligands by cyclometalation.²

The actual term “pincer complex” was not introduced until 1989 by van Koten to describe monoanionic NCN-pincer complexes of tin, platinum and nickel.⁴ One key emphasis of van Koten’s studies of these pincer ligands with “hard” flanking amine donors was the influence of remote *para* substituents on the ligand aromatic backbone (**Scheme 1.2**).⁵⁻⁶ Both electron-withdrawing and donating substituents were introduced onto the ligand backbone and found to affect both the resulting complex’s redox and catalytic activity. In the former case, more donating substituents lowered the potential necessary for Ni(II) to Ni(III) oxidation. Over the variety of substituents tested a potential range of 0.13 V was observed. Introduction of an inductively-donating amino substituent similarly provided the most reactive catalyst for the Kharasch addition of polyhalogenated alkanes to olefins.⁷ The proposed reason for enhanced reactivity lies in the single electron oxidation of the metal center which occurs in the catalytic reaction’s rate determining step.



Scheme 1.2. NCN nickel complexes reported by van Koten for Kharasch additions.⁶

Since Shaw's disclosure, a wide array of pincer complexes with numerous donor configurations have been described in the literature (**Figure 1.1**).⁸ In complexes with arenes as the central donor, both anionic and neutral arenes have been utilized. In the latter case, pyridines and other N-heterocyclic arenes are especially common.⁹⁻¹⁰ Relatively "soft" non-phosphines like N-heterocyclic carbenes have also been incorporated as the flanking donors and displayed significantly different reactivity than their phosphine containing counterparts.¹¹⁻¹³ Central anionic nitrogen based donors such as diarylamido and pyrrole-based pincers are another interesting class of ligands.¹⁴⁻¹⁵

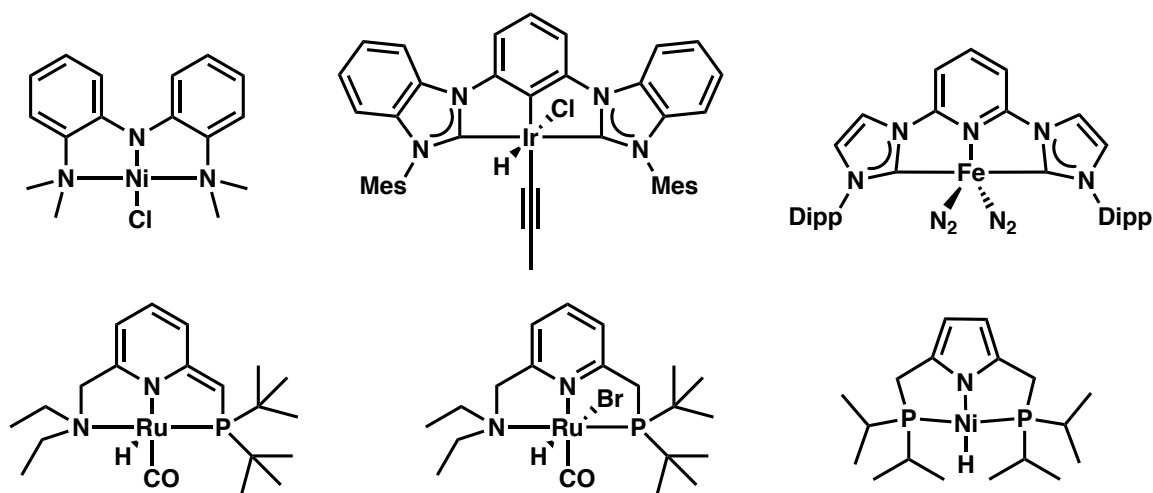
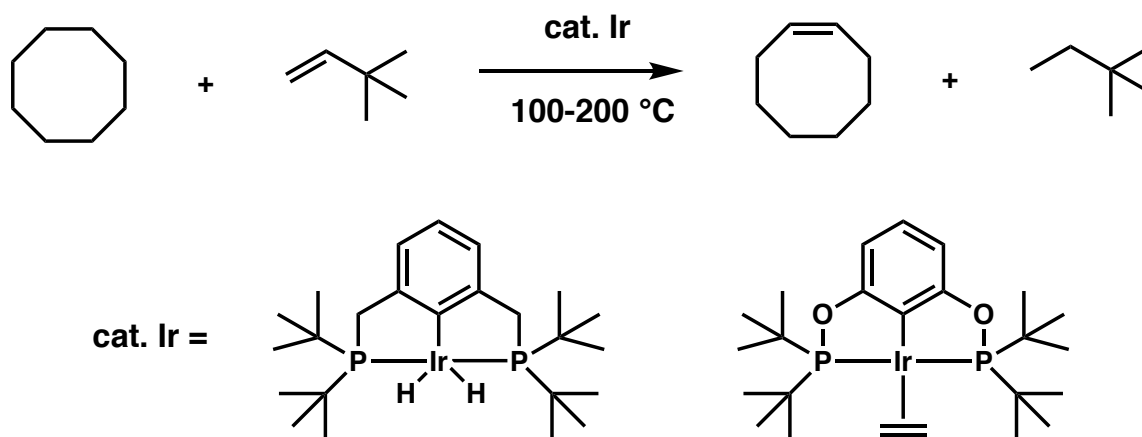


Figure 1.1. Variety of late transition metal pincer complexes.⁸⁻¹⁵ Mes = 2,4,6-trimethylphenyl. Dipp = 2,6-diisopropylphenyl

The seemingly endless combinations of metals and pincer ligand configurations has led to several interesting examples of reactivity. Due in part to the high thermal stability imparted by tridentate coordination and bulky terminal phosphine donors, PCP complexes of group 9 metals have displayed impressive activity in the homogeneous transfer

dehydrogenation of alkanes (**Scheme 1.2**).¹⁶ A notable example of the effect seemingly small changes in pincer ligand structure can have on a complex's overall reactivity is the difference in alkane dehydrogenation catalysis between iridium bis(phosphine) PCP complexes and their bis(phosphinite) POCOP analogs. While the former complexes catalytically dehydrogenate linear alkanes, they exhibit little to no activity for the dehydrogenation of cyclic alkanes such as cyclooctane (COA).¹⁷⁻¹⁸ In contrast, iridium POCOP complexes are capable of dehydrogenating COA with high TON's.¹⁸⁻²⁰



Scheme 1.3. Homogeneous alkane transfer dehydrogenation by iridium PCP and POCOP pincer complexes.¹⁶

Computational studies by Goldman and Krogh-Jespersen suggest that electronic differences are only modestly responsible for the disparity in observed reactivity given the relative similarity in electron density at iridium for each system.²¹ Steric factors are thought to be significantly more important. Because of shorter phosphorus-oxygen bonds compared to phosphorus-carbon bonds, iridium hydrido chloride POCOP complexes possess a more acute P-Ir-P bond angle (159.9 °) than in the analogous PCP complexes (164.3 °) and are

thus more “open” with respect to coordinating a substrate at the site trans to the central pincer ligand donor. The same disparity was measured by Koridze for the corresponding Ir(I) carbonyl complexes, with a P-Ir-P angle difference of 7 °. However, a difference in reactivity has been seen for POCOP complexes with varying substitution on the central arene of the ligand backbone.²⁰ Catalysts with electron-withdrawing substituents *para* to the iridium-bound *ipso* carbon tend to show higher TON's than those with more donating substituents. Although a great deal of this enhanced reactivity can be attributed to initial high rates of catalysis, overall TON's are greater for relatively electron-poor complexes as well.²⁰ Wendt's report of a bis(trifluoromethyl)-substituted POCOP ligand and the resulting iridium complex which is a very active pre-catalyst for COA transfer dehydrogenation with neohexene as hydrogen acceptor is especially interesting.²³ The overall TONs observed under comparable conditions for Wendt's complex are approximately 50% higher than for other backbone-substituted pincer complexes.^{18-20,23} While the -CF₃ groups on the backbone of Wendt's catalyst were certainly electron-withdrawing, their lipophilicity probably improves their solubility under the catalytic reaction conditions and may be a contributing factor to the observed performance.²⁴

In contrast to the wide array for synthetic pincer complexes currently known, in 2015 a natural pincer complex was discovered in the bacterial enzyme lactate racemase (LarA).²⁵⁻²⁶ Lactate racemase catalyzes the interconversion of the L and D stereoisomers of lactic acid and was previously known to contain a nickel-cofactor critical to this reactivity.^{27-28,31} Hausinger, Hu and coworkers employed a combination of mass spectrometry and x-ray crystallography to analyze the active site of the enzyme and deduced the structure of a nickel pincer complex derived from niacin. The unsymmetrical SCS nickel pincer complex consists

of a thiocarboxylate and thioamide as flanking donors and a central pyridine coordinated to nickel through the carbon *para* to the nickel atom (**Figure 1.2**). The pyridine nitrogen is bound to a phosphorylated adenine which tethers the cofactor to the rest of the enzyme along with the thioamide-nitrogen bond to a lysine residue (Lys184). Thus, the pyridine is “reversed” from what is considered normal binding and is an anionic rather than neutral donor.

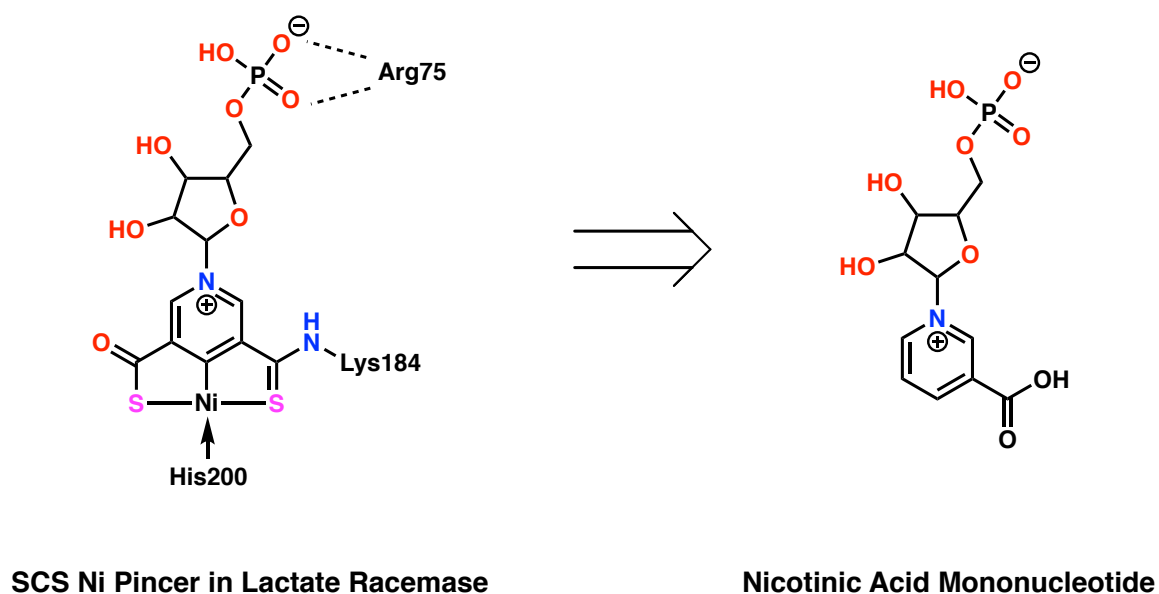
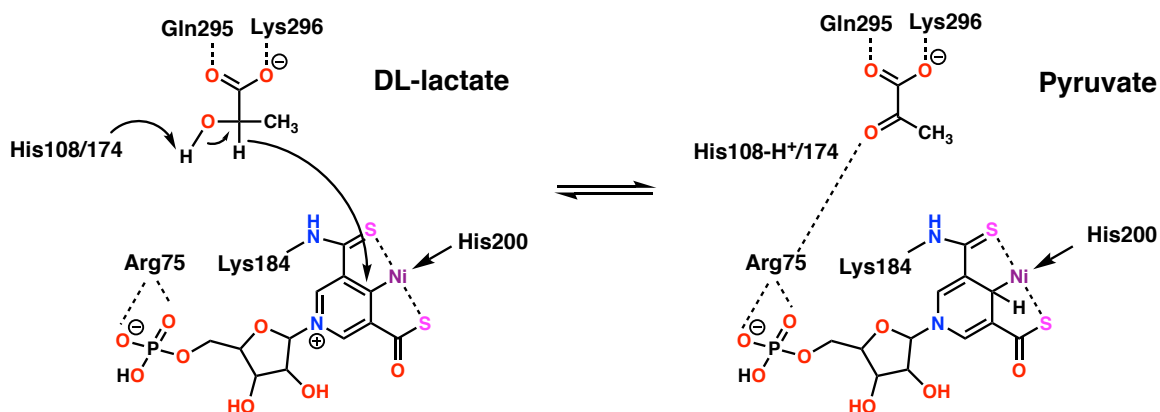


Figure 1.2. Structure of SCS nickel pincer in lactate racemase.

The mechanism of lactate racemization with this nickel pincer complex is understandably a matter of debate. A general proposal involves reversible hydride transfer from lactate to the nickel bound *ipso* carbon to the pincer, which is reminiscent of hydride transfers with nicotinamide adenine dinucleotide (**Scheme 1.4**).²⁶ The hydride migration would convert the sp^2 *ipso* carbon to sp^3 -hybridization and the pyridinium ring to a dihydropyridine. The steric

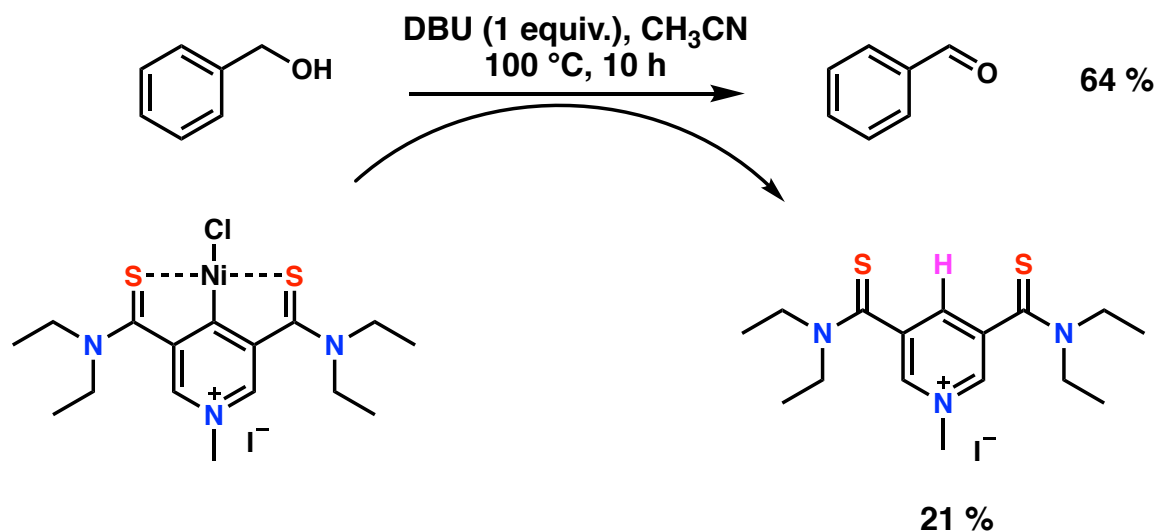
environment in the rest of the enzyme active site could favor one isomer of lactate over the other and vary with different bacterial strains or environmental conditions. Wang and Shaik have argued for a PCET mechanism in which the nickel center acts as a single-site “electrode” and “electron-relay” catalyst, facilitating C-C cleavage of lactate to form CO₂ radical anion and acetaldehyde.²⁹ Subsequently the acetaldehyde rotates and is prepared to form the opposite isomer of lactate via back PCET. While the exact mechanism for lactate racemase activity can never be known, it is clear that nature selected for the particular nickel pincer cofactor structure for some reason related to its ability to efficiently facilitate the needed transformation.



Scheme 1.4. Proposed mechanism of lactate racemization in LarA.²⁶

In an effort to explore the potential of “reverse pyridine” *ipso*-carbon involvement in hydride transfer, the group of Xile Hu synthesized a SCS pincer complex meant to model the active site of lactate racemase.³⁰ In order to approximate the coordination of the biological

pincer, flanking thioamide donors and a lutidine-based core were employed. Interestingly, alkylation of the pyridine nitrogen with methyl iodide afforded a pyridinium ligand which could be metalated even more efficiently with Ni(COD)_2 than the free base ligand. Attempted alkylation of the nickel complex with a free pyridine nitrogen was unsuccessful. Stoichiometric reaction of the SCS nickel pincers with benzyl alcohol in the presence of DBU permitted dehydrogenation, with the alkylated complex producing benzaldehyde in 64% yield while the non-alkylated complex only did so in only 8% yield (**Scheme 1.5**).



Scheme 1.5. Alcohol dehydrogenation by an SCS reverse pyridine pincer complex.³⁰

Furthermore, one isolated byproduct of the dehydrogenation reaction was demetalated pyridinium ligand with a hydrogen bound at the formerly nickel-bound *ipso* carbon. DFT calculations suggested that hydride addition from benzyl alcohol to the *ipso* carbon of the pyridinium ring rendered the the overall dehydrogenation exergonic, as opposed to

endergonic dehydrogenation by the nickel pincer with a free pyridine backbone.³⁰ Thus, functionalization of a reverse pyridine pincer backbone through modification of the pyridyl nitrogen can have a profound effect on the complex's overall reactivity.

Other previously reported pincer complexes featuring the “reverse pyridine” structural motif are shown in **Figure 1.3**.

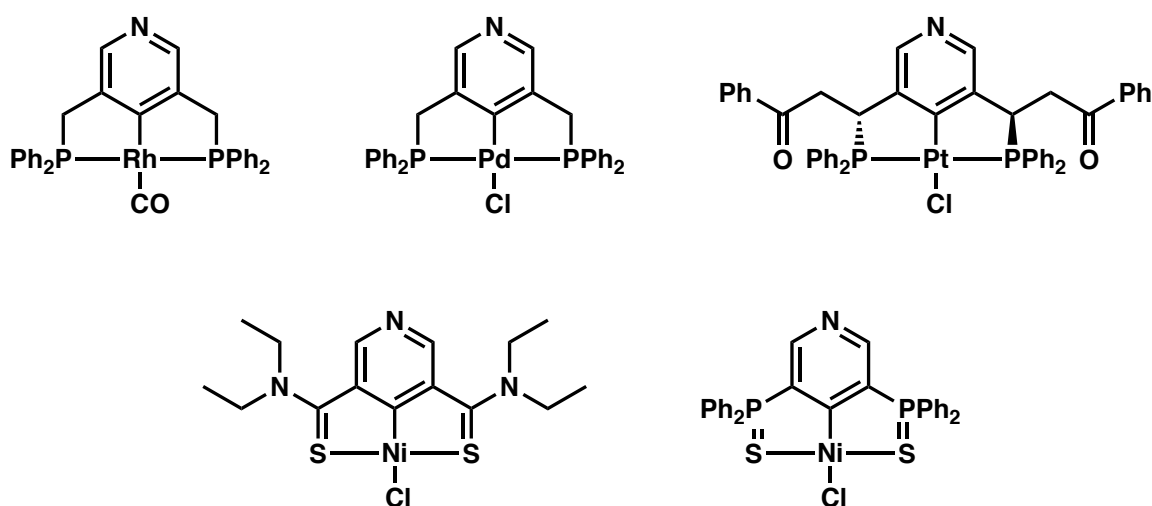
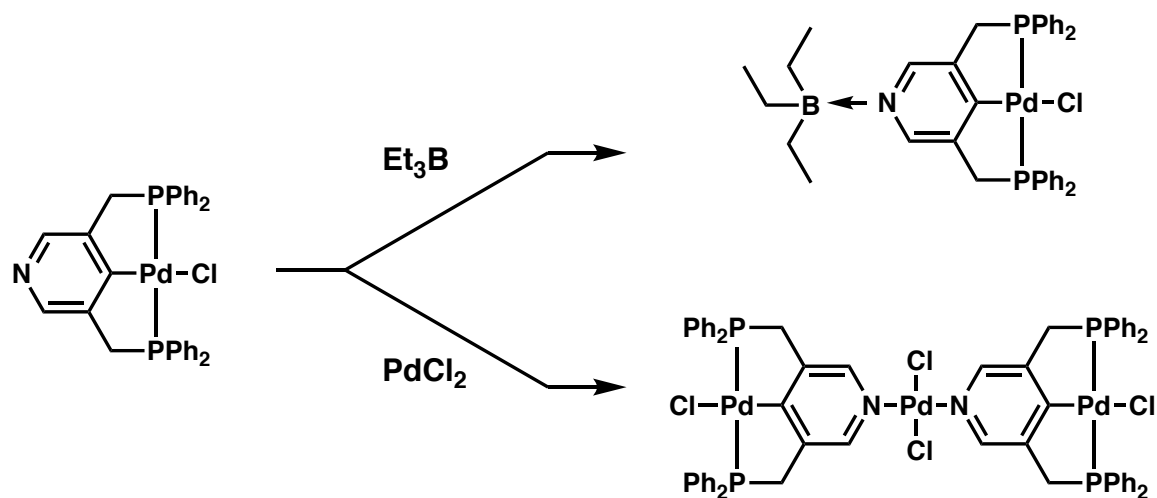


Figure 1.3. Previously synthesized reverse pyridine pincer complexes.³²⁻³⁴

Most notably in 1996 Milstein detailed the synthesis and complexation of a 3,5-lutidine-based phosphine pincer ligand.³² Despite an overall very low yielding synthetic route, the ligand 3,5-bis(diphenylphosphino)methylpyridine was successfully isolated on a multigram scale. Both rhodium and palladium complexes of the reverse pyridine PCP ligand were formed, and the presence of added trimethylamine was found to be critical for metalation reactions in which an equivalent of HCl were generated. Without exogenous base,

intractable mixtures were formed. Additionally, coordination of the metallic Lewis acid palladium dichloride to the pyridine nitrogen permitted formation of a trimetallic palladium complex (**Scheme 1.6**). N-coordination of triethylborane was also reported, and both Lewis acid coordinated products displayed spectroscopic features indicating withdrawal of electron density from the main pincer metal center. Kanbara and coworkers reported a series of SCS reverse pyridine pincer complexes for which functionalization of the pyridine was also achieved with metallic species.³³ Quaternization through alkylation with methyl iodide was described as well. Wong et. al. synthesized palladium and platinum PCP reverse pyridine complexes with flanking chiral phosphine donors.³⁴ Modest activity for asymmetric olefin hydrophosphination was also reported.



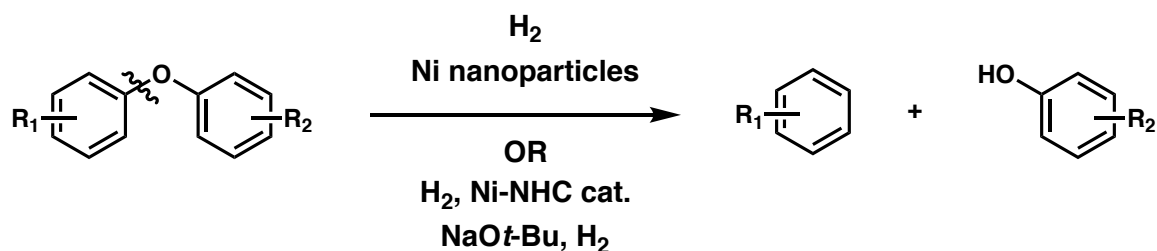
Scheme 1.6. Milstein's reverse pyridine pincer complex with N-coordinated Lewis acids.³²

Proposed Pincer Research

Given the relative dearth of reverse pyridine pincer ligands and complexes in the literature compared to the wider body of pincer compounds, we set out to synthesize a reverse pyridine bis(phosphinite) or POCOP pincer ligand as described in Chapter 2. Exploration of the potential for Lewis acid coordination to the pyridine nitrogen and its subsequent influence on the resulting complexes structural, spectroscopic and electronic properties was pursued. Additionally, both stoichiometric and catalytic transformations were targeted to discern the potential of remote electronic tuning with Lewis acids on organometallic reactivity.

C-X Bond Cleavage

The cleavage of strong C-X bonds in organic synthesis is a challenge best exemplified by efforts towards the cleavage of strong carbon-oxygen bonds in non-food biomass.³⁵⁻³⁷ A great deal of work has been dedicated in recent years to C-O bond cleavage via transition metal catalysis. Hartwig has disclosed multiple nickel catalyzed methods for the breaking of C-O bonds in aryl ethers using hydrogen gas as reductant (**Scheme 1.7**).³⁸⁻⁴⁰



Scheme 1.7. Hartwig's nickel-catalyzed C-O cleavage with hydrogen as reductant.³⁸⁻⁴⁰

Both apparently homogeneous N-heterocyclic carbene-ligated nickel systems and heterogeneous systems based on nickel nanoparticles have been explored. Martin and Chatani have reported aryl alkyl ether cleavage with tertiary silanes as reductants.⁴¹⁻⁴² With respect transition metal free systems, the use of excess alkali metals is a classic but impractical approach.⁴³⁻⁴⁴ In Chapter 3 we describe a surprising transition metal free cleavage of diaryl and aryl alkyl ethers mediated by alkoxide bases using silanes as reductants. Further reactivity in carbon-sulfur bond cleavage is also described.

References

- (1) Morales-Morales, D. *Pincer Compounds Chemistry and Applications*; Elsevier: Amsterdam, 2018.
- (2) Moulton, C.J.; Shaw, B.L.; *J. Chem. Soc. Dalton. Trans.* **1976**, 0, 1020.
- (3) Albrecht, M. *Chem. Rev.* **2010**, 110, 576.
- (4) van Koten, G. *Pure Appl. Chem.* **1989**, 61, 1681.
- (5) Gossage, R.A.; van de Kuil, L.A.; van Koten, G. *Acc. Chem. Res.* **1998**, 31, 423.
- (6) van de Kuil, L.A.; Luitjes H.; Grove, D.M.; Zwikker, J.W.; van der Linden, J.G.M.; Roelofsen, A.M.; Jenneskens, L.W.; Drenth, W.; van Koten, G. *Organometallics*, **1994**, 13, 468.
- (7) van de Kuil, L.A.; Grove, D.M.; Gossage, R.A.; Zwikker, J.W.; Jenneskens, L.W.; Drenth, W.; van Koten, G. *Organometallics* **1997**, 16, 4985.
- (8) Peris, E.; Crabtree, R.H. *Chem. Soc. Rev.* **2018**, 47, 1959
- (9) Gunanathan, C.; Ben-David, Y.; Milstein, D. *Science* **2007**, 317, 790.
- (10) Gunanathan, C.; Milstein, D. *Angew. Chem. Int. Ed.* **2008**, 47, 8661.
- (11) Andrew, R.E.; Gonzales-Sebastian, L.; Chaplin, A.B. *Dalton Trans.*, **2016**, 45, 1299.

- (12) Chianese, A.R.; Drance, M.J.; Jensen, K.H.; McCollom, S.P.; Yusufova, N.; Shaner, S.E.; Shopov, D.Y.; Tandler, J.A. *Organometallics* **2014**, *33*, 457.
- (13) Yu, R.P.; Darmon, J.M.; Milsman, C.; Margulieux, G.W.; Stieber, S.C.E.; DeBeer, S.; Chirik, P.J. *J. Am. Chem. Soc.* **2013**, *135*, 13168.
- (14) Garcia, P.M.P.; Ren, P.; Scopelliti, R.; Hu, X.L. *ACS Catal.* **2015**, *5*, 1164.
- (15) Kreye, M.; Freytag, M.; Jones, P.G.; Williard, P.G.; Bernskoetter, W.H.; Walter, M.D. *Chem. Commun.* **2015**, *15*, 2946.
- (16) Choi, J.; Roy MacArthur, A.H.; Brookhart, M.; Goldman, A.S. *Chem. Rev.* **2011**, *111*, 1761.
- (17) Liu, F.; Pak, E.B.; Singh, B.; Jensen, C.M.; Goldman, A.S. *J. Am. Chem. Soc.* **1999**, *121*, 4086.
- (18) Göttker-Schnetmann, I.; White, P.S.; Brookhart, M. *J. Am. Chem. Soc.* **2004**, *126*, 1804.
- (19) Göttker-Schnetmann, I.; Brookhart, M. *J. Am. Chem. Soc.* **2004**, *126*, 9330.
- (20) Göttker-Schnetmann, I.; Brookhart, M. *Organometallics* **2004**, *23*, 1766.
- (21) Zhu, K.; Achord, P.D.; Zhang, X.; Krogh-Jespersen, K.; Goldman, A.S. *J. Am. Chem. Soc.* **2004**, *126*, 13044.
- (22) Kulkin, S.A.; Sheloumov, A.M.; Dolgushin, F.M.; Ezernitskaya, M.G.; Pergudov, A.S.; Petrovskii, P.V.; Koridze, A.A. *Organometallics* **2006**, *25*, 5466.
- (23) Kovalenko, O.O.; Wendt, O.F. *Dalton Trans.* **2016**, *45*, 15963.
- (24) Yale, H.L. *Journal of Medicinal and Pharmaceutical Chemistry* **1959**, *1*, 121.
- (25) Desguin, B.; Zhang, T.; Soumillion, P.; Hols, P.; Hu, J.; Hausinger, R.P. *Science* **2015**, *349*, 66.
- (26) Xu, T.; Bauer, G.; Hu, X. *ChemBioChem* **2016**, *17*, 31.
- (27) Desguin, B.; Goffin, P.; Viaene, E.; Kleerebezem, M.; Diaconescu, V.M.; Maroney, M.J.; Declercq, J.-P.; Soumillion, P.; Hols, P. *Nat. Commun.* **2014**, *5*, 3615.
- (28) Dennis, D.; Reichlin, M.; Kaplan, N.O. *Ann. NY Acad. Sci.* **1965**, *119*, 868.
- (29) Wang, B.; Shaik, S. *Angew. Chem. Int. Ed.* **2017**, *56*, 1.

- (30) Xu, T.; Wodrich, M.D.; Scopelliti, R.; Corminboeuf, C.; Hu, X. *Proc. Natl. Acad. Sci. USA* **2017**, *114*, 1242.
- (31) Desguin, B.; Soumillion, P.; Hols, P.; Hausinger, R.P. *Proc. Natl. Acad. Sci. USA* **2016**, *113*, 5598.
- (32) Weisman, A.; Gozin, M.; Kraatz, H.-B.; Milstein, D. *Inorg. Chem.* **1996**, *35*, 1792.
- (33) Meguro, H.; Koizumi, T.; Yamamoto, T.; Kanbara, T. *Journal of Organometallic Chemistry* **2008**, *693*, 1109.
- (34) Wong, E.H.Y.; Jia, Y.-X.; Li, Y.; Pullarkat, S.; Leung, P.-H. *Journal of Organometallic Chemistry* **2018**, 862, 22.
- (35) Hicks, J.C. *J. Phys. Chem. Lett.* **2011**, *2*, 2280.
- (36) Zakzeski, J.; Bruijninx, P.C.A.; Jongerius, A.L.; Weckhuysen, B.M. *Chem. Rev.* **2010**, *110*, 3552.
- (37) Parthasarathi, R.; Romero, R.A.; Redondo, A.; Gnankaran, S. *J. Phys. Chem. Lett.* **2011**, *2*, 2660.
- (38) Sergeev, A.G.; Hartwig, J.F. *Science* **2011**, *332*, 439.
- (39) Sergeev, A.G.; Webb, J.D.; Hartwig, J.F. *J. Am. Chem. Soc.* **2012**, *134*, 20226.
- (40) Gao, F.; Webb, J.D.; Hartwig, J.F. *Angew. Chem. Int. Ed.* **2016**, *55*, 1474.
- (41) Alvarez-Bercedo, P.; Martin, R. *J. Am. Chem. Soc.* **2010**, *132*, 17352.
- (42) Tobisu, M.; Yamakawa, K.; Shimasaki, T.; Chatani, N. *Chem. Commun.* **2011**, 47, 2946.
- (43) Grobelny, Z. *Eur. J. Org. Chem.* **2004**, 2973.
- (44) Maercker, A. *Angew. Chem. Int. Ed.* **1987**, *26*, 972.
- (45) Keumi, T.; Murata, C.; Sasaki, Y.; Kitajima, H. *Synthesis* **1980**, 634.

Chapter 2

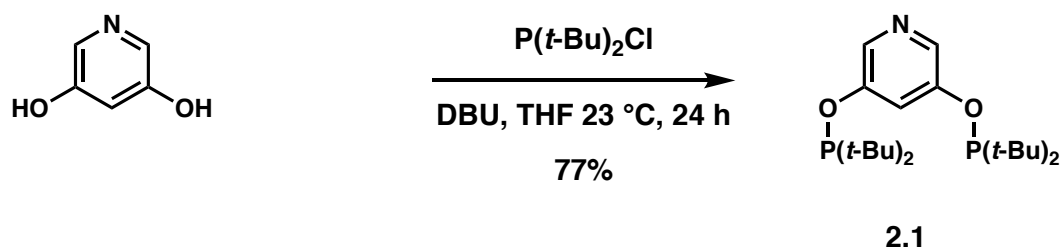
Synthesis, Characterization and Reactivity of “Reverse Pyridine” POCOP Pincer Complexes

Abstract

This chapter describes the synthesis of a “reverse pyridine” POCOP pincer ligand from 3,5-dihydroxy pyridine and the formation of a subsequent adduct between the pyridyl nitrogen and the potent Lewis acid tris(pentafluorophenyl)borane (BCF). The factors affecting ligand cyclometalation with group 9 and 10 metal precursors are discussed. Spectroscopic, electrochemical, and structural characterization of rhodium, iridium, and nickel complexes are presented. The synthesis of a nickel hydride complex of the ligand with BCF coordinated and insertion reactivity with carbon dioxide is described. Attempts at catalytic alkane transfer dehydrogenation with iridium complexes are also discussed.

Introduction and Ligand Synthesis

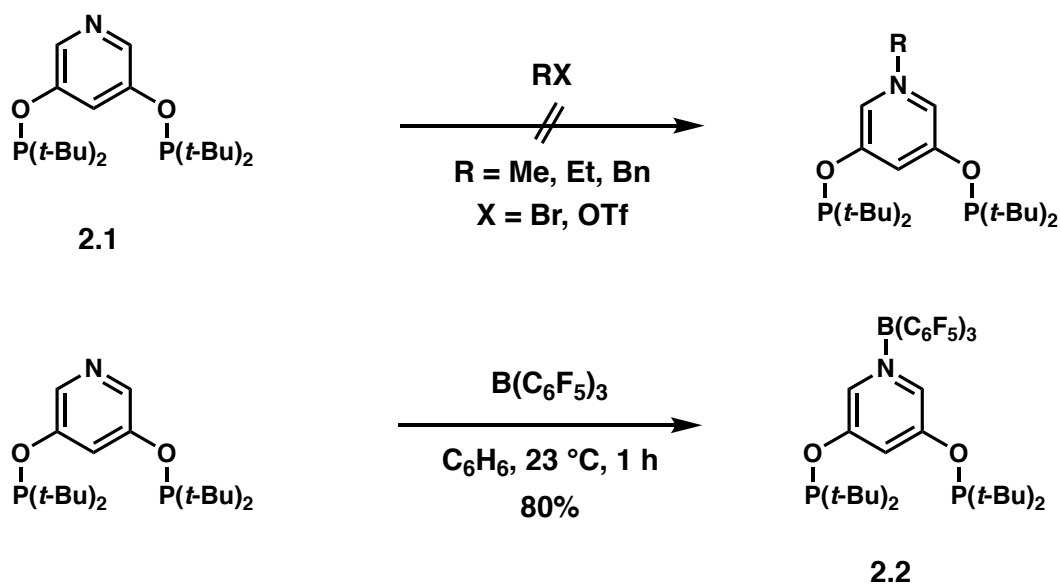
Given the synthetic utility of late transition metal bis(phosphinite) pincer complexes with a central resorcinol core, further elaborations on this ligand class are warranted.¹⁻² Thus the development of a “reverse pyridine” POCOP variant was pursued, beginning with the synthesis of the bis(phosphinite) ligand itself. Brookhart and Jensen first reported the synthesis of POCOP ligands starting from substituted resorcinols, base and dialkylchloro- or diarylchlorophosphines.³⁻⁵ Modern methods have varied little from this approach other than in the identity of the base and reaction solvent and temperature.⁶ Starting from commercially available 3,5-dihydroxypyridine, we screened reaction conditions using di-*tert*-butylchlorophosphine as a coupling partner. In contrast to the use of alkali metal hydride or amine bases common for regular POCOP ligand synthesis, we found DBU to be the only base which gave our target bis(phosphinite) ligand **2.1** with good selectivity (**Scheme 2.1**).



Scheme 2.1. Synthesis of a reverse pyridine POCOP pincer ligand **2.1**.

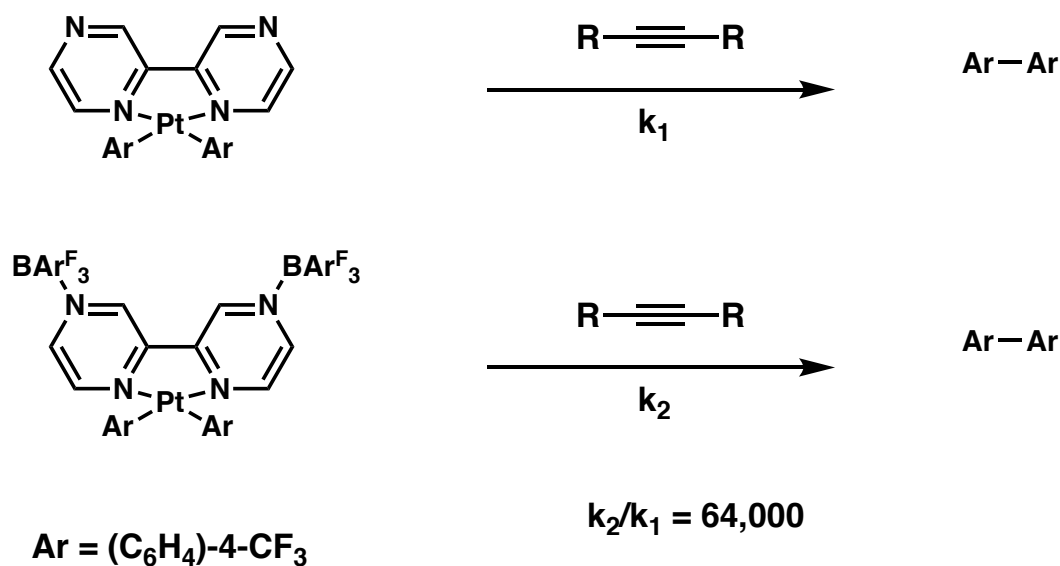
The importance of the organic base DBU probably stems from the enhanced solubility of the *in situ* generated aryloxide anion generated in contrast with more typical alkali metal cations associated with metal hydride bases. After minor purification 3,5-bis(di-*tert*-butylphosphinito)pyridine **2.1** was synthesized in good yield (77%).

Given the appeal of remote tuning of pincer complex electronic through the ligand backbone, we also pursued the formation of adducts between **2.1** and Lewis acids. Electrophilic alkyl sources such as methyl iodide, methyl triflate, and benzyl bromide failed to react selectively with the pyridine nitrogen, instead favoring O- and P-alkylation to a high degree (**Scheme 2.2**).



Scheme 2.2. Attempted alkylation of **2.1** and successful BCF N-coordination.

To that end, we sought a bulkier Lewis acid which would promote N-coordination. The ubiquitous and potent Lewis acid tris(pentafluorophenyl)borane (BCF) was chosen due to its large steric profile and historical use in similar applications. Bergman and Tilley utilized $B(C_6F_5)_3$ for remote tuning of the electronics in platinum bipyrazine complexes.⁷ They found that biaryl reductive elimination from square planar platinum “20hydroxy” complexes could be accelerated by a factor of 64,000 via BCF coordination to the backbone of their bidentate ligands (Scheme 2.3). Further work on 2,2'-bipyrimidyl platinum complexes with coordinated Lewis acids revealed a more complex mechanistic picture involving nitrogen ligand dissociation from platinum prior to reductive elimination.⁸



Scheme 2.3. Effect of remote Lewis acid binding on platinum biaryl complex reductive elimination.⁸

Jordan and coworkers observed “allosteric” effects due to remote binding of BCF to bidentate phosphine-phosphinate ligands of palladium complexes for ethylene polymerization.⁹ In these complexes the binding of BCF to a ligand phosphinate oxygen was thought to render the palladium center significantly more electrophilic and subsequently increase polyethylene chain growth rate. Importantly, detailed studies suggest that the catalysis promoting effects of BCF binding in this system were primarily electronic in nature and not due to significant structural or steric changes. In 2015 Horak et. al. disclosed a pyridine diphosphine ligand with π -coordinated metals and further demonstrated tuning of the metal electronic through remote Lewis acid coordination to the pyridine nitrogen.¹⁰ In a systematic investigation, N-coordination was achieved with BCF and other boron Lewis acids in addition to alkylation and protonation.

Thankfully, coordination of BCF to ligand **2.1** proved straightforward as stirring of the Lewis acid and pyridine ligand in benzene at ambient temperature afforded the desired N-adduct **2.2** in high yield (**Scheme 2.2**). The spectroscopic features of **2.2** are consistent with N-coordination of the boron Lewis acid. The ³¹P NMR spectrum of **2.2** features a signal at 170 ppm, approximately 12 ppm downfield of borane-free ligand **2.1**. The shifts observed in the ¹H NMR spectra between the two compounds are unremarkable (see Experimental Section). In the ¹⁹F spectrum the observed separation between the *meta* and *para* (approximately 7 ppm) fluorine resonances indicates coordination to a N-heterocycle and four-coordinate boron overall.¹¹⁻¹²

Metalation of the free pyridine ligand **2.1** was attempted with a variety of group 9 and 10 metal precursors. As shown in **Tables 2.1-2.3**, cyclometalation of the reverse pyridine POCOP with common iridium, rhodium, nickel, and palladium precursors was unsuccessful.

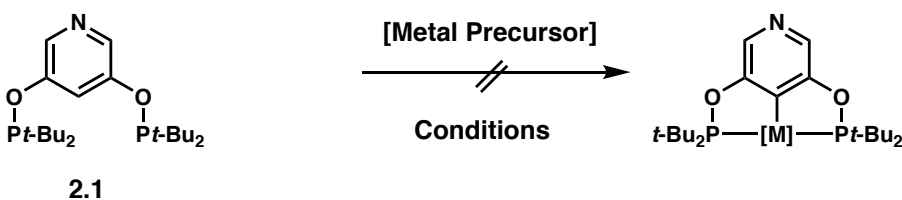
					
Entry	Metal Precursor	Base	Solvent	Temp. (°C)	Time (h)
1	$[\text{Ir}(\text{COD})\text{Cl}]_2$	-	Toluene	120	24
2	$[\text{Ir}(\text{COD})\text{Cl}]_2$	Et_3N	Toluene	120	24
3	$[\text{Ir}(\text{COD})\text{Cl}]_2$	Pyridine	Toluene	120	24
4	$[\text{Ir}(\text{COD})\text{Cl}]_2$	-	Benzene	80	24
5	$[\text{Ir}(\text{COE})_2\text{Cl}]_2$	-	Toluene	120	24
6	$[\text{Ir}(\text{COE})_2\text{Cl}]_2$	-	Toluene	80	24
7	$[\text{Ir}(\text{COE})_2\text{Cl}]_2$	Et_3N	Toluene	120	24
8	$[\text{Ir}(\text{COE})_2\text{Cl}]_2$	Pyridine	Toluene	120	24
9	$\text{IrCl}_3 \cdot x\text{H}_2\text{O}$	NaHCO_3	<i>i</i> -PrOH	80	24
10	$\text{IrCl}_3 \cdot x\text{H}_2\text{O}$	-	THF	80	24
11	$\text{IrCl}_3 \cdot x\text{H}_2\text{O}$	Et_3N	THF	80	24
12	$[\text{Ir}(\text{C}_2\text{H}_4)_2\text{Cl}]_2$	-	THF	25	12
13	$[\text{Ir}(\text{C}_2\text{H}_4)_2\text{Cl}]_2$	-	Toluene	25	12
14	$[\text{Ir}(\text{C}_2\text{H}_4)_2\text{Cl}]_2$	Pyridine	Toluene	25	12

Table 2.1. Attempted metalation of free pyridine ligand **2.1** with iridium precursors.

Intractable mixtures of mostly insoluble material were obtained upon heating **2.1** with common Ir(I) precursors used for pincer ligand cyclometalation like $[\text{Ir}(\text{COD})\text{Cl}]_2$ and $[\text{Ir}(\text{COE})_2\text{Cl}]_2$.^{3-4,13-14} Although formation of the expected product of such reactions, an Ir(III) hydrido chloride complex, would not involve generation of an equivalent of hydrogen chloride, the addition of an equivalent of triethylamine or pyridine had no effect on the course of the reaction. The use of $\text{IrCl}_3 \cdot x\text{H}_2\text{O}$ as an iridium precursor was similarly unsuccessful (**Table 2.1, entries 9-11**).

A plausible explanation for the failure of ligand **2.1** to cyclometalate to a pincer complex smoothly is that formation of coordination polymers or oligomers, particularly through the pyridine nitrogen, is more favorable than formation of tridentate pincer complexes under the experimental conditions. Milstein noted the formation of oligomeric species in iron pyrazine-based PNP pincer complexes under certain reaction conditions (**Figure 2.1**).¹⁵ Introduction of hydrogen or carbon dioxide resulted in disassembly of the oligomeric species. In the case of ligand **2.1**, it is also possible to envision oligomeric or polymeric species which do not contain a cyclometalated pincer complex at all. Phosphinite pincer complexes have previously been known to form likely coordination polymers through the phosphinite groups linking multiple ligands through iridium, although this was only observed with alkyl phosphorous substituents smaller than *tert*-butyl.¹⁶ However, in the present case, intermolecular coordination between a phosphinite, iridium metal and pyridine on another molecule of **2.1** could enable formation of insoluble polymeric materials. Given the high temperatures typically needed for the desired pincer cyclometalation with the aforementioned iridium precursors, we attempted metalation at lower

temperature with $[\text{Ir}(\text{C}_2\text{H}_4)_2\text{Cl}]_2$, but this precursor was not reactive enough to cyclometalate ligand **2.1** (Table 2.1, entries 12-14).

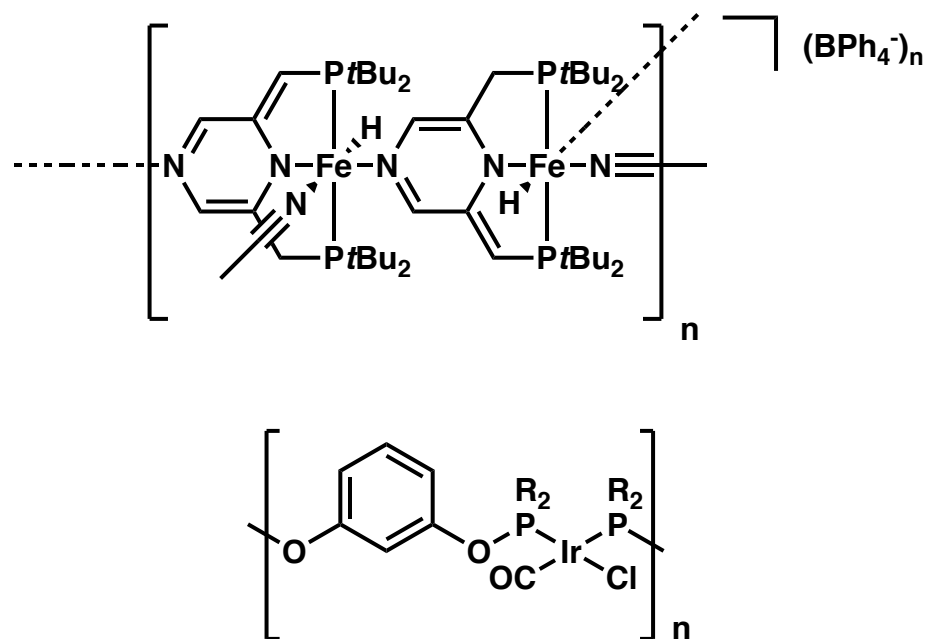


Figure 2.1. Coordination polymers previously postulated for pyrazine PNP and POCOP pincer ligands.¹⁵⁻¹⁶

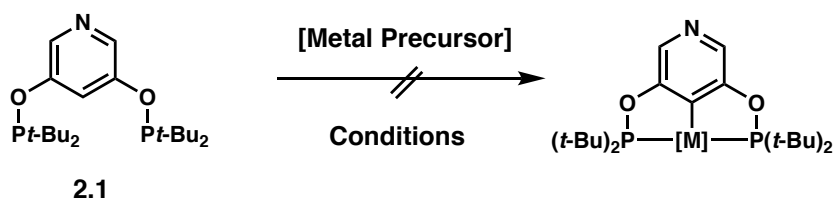
Similar results were obtained with common rhodium precursors (Table 2.2). $[\text{Rh}(\text{COD})\text{Cl}]_2$, $[\text{Rh}(\text{COE})_2\text{Cl}]_2$ and $[\text{Rh}(\text{C}_2\text{H}_4)_2\text{Cl}]_2$ all gave similar insoluble, intractable mixtures as was the case with iridium. The addition of pyridine was carried out in an attempt to enforce the desired pincer cyclometalation by disaggregating any potential coordination polymer. The insoluble materials obtained from all reactions were also subjected to sonication with excess pyridine or reaction with H_2 or CO and subsequent heating, but the crude reaction materials remained intractable.

2.1

Entry	Metal Precursor	Base	Solvent	Temp. (°C)	Time (h)
1	[Rh(COD)Cl] ₂	-	Toluene	120	24
2	[Rh(COD)Cl] ₂	Et ₃ N	Toluene	120	24
3	[Rh(COD)Cl] ₂	Pyridine	Toluene	120	24
4	[Rh(COE) ₂ Cl] ₂	-	Toluene	120	24
5	[Rh(COE) ₂ Cl] ₂	-	THF	80	24
6	[Rh(COE) ₂ Cl] ₂	Et ₃ N	Toluene	120	24
7	[Rh(COE) ₂ Cl] ₂	Pyridine	Toluene	120	24
8	[Rh(C ₂ H ₄) ₂ Cl] ₂	-	THF	25	12
9	[Rh(C ₂ H ₄) ₂ Cl] ₂	-	Toluene	25	12
10	[Rh(C ₂ H ₄) ₂ Cl] ₂	Pyridine	Toluene	25	12
11	[Rh(C ₂ H ₄) ₂ Cl] ₂	-	Toluene	100	24

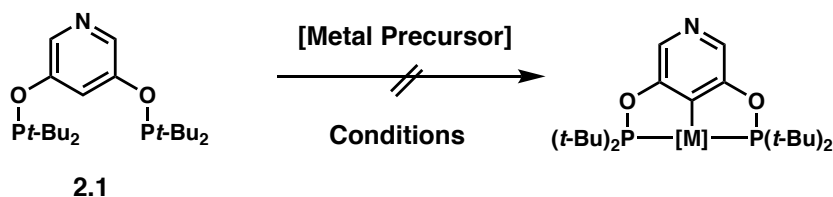
Table 2.2. Attempted metalation of ligand **2.1** with rhodium precursors.

Efforts at metalation of ligand **2.1** with group 10 precursors proved similarly futile (**Tables 2.3-2.4**). Addition of triethylamine to act as a sink for acid generated from divalent nickel and palladium halide salts and precursors had no effect on the outcome of the reactions. Even reagents such as the polymeric nitrile ligated reagent $\{(i\text{-PrCN})\text{NiBr}_2\}_n$ which have been shown to metalate POCOP ligands at ambient temperature were unsuccessful (**Table 2.4, entries 5-8**).¹⁷



Entry	Metal Precursor	Base	Solvent	Temp. (°C)	Time (h)
1	PdCl ₂	-	Toluene	120	24
2	PdCl ₂	Et ₃ N	Toluene	120	24
3	PdCl ₂	Pyridine	Toluene	120	24
4	PdCl ₂	Et ₃ N	THF	80	24
5	Pd(COD)Cl ₂	-	Toluene	120	24
6	Pd(COD)Cl ₂	Et ₃ N	Toluene	110	24
7	Pd(COD)MeCl	Et ₃ N	Toluene	120	24
8	Pd(COD)MeCl	-	Toluene	120	24
9	Pd(COD)MeCl	Et ₃ N	THF	80	24
10	Pd ₂ (dba) ₃	-	Toluene	80	24
11	Pd ₂ (dba) ₃	-	THF	80	24
12	Ni(DME)Br ₂	-	Toluene	110	24
13	Ni(DME)Br ₂	Et ₃ N	Toluene	110	24
14	Ni(DME)Br ₂	Pyridine	Toluene	110	24
15	Ni(DME)Br ₂	Pyridine	THF	80	24

Table 2.3. Attempted metalation of ligand **2.1**. with group 10 precursors.

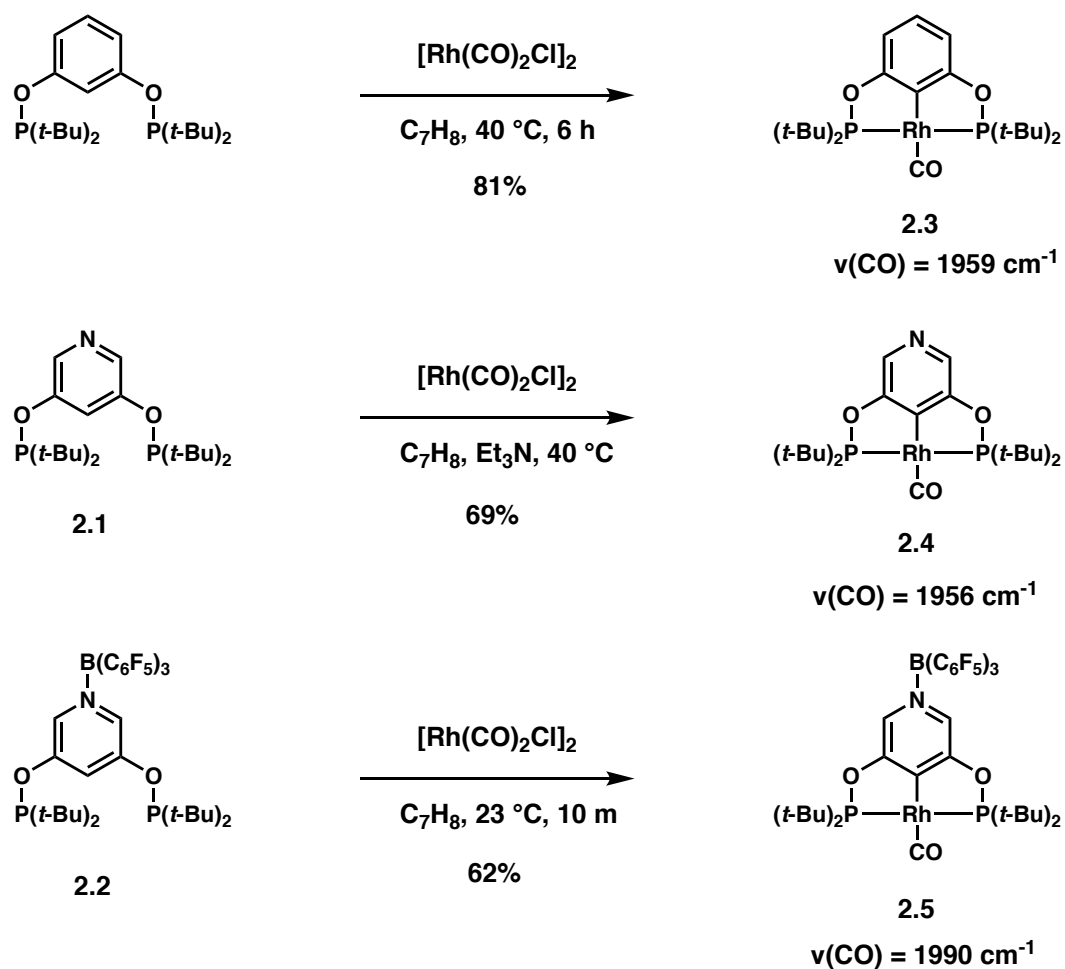


Entry	Metal Precursor	Base	Solvent	Temp. (°C)	Time (h)
1	NiCl ₂	-	Toluene	110	24
2	NiCl ₂	Et ₃ N	Toluene	110	24
3	NiCl ₂	Pyridine	Toluene	110	24
4	NiCl ₂	Et ₃ N	THF	80	24
5	(<i>i</i> -PrCN)NiBr ₂	Et ₃ N	THF	80	24
6	(<i>i</i> -PrCN)NiBr ₂	Et ₃ N	Toluene	100	24
7	(<i>i</i> -PrCN)NiBr ₂	Et ₃ N	THF	25	24
8	(<i>i</i> -PrCN)NiBr ₂	Et ₃ N	Toluene	25	24

Table 2.4. Attempted metalation of ligand **2.1** with nickel precursors.

When metalation of ligand **2.1** was attempted with Vaska's complex [IrCl(CO)(PPh₃)₂], some soluble products which could be attributed to the desired cyclometalation were observed by ³¹P NMR spectroscopy in C₆D₆ after heating at 80 °C for several hours. It seemed possible that the combination of phosphine and carbonyl ligands on Vaska's complex provided the necessary coordination environment to permit pincer cyclometalation. Given the undesirability of additional phosphines for complex purification and promoting further reactivity, we examined

metalation with rhodium carbonyl chloride dimer $[\text{Rh}(\text{CO})_2\text{Cl}]_2$ as a suitable starting material. Thankfully, reaction between ligand **2.1** and $[\text{Rh}(\text{CO})_2\text{Cl}]_2$ in the presence of triethylamine yielded the desired cyclometalated pincer rhodium carbonyl complex **2.4** (Scheme 2.4). Gentle heating was required to push the reaction towards completion and eliminate HCl from the metal coordination sphere.



Scheme 2.4. Metalation of POCOP ligands with rhodium carbonyl chloride dimer.

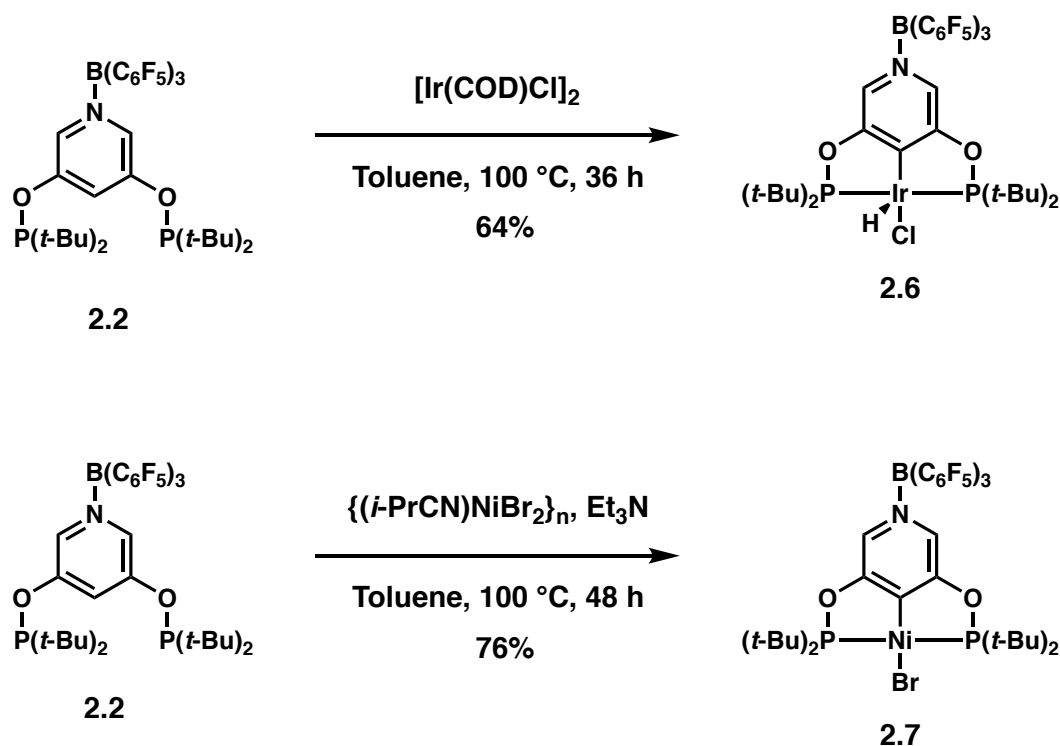
The relatively high acidity of such pincer rhodium chloro carbonyl hydrides has been previously observed.¹⁸⁻²⁰ The parent POCOP ligand can be similarly metalated

with $[\text{Rh}(\text{CO})_2\text{Cl}]_2$ without added base if sufficiently heated to drive off HCl in an open flask (**Scheme 2.4**). Reaction of the BCF POCOP adduct **2.2** with $[\text{Rh}(\text{CO})_2\text{Cl}]_2$ yielded the desired pincer carbonyl complex **2.5** in high yield in a remarkably short reaction time of approximately ten minutes. A plausible mechanism would involve formation of a six-coordinate, pincer cyclometalated rhodium carbonyl hydrido chloride complex followed by dissociation of chloride anion which could act as a base to deprotonate the resulting rhodium hydride carbonyl species. Thus, the faster reaction rate observed for metalation of ligand **2.2** may derive from the significantly higher expected acidity of an intermediate hydride species. In the case of ligand **2.1**, added base enabled formation of reverse pyridine pincer complex **2.4** with an uncoordinated nitrogen backbone. The relatively low temperature required to induce cyclometalation was probably also a key factor in avoiding formation of undesirable oligomeric or polymeric materials.

Comparing the spectroscopic data from both new rhodium compounds revealed the significant effect Lewis acid coordination to a reverse pyridine pincer complex can exert. The ^{31}P NMR signal for **2.4** appeared at 220 ppm as a doublet ($^1J_{\text{Rh-P}} = 155 \text{ Hz}$), while for BCF-coordinated **2.5** the resonance was shifted downfield to 228 ppm ($^1J_{\text{Rh-P}} = 152 \text{ Hz}$). Infrared analysis of each carbonyl compound revealed a gap of 34 cm^{-1} for the strong carbonyl stretching band observed for **2.4** (1956 cm^{-1}) and **2.5** (1960 cm^{-1}). Therefore, coordination of Lewis acid to pyridine results in a higher observed stretching band as the more electron-deficient pincer backbone competes with the carbonyl group as a pi-acceptor. Interestingly, the gap between the free base reverse pyridine complex and BCF-coordinated analog was many times greater than

that between the unadorned reverse pyridine complex **2.4** and the parent POCOP complex **2.3** (1959 cm^{-1}). Therefore, Lewis acid coordination accounts for a greater effect than switching the POCOP ligand backbone from one based on resorcinol to one based on bis(3-hydroxy)pyridine (3 cm^{-1}). A similar observation was made by Horak and Agapie during the study of pyridine diphosphine complexes with N-coordinated Lewis acids.¹⁰

Given the ease with which borane-bound ligand **2.2** was metalated with a rhodium precursor, we returned to attempted cyclometalation with nickel and iridium precursors. In the latter case, heating a toluene solution of **2.2** and $[\text{Ir}(\text{COD})\text{Cl}]_2$ for one day cleanly afforded the desired Ir(III) hydrido chloride complex **2.6** in good yield (**Scheme 2.5**). Similarly, reaction of **2.2** and $\{(i\text{-PrCN})\text{NiBr}_2\}_n$ and triethylamine furnished the desired cyclometalated nickel bromide complex **2.7**. The high reaction temperature needed for nickelation is consistent with an electrophilic mechanism, as the electron-withdrawing nature of the backbone of **2.2** would slow such a reaction.²⁴ The relative ease with which the borane-bound reverse pyridine pincer ligands were cyclometalated compared to the free base ligand is illustrative of a potential pitfall with this ligand motif. Even with bulky alkyl substituents on phosphinite groups, the presence of the “unprotected” free pyridine limits cyclometalation options due to likely formation of intractable oligomeric or polymeric materials which are favored over cyclometalation under certain conditions.²⁵

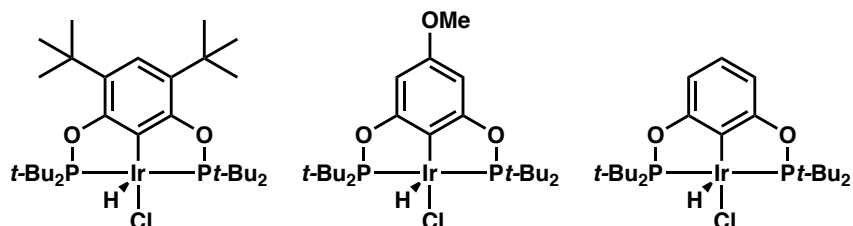


Scheme 2.5. Metalation of BCF-bound ligand **2.2** with iridium and nickel.

Structural Characterization

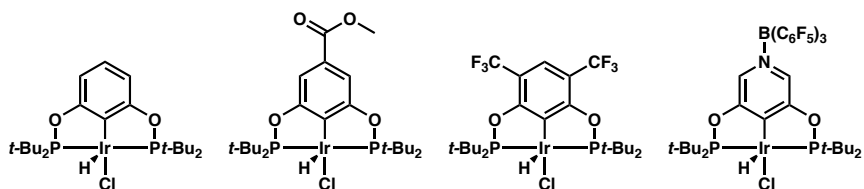
Structural analysis of complexes **2.6** and **2.7** was performed after the growth of x-ray quality single crystals. Iridium hydrido chloride complex **2.6** adopts a distorted square pyramidal structure with the hydride assumed in the apical position and with a C_{ipso} -Ir-Cl angle of approximately 170° . The P-Ir-P angle of 160.5° is in line with the range of analogous POCOP Ir(III) pincer complexes as shown in **Tables 2.5** and **2.6**.^{3-4,21-23} The measured Ir-Cl bond length of $2.3721(9)\text{ \AA}$ is approximately 0.023 \AA shorter than that of the parent POCOP Ir(III) complex, but follows the trend observed for increasing electron-withdrawing character of the ligand backbone. Similarly, the

Ir-C_{ipso} distance of 1.977(2) Å is 0.023 Å shorter than for the parent complex and in line with a similar pattern.



Ir-Cl (Å)	2.4115(12)	2.4044(14)	2.3947(12)
Ir-C(1) (Å)	2.014(4)	2.004(5)	2.000(3)
P(1)-Ir-P(2) (°)	161.07(40)	159.79(5)	159.9(4)

Table 2.5. Structural parameters of POCOP Ir(III) complexes.^{3-4,21}



Ir-Cl (Å)	2.3947(12)	2.3933(13)	2.3840(16)	2.3721(9)
Ir-C(1) (Å)	2.000(3)	1.992(4)	1.997(5)	1.977(2)
P(1)-Ir-P(2) (°)	159.9(4)	160.37(4)	160.59(5)	160.53(3)

Table 2.6. Structural parameters of POCOP Ir(III) complexes with electron-withdrawing backbones.^{3-4,22-23}

One possible explanation for the contracted bond lengths observed with increasing electron-withdrawing character of the ligand backbones is that such an inductive effect causes a more polarized Ir-C_{ipso} interaction in the direction of C_{ipso}. Therefore, the Coulombic attraction between the two atoms. A similar effect would explain the shortening of Ir-Cl. In the nickel bromide complex **2.7**, the Ni-Br distance of 2.3163(6) Å is approximately 0.022 Å shorter than that observed for the parent complex (**Table 2.7**).¹⁷ This again could reflect an interaction polarized more from Ni towards C_{ipso} and subsequent greater Coulombic attraction between Ni⁺ and Br⁻. The contraction could also be a function of increased Br to Ni pi-donation.

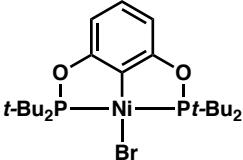
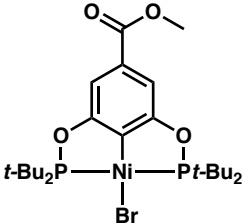
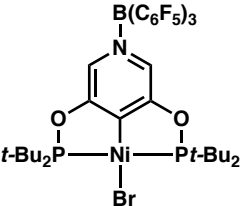
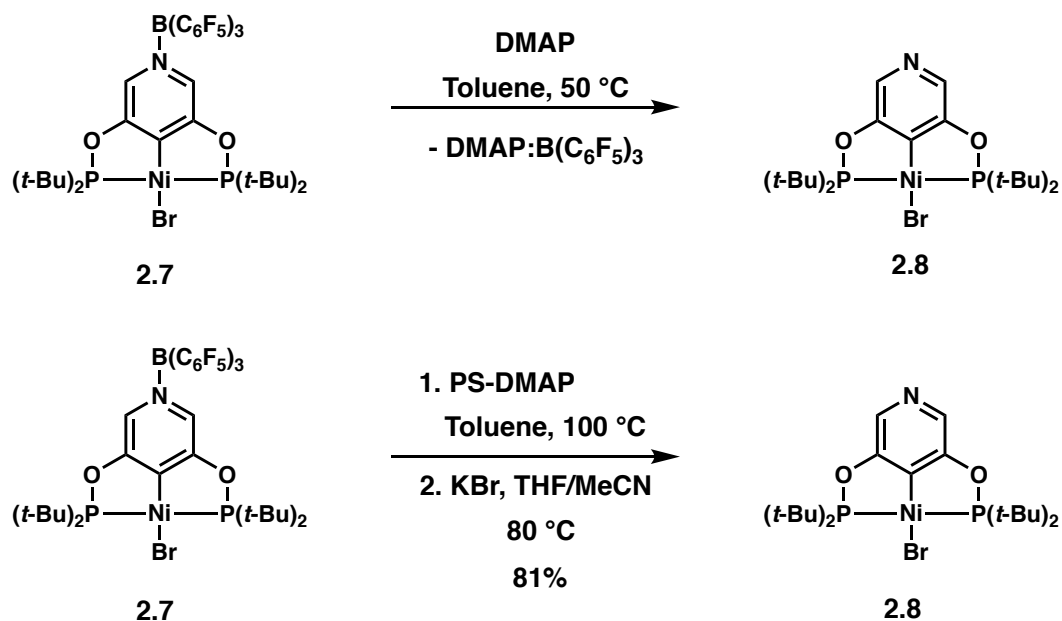
			
Ni-Br (Å)	2.338(2)	2.321(1)	2.3163(6)
Ni-C(1) (Å)	1.887(2)	1.877(2)	1.863(1)
P(1)-Ni-P(2) (°)	164.13(3)	164.58(3)	164.01(3)

Table 2.7. Structural parameters for POCOP Ni complexes with electron-withdrawing backbone substituents.¹⁷

A similar effect is seen for shortening of the Ni-C_{ipso} length (**Table 2.7**). The contraction is greater for both bonds than for those observed by Zargarian for an analogous 4-methyl ester-substituted complex. Thus, the reverse pyridine POCOP

motif with N-coordinated Lewis acid represents a potentially more powerful means of pincer complex tuning with remote substituents than more conventional, reported substituents.

Given the difficulty encountered with cyclometalation of “unprotected” reverse pyridine POCOP ligand **2.1**, we sought to examine the reversibility of borane binding to adduct **2.2**. Heating an equimolar mixture of **2.2** and DMAP in toluene at 50 °C for several hours cleanly gave a 1:1 mixture of a DMAP-B(C₆F₅)₃ adduct and a new pincer complex (**Scheme 2.6**).¹² While the ¹H NMR signals for the new species were not very different from those of **2.7**, a new ³¹P resonance at 195.9 ppm was recorded, approximately 9 ppm upfield of the starting complex. Given the inherent difficulty in separating the two products of the reaction, commercially available polystyrene-supported DMAP was used instead (**Scheme 2.6**).



Scheme 2.6. Removal of N-coordinated B(C₆F₅)₃ from complex **2.7**

Thankfully, use of the heterogeneous DMAP source proved successful and “unprotected” reverse pyridine POCOP nickel bromide complex **2.8** was obtained. A small (2-3%) side product in the crude reaction mixture suggested possible halogen exchange from chloride impurities present in the solid-supported DMAP. Addition of an excess of KBr and heating in a tetrahydrofuran/acetonitrile mixture cleanly converted the balance of material to bromide complex **2.8**.

UV-Visible Absorption Spectroscopy

With both borane-bound complex **2.7** and borane-free complex **2.8** in hand, we decided to compare the two by their UV-visible absorption spectra. Figure 2.2 shows the absorption spectrum for the parent complex at ambient temperature in dichloromethane, which was reported by Zargarian but reproduced independently.¹⁷

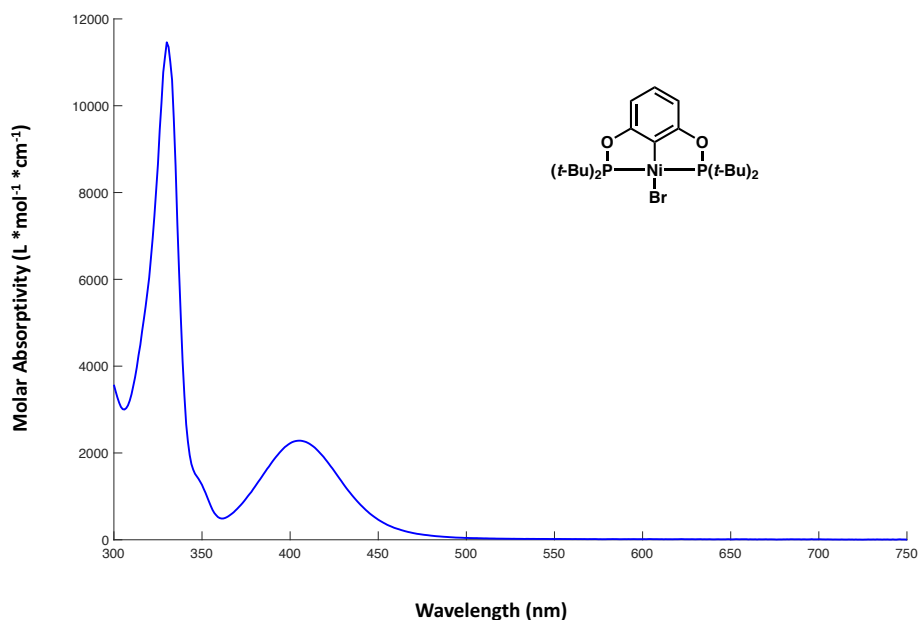


Figure 2.2. UV-visible spectrum of (POCOP)NiBr in dichloromethane.

Two features are notable in the spectrum which do not appear in the spectrum of the POCOP ligand itself.¹⁷ An absorbance at 335 nm ($\epsilon = 11,088 \text{ L}\cdot\text{mol}^{-1}\cdot\text{cm}^{-1}$) is attributed to MLCT, while the much less intense absorption at 405 nm is considered a spin-forbidden d-d transition.²⁸⁻³⁰ Prior work with backbone-substituted POCOP nickel complexes has shown the energy of the charge transfer band to be sensitive to backbone-ring substitution *para* to the metal.¹⁷ Specifically, a POCOP derivative with an alkyl ester at the 4-position of the backbone ring exhibited a MLCT band red-shifted by 26 nm compared to the parent nickel bromide complex. This energy difference corresponds to approximately 2000 cm^{-1} . A potential rationalization of this shift to lower energy absorption is that electron-withdrawing substituents on the ligand backbone help delocalize and thus stabilize charge in the complex's excited state.

Figure 2.3 shows the spectrum of complex **2.8**. While the two features observed in the spectrum of **2.7** are again noticeable, the tail of a feature at a shorter wavelength is apparent near the lower wavelength limit. This is most likely due to a $\pi\text{-}\pi^*$ transition centered on the ligand which is red-shifted compared to that of the parent POCOP ligand. The metal charge transfer band occurs at 339 nm, a minimal change from the parent complex. The molar absorptivity ($\epsilon = 10,853 \text{ L}\cdot\text{mol}^{-1}\cdot\text{cm}^{-1}$) is similarly nearly unchanged.

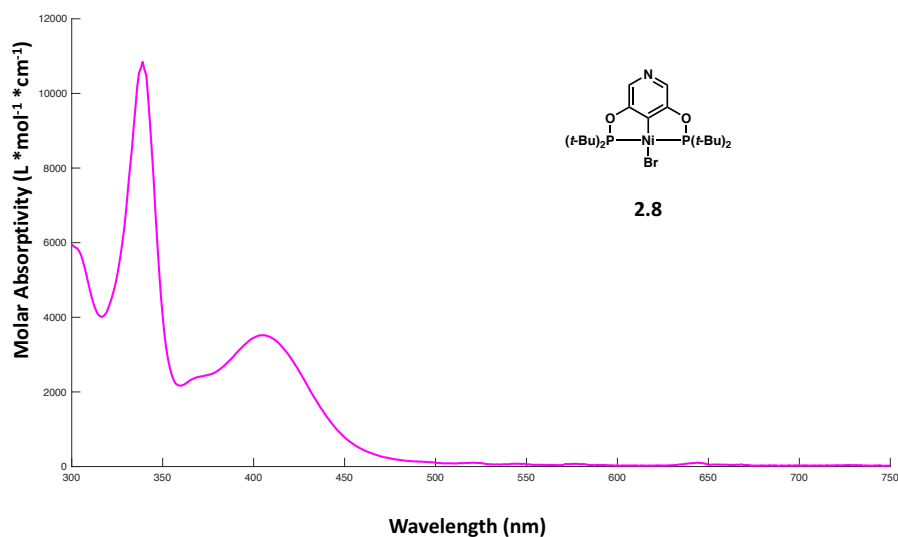


Figure 2.3. UV-visible absorption spectrum for **2.8** in DCM at ambient temperature.

Figure 2.4 displays the spectrum of **2.7** in dichloromethane at ambient temperature. Immediately the large shift in the charge transfer band from 335 nm in the parent complex to 372 nm in the borane-bound complex is apparent. The gap corresponds to an approximately 3000 cm^{-1} energy difference. Thus, Lewis acid coordination to the reverse pyridine pincer was found to have a very significant effect on the energetics of charge transfer, which could have relevance to the future design of photosensitizers.

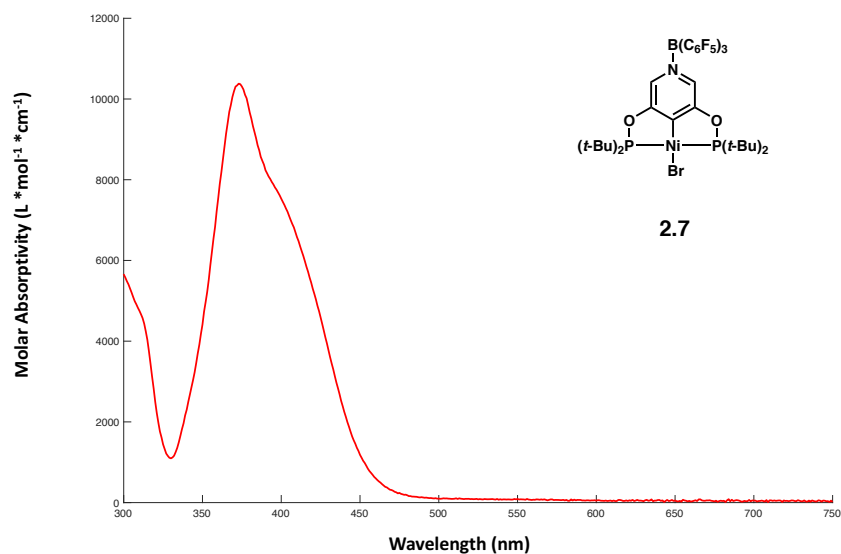


Figure 2.4. UV-visible spectrum of BCF-POCOP complex **2.7**.

Electrochemistry

Since the early work of van Koten, nickel pincer complexes which support oxidative chemistry have been widely studied.²⁶ Cyclic voltammetry offers an excellent opportunity to investigate the energetics of oxidation to Ni(III) starting from Ni(II) pincer complexes. As previously seen by Zargarian, the parent POCOP nickel bromide complex exhibits a reversible oxidative wave in dichloromethane.¹⁷ This complex was analyzed in our hands with respect to the decamethylferrocenium couple as shown in **Figure 2.5**. Again, a reversible wave with $E_{1/2} = 1.15$ V was observed. The peak oxidation potential E_{ox} was recorded as 1.23 V vs. Fc^{*+}/Fc^* .

Next, we examined the behavior of reverse pyridine complex **2.8**. Interestingly, a non-reversible wave was observed with E_{ox} of 1.54 V vs. Fc^{*+}/Fc^* (**Figure 2.6**). The 310 mV shift in peak oxidation potential is large but not necessarily surprising

in light of the inherent electron-deficiency of pyridine versus a benzene ring. Furthermore, Zargarian has measured individual backbone substituents in nickel POCOP complexes accounting for a shift in E_{ox} of approximately 200 mV. Discerning why the oxidation is irreversible raises the question of the nature of the oxidized species, which warrants future study.

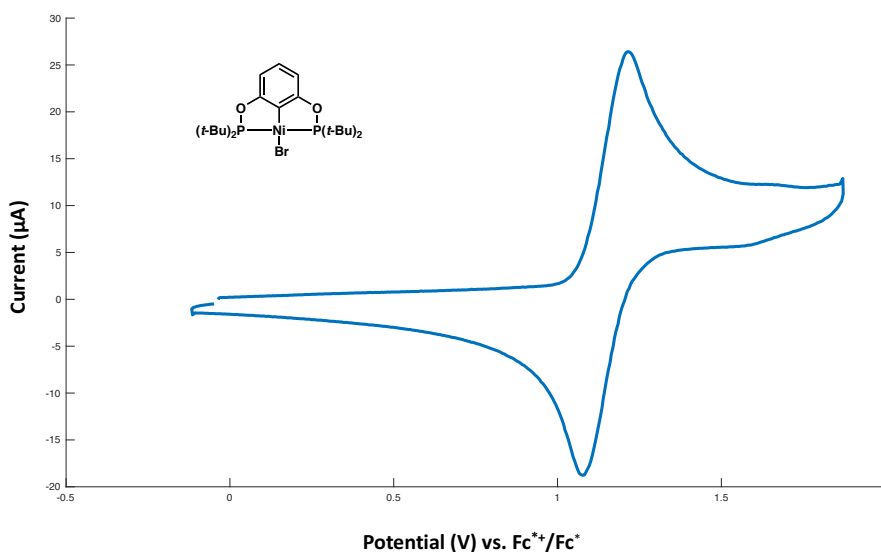


Figure 2.5. CV of parent POCOP nickel bromide complex in DCM. Scan rate = 100 mv/s.

Finally, the borane-bound complex **2.7** was examined and found to exhibit a non-reversible oxidation with $E_{\text{ox}} = 1.79 \text{ V vs Fc}^{*+}/\text{Fc}^{*\cdot}$. In light of the expected large inductive effect for the potent Lewis acid $\text{B}(\text{C}_6\text{F}_5)_3$, this further shift by approximately 250 mV is not surprising. Unfortunately, the tailing end of this oxidative event began to fall out of the solvent window for dichloromethane. Future study in a more oxidatively robust solvent such as acetonitrile is needed.

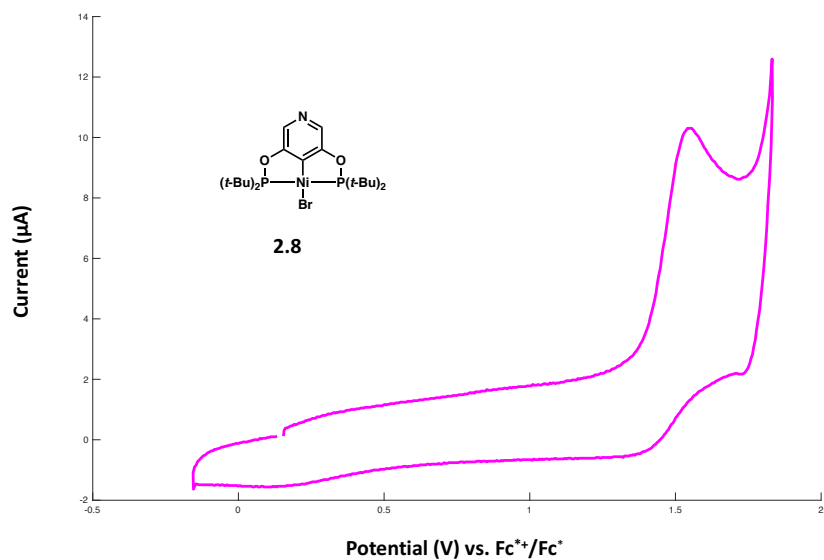


Figure 2.6. CV of reverse pyridine nickel bromide pincer complex **2.8** in DCM. Scan rate 100 mV/s.

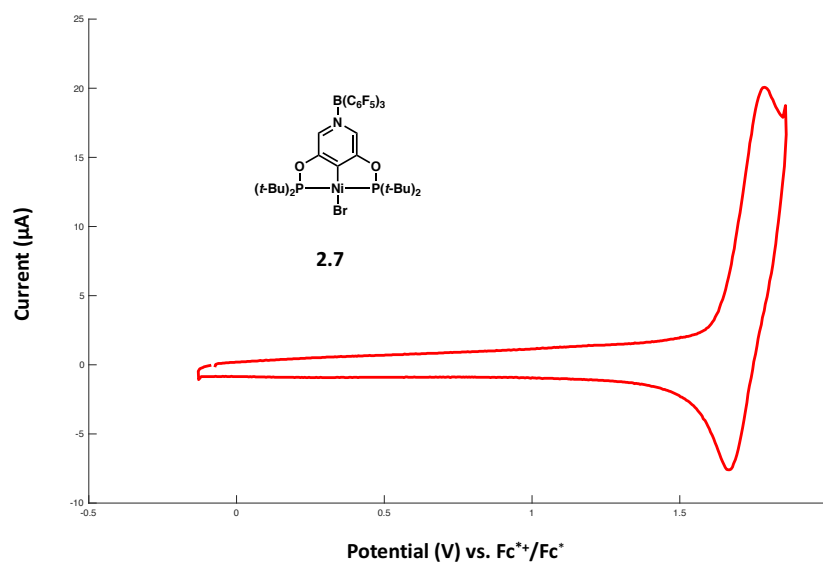
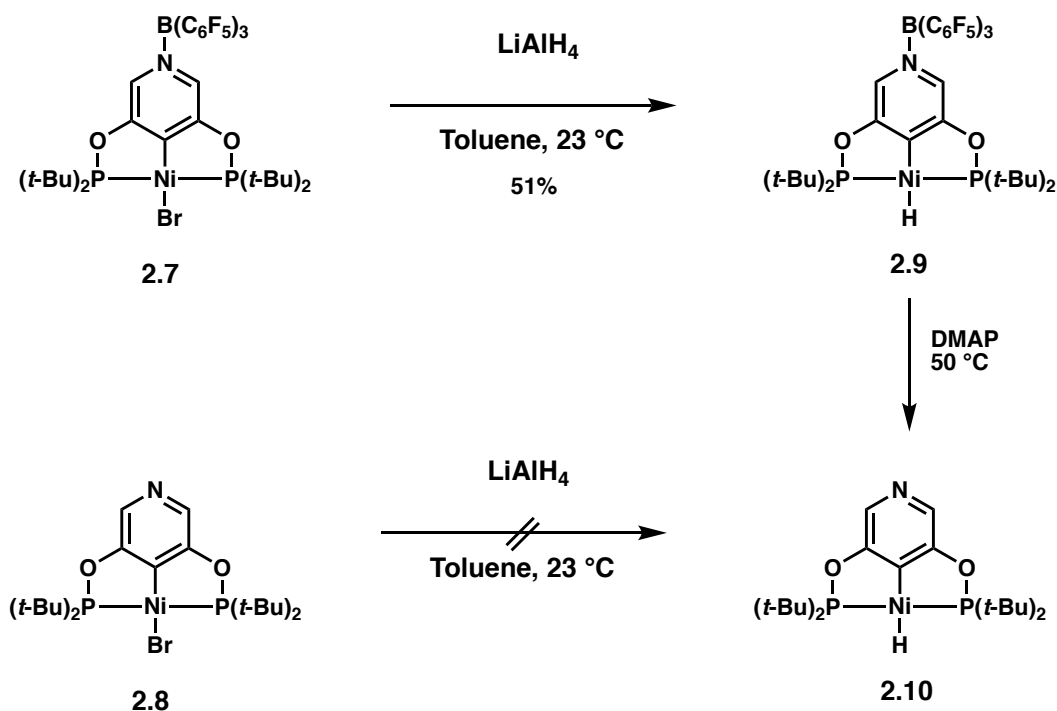


Figure 2.7. CV of BCF coordinated reverse pyridine nickel bromide pincer complex **2.7** in DCM. Scan rate 100 mV/s.

Nickel Hydride Reactivity

In order to study more reactive reverse pyridine nickel pincer complexes, we pursued synthesis of the corresponding metal hydrides from our bromide complexes. Reaction of **2.7** with an excess of lithium aluminum hydride in toluene provided the desired pincer nickel hydride **2.9** in moderate yield (**Scheme 2.7**). Although Guan and coworkers were able to obtain POCOP nickel hydrides using the same synthetic method in very high yields, it is possible that interactions between the borane in **2.7** and excess lithium and aluminum salts enabled decomposition pathways which lowered the obtained yield.²⁷ Complex **2.9** is a bright yellow solid with two notable spectroscopic features distinguishing the metal hydride: a triplet in the ^1H NMR spectrum (-7.92 ppm, $^2J_{\text{P-H}} = 52.0$ Hz) and a stretch in the IR spectrum at 1804 cm^{-1} . Unfortunately, the borane-free nickel hydride could not be obtained cleanly by reacting **2.8** with LiAlH_4 . This is most likely due to a combination of hydride reduction of the ligand pyridine backbone and pyridine coordination to lithium and aluminum salts. Instead, the hydride could be generated as a mixture by heating the borane-bound nickel hydride with one equivalent of DMAP at $50\text{ }^\circ\text{C}$ (**Scheme 2.7**). Use of polymer-supported DMAP requires higher temperatures to overcome relatively sluggish kinetics, and at these higher temperatures hydride **2.9** steadily decomposes to insoluble material.



Scheme 2.7. Synthesis of pincer nickel hydride complexes.

Figure 2.8 displays a series of pincer nickel hydrides known in the literature along with their signature IR hydride stretches. A variety of central pincer donor atoms are represented, including anionic carbon, nitrogen and silicon donors, each with a different level of σ -basicity.³¹ A reaction common to many nickel hydrides is carbon dioxide insertion to generate metal formate complexes.³²⁻³⁶ Until recently, studies on the mechanism of this insertion were limited to theoretical calculations.³⁷ However, work by Mayer, Bernskoetter, and Hazari using stop-flow time resolved spectroscopy has helped elucidate more details of this important transformation relevant to CO₂ reduction and catalysis.³⁸⁻³⁹ They found that an inner-sphere pathway

is favored with sterically accessible metal hydrides, and that the rate of insertion increases with ancillary ligand basicity. Empirically this correlation of ligand basicity and CO₂ insertion rates has been well known for pincer metal hydrides (Figure 2.9).³¹

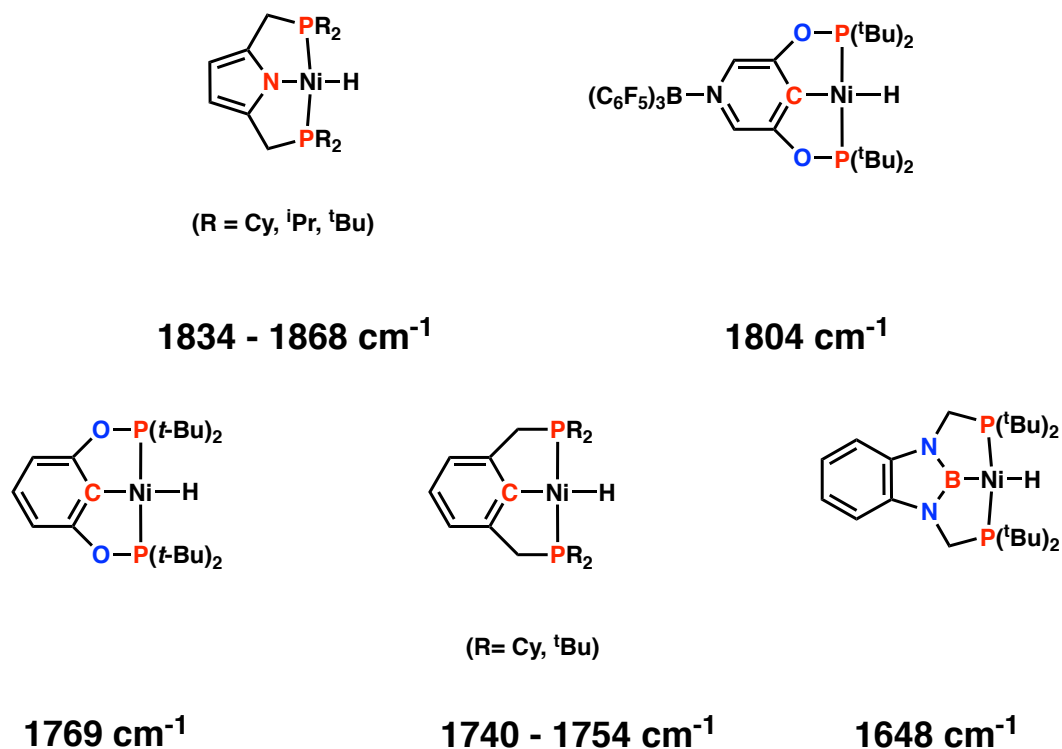
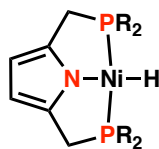


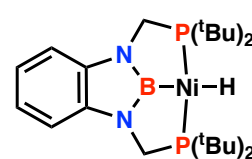
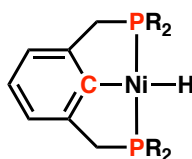
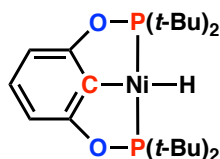
Figure 2.8. Known pincer nickel hydride complexes and their IR hydride stretches.³¹

For pincers with highly basic anionic carbon central donors, the rate of CO₂ insertion is fast, on the order of microseconds for some PCP pincer complexes.³⁸⁻³⁹ Slower insertion is observed for complexes with less basic central donors, like an amido or pyrrole donor (Figure 2.9).



(R = Cy, ⁱPr, ^tBu)

Slow CO₂ Insertion at 25 °C



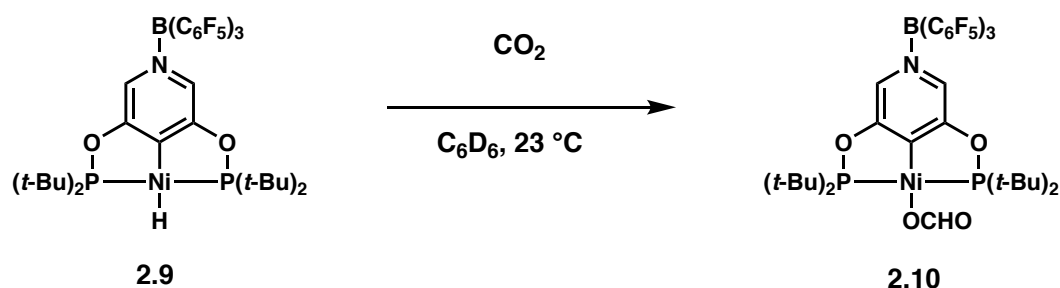
(R = Cy, ^tBu)

Fast CO₂ Insertion at 25 °C

Figure 2.9. Relative rates of CO₂ insertion by pincer nickel hydrides.³¹

We sought to examine the rate of carbon dioxide insertion for our reverse pyridine nickel hydride complex. Exposure of **2.9** to 1 atmosphere of CO₂ in C₆D₆ led to slow and clean conversion to a nickel formate complex **2.11** over the course of 16 hours at ambient temperature (**Scheme 2.8**). A distinct formyl proton was observed in the ¹H NMR spectrum at 7.99 ppm. This rate of insertion is similar to that observed for a PNP pyrrole-based nickel pincer complex.⁴⁰ Therefore, coordination of a borane Lewis acid to the reverse pyridine POCOP pincer framework enabled a shift in the rate of an insertion reaction to that seen for a pincer with an entirely different central donor atom. Furthermore, the steric environment around the pyrrole pincer is prone

to congestion such that less bulky *iso*-propyl groups on the phosphines were needed to permit full conversion from hydride to formate. Remote electronic modification in the reverse pyridine case comes without appreciable steric modification of the reactive portion of the pincer complex.

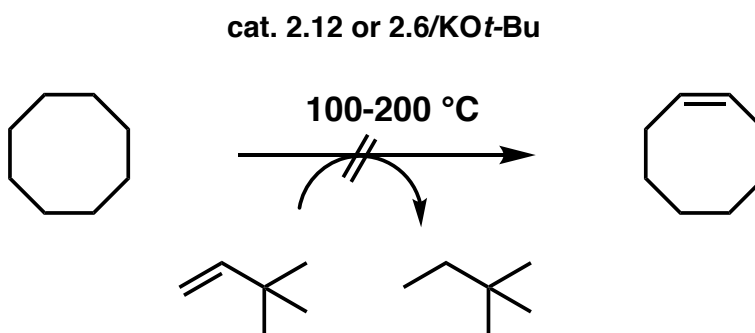
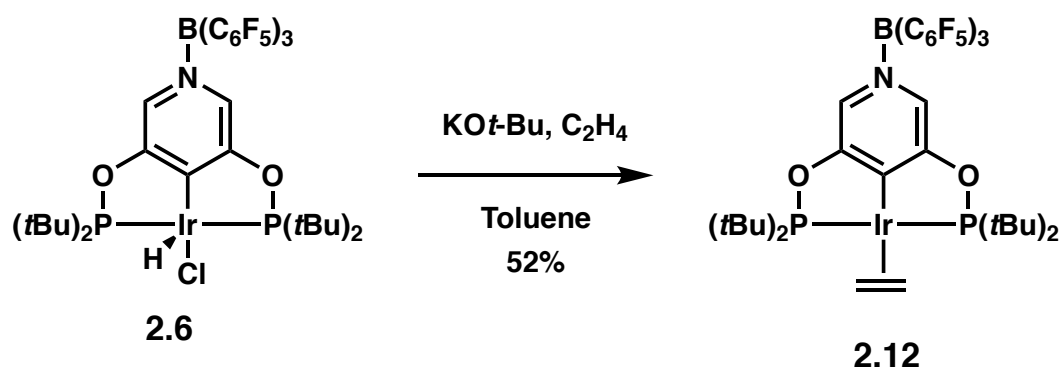


Scheme 2.8. Carbon dioxide insertion by complex **2.9**.

For the parent POCOP nickel hydride complex, the fast and thermodynamically favorable CO_2 insertion is matched by an unfavorable but kinetically accessible decarboxylation to regenerate the metal hydride.³⁶ This microscopic reverse of the insertion reaction is clean for the parent complex under vacuum at 60 °C. In our hands formate complex **2.11** decomposed to insoluble material under similar conditions. Heating under an atmosphere of nitrogen at 60 °C led to slow conversion to hydride along with simultaneous decomposition, probably of both the formate and hydride. Heating the formate complex to 60 °C under an atmosphere of CO_2 similarly led to decomposition, most notably to oxidized phosphine species. Such species may stem from activation of the phosphinite donors to P-O and C-O cleavage by the reverse pyridine framework.

Iridium Complex Reactivity

We next sought to examine possible catalysis with iridium complex **2.6**. We attempted alkane transfer dehydrogenation with *tert*-butyl ethylene as hydrogen acceptor and both cyclooctane and octane as substrate. Unfortunately, over a range of temperatures, none of the desired olefin product was observed using catalytic **2.6** with added alkoxide base. Conversion of **2.6** to the ethylene complex **2.12** was successful, but **2.12** was similarly inactive as a catalyst (**Scheme 2.9**). Heating a solution of **2.12** in *p*-xylene- d_{10} over the course of a day at 150 °C led to some apparent decomposition, but enough starting material remained to suggest that over the course of a catalytic reaction enough compound would be available for productive reactivity. Although relatively electron-poor iridium pincer complexes are generally more active for alkane transfer dehydrogenation, this phenomenon is poorly understood and may in some cases be a factor of catalyst or precatalyst solubility.^{3-4, 23} It is likely that the significant electronic modification of pincer electronics derived from the reverse pyridine pincer core and Lewis acid coordination interfere with the necessary steps for catalysis. Attempted removal of the N-coordinated borane from **2.6** with either DMAP or solid-supported DMAP were unsuccessful, most likely due to preferential binding of DMAP to the iridium metal center rather than the coordinated borane.



Scheme 2.9. Unsuccessful alkane transfer dehydrogenation with **2.6** and **2.12**.

Conclusion

We have synthesized a new “reverse pyridine” POCOP pincer complex and an N-coordinated borane adduct. The factors affecting successful metalation of both ligands have been elucidated. The free pyridine ligand is difficult to cycloemetalate due to likely pathways towards coordination polymers or oligomers. The $\text{B(C}_6\text{F}_5)_3$ adduct proved much more amenable to metalation. Borane removal through use of solid-supported DMAP enabled access to free pyridine nickel complexes.

Spectroscopic and electrochemical investigation of borane-bound and borane-free versions of nickel pincer complexes revealed significant effects of Lewis acid binding on the complex's overall properties. A nickel hydride complex was synthesized and found to insert carbon dioxide at a rate similar to a pincer complex with a central anionic nitrogen donor instead of carbon. Attempted catalysis with borane-coordinated iridium reverse pyridine pincer complexes was unsuccessful.

Future direction should focus on alternative Lewis acids and different central metals for the reverse pyridine pincer complexes. Protonation of the free pyridine backbone, especially with respect to protonation at the metal center, would be a worthwhile pursuit. Catalytic reactions taking advantage of enhanced metal electrophilicity due to remote Lewis acid binding should be investigated.

Experimental Details

Materials and Methods

Unless otherwise noted, all reactions were performed under an inert atmosphere of argon using standard Schlenk techniques or in a nitrogen or argon filled glovebox. Proteo-solvents were dried by passage through a column of activated alumina with nitrogen. All deuterated solvents were purchased from Cambridge Isotope Laboratories Inc. C_6D_6 was dried by passage through two columns of activated neutral alumina. Toluene- d_8 was distilled over sodium/benzophenone ketyl and degassed via freeze-pump-thaw. CD_2Cl_2 was dried over calcium hydride and vacuum transferred prior to use. $B(C_6F_5)_3$ was purchased from Strem and sublimed under vacuum (0.1 mtorr, 90 °C) prior to use. $[Ir(COD)Cl]_2$, $[Rh(CO)_2Cl]_2$ and $Ni(COD)_2$ were purchased from Strem. $\{(i\text{-PrCN})NiBr_2\}_n$ was prepared according to the literature method reported by Zargarian and stored under nitrogen. $IrCl(CO)(PPh_3)_2$ was purchased from Aldrich. Di-*tert*-butylchlorophosphine (96%), potassium *tert*-butoxide (99.99% sublimed grade) lithium aluminum hydride powder (95%) and 4-(dimethylamino)pyridine (99%) were purchased from Aldrich and used as received. 1,8-diazabicyclo[5.4.0]undec-7-ene (98%) was purchased from Aldrich and stored over KOH pellets. Cyclooctane (99%) was purchased from Aldrich and distilled over sodium/benzophenone ketyl. *tert*-Butyl ethylene was purchased from Alfa Aesar, degassed via three freeze-pump-thaw cycles, stirred over freshly prepared sodium/potassium alloy (NaK) for 3 days, and vacuum transferred for

storage in the dark prior to use. 3,5-dihydroxypyridine was purchased from Enamine Ltd. Polymer-supported DMAP was purchased from Oakwood Chemical at a 3.00 mmol/g loading.

^1H , ^{31}P , and ^{19}F NMR spectra were taken on a Varian Inova 400 MHz spectrometer. ^{13}C NMR spectra were taken on a Bruker AscendTM 400 MHz spectrometer. ^1H and ^{13}C NMR spectra were referenced to residual proteo solvent consistent with accepted literature values. ^{31}P spectra were externally referenced to H_3PO_4 . ^{19}F spectra were referenced to CFCl_3 (δ 0 ppm). NMR spectral data are reported according to the format chemical shift (δ ppm) (multiplicity, coupling constant (Hz), integration, identity assignment). The abbreviations for multiplicity s = singlet, d = doublet, t = triplet, m = multiplet, dt = doublet of triplets, dm = doublet of multiplets, and td = triplet of doublets were employed. All NMR spectra were analyzed using MestReNOVA version 11.0.2.

IR measurements were taken on a Bruker ALPHA ATR-IR as thin films using the Platinum Sampling Module and OPUS software package at 2 cm^{-1} resolution. HRMS data were collected on a JEOL JMS-600H High Resolution Mass Spectrometer at the Caltech Department of Chemistry Mass Spectral Facility. UV-Vis spectra were recorded in dry dichloromethane on an Agilent Cary 60 UV-Vis Spectrophotometer using quartz cuvettes. Combustion analyses were performed at the California Institute of Technology on a PerkinElmer 2400 Series II CHN Elemental Analyzer. Electrochemical experiments were performed using a Pine Instrument Company AFCBP1 biopotentiostat and the Aftermath software package.

Cyclic voltammograms were recorded in three-electrode cells under nitrogen. Glassy carbon working electrode, silver wire reference electrodes and platinum wire counter electrodes were used. All measurements were taken in dry dichloromethane with decamethylferrocene as internal standard.

Synthetic Procedures

Synthesis of 3,5-bis(di-*tert*-butylphosphinito)pyridine (2.1)

In a nitrogen-filled glovebox a 250-mL round-bottom Schlenk flask was charged with 3,5-dihydroxypyridine (1.00 g, 9.00 mmol) and a large Teflon stir bar. The flask was removed from the glovebox and while open to a flow of argon, THF (60 mL) was added via syringe. To the suspension was added di-*tert*-butylchlorophosphine (3.42 mL, 3.26 g, 18.00 mmol) all at once followed by DBU (2.70 mL, 2.74 g, 18.00 mmol) dropwise. The order of addition is important for the selectivity of the reaction. Within minutes of the addition of DBU a colorless precipitate was observed. The mixture was stirred at ambient temperature for 24 h and then the solvent was removed *in vacuo*. The resulting material was extracted with toluene (3 x 30 mL), and filtered via cannula over a thin pad of Celite on a coarse-fritted Schlenk filter. Removal of toluene *in vacuo* afforded a light brown solid which was further heated under vacuum at 60 °C for 24 h to remove traces of di-*tert*-butylchlorophosphine. The tan powder (2.76 g, 77%) was found to be sufficiently pure via NMR spectroscopy and used without further purification.

^1H NMR (400 MHz, 23 °C, C_6D_6) δ 8.55 (t, $^4J_{\text{P-H}} = 4.0$ Hz, 2H, 2,6-H), 7.75 (t, $^4J_{\text{P-H}} = 4.0$ Hz, 1H, 4-H), 1.00 [d, $^3J_{\text{P-H}} = 12.0$ Hz, 36H, 2 x P(*t*Bu) $_2$].

$^{13}\text{C}\{^1\text{H}\}$ NMR (101 MHz, 23 °C, C_6D_6) δ 156.8 (d, $^2J_{\text{P-C}} = 9.1$ Hz, C3 and C5), 134.7 (d, $^3J_{\text{P-C}} = 9.1$ Hz, C2 and C6), 114.3 (t, $^3J_{\text{P-C}} = 14.1$ Hz, C4), 35.4 [d, $^1J_{\text{P-C}} = 27.3$ Hz, 2 x P(*t*Bu) $_2$], 26.9 [d, $^2J_{\text{P-C}} = 15.2$ Hz, 2 x P(*t*Bu) $_2$].

$^{31}\text{P}\{^1\text{H}\}$ NMR (162 MHz, 23 °C, C_6D_6) δ 157.7 (s).

HRMS: (FAB+) calcd. for $\text{C}_{21}\text{H}_{40}\text{O}_2\text{P}_2\text{N}$ [M+H] $^+$ 400.2534, found 400.2544.

Synthesis of *N*-tris(pentafluorophenyl)borane-3,5-bis(di-*tert*-butylphosphinito)pyridine [BCF-pyrPOCOP] (**2.2**)

In a nitrogen-filled glovebox a scintillation vial was charged with compound **2.1** (0.500 g, 1.25 mmol) and a Teflon stir bar and dissolved in 10 mL benzene. Another scintillation vial was charged with $\text{B}(\text{C}_6\text{F}_5)_3$ (0.641 g, 1.25 mmol) and dissolved in 10 mL benzene. The solution of BCF in benzene was added slowly to the solution of **2.1** and stirred at ambient temperature for 3 h. The reaction solution was then frozen at -35 °C and carefully lyophilized to remove benzene. The resulting solid was washed (3 x 5 mL) with dry acetonitrile, dissolved in THF (6 mL) and passed through a very thin plug of dried silica gel. Evaporation of solvent gave analytically pure **2.2** (0.912 g, 80%) as a colorless powder.

^1H NMR (400 MHz, 23 °C, C_6D_6) δ 8.65 (s, 2H, 2,6-H), 7.58 (m, 1H, 4-H), 0.84 [d, $^3J_{\text{P-H}} = 12.0$ Hz, 36H, 2 x P(*t*Bu) $_2$].

$^{13}\text{C}\{^1\text{H}\}$ NMR (101 MHz, 23 °C, C_6D_6) δ 158.4 (d, $^2J_{\text{P-C}} = 9.1$ Hz, C3 and C5), 147.9 (dm, $^1J_{\text{C-F}}$, 242.4 Hz, C-F), 140.2 (dm, $^1J_{\text{C-F}}$, 276.7 Hz, C-F), 137.5 (dm, $^1J_{\text{C-F}} = 259.6$ Hz, C-F), 131.6 (d, $^3J_{\text{P-C}} = 19.2$ Hz, C2 and C6), 121.1 (t, $^3J_{\text{P-C}} = 9.1$ Hz, C4), 35.6 [d, $^1J_{\text{P-C}} = 28.3$ Hz, 2 x P(*t*Bu) $_2$], 26.4 [d, $^2J_{\text{P-C}} = 16.2$ Hz, 2 x P(*t*Bu) $_2$].

$^{31}\text{P}\{^1\text{H}\}$ NMR (162 MHz, 23 °C, C_6D_6) δ 170.2 (s).

$^{19}\text{F}\{^1\text{H}\}$ NMR (376 MHz, 23 °C, C_6D_6) δ -131.5 (d, $^3J_{\text{F-F}}$, 22.6 Hz, *o*-F), -155.75 (t, $^3J_{\text{F-F}}$, 18.8 Hz, *p*-F), -163.0 (t, $^3J_{\text{F-F}}$, 18.8 Hz, *m*-F).

Elemental Analysis Calculated for $\text{C}_{39}\text{H}_{39}\text{NBF}_{15}\text{O}_2\text{P}_2$ (911.47): C, 51.39; H, 4.31; N, 1.54. **Found:** C, 51.75; H, 4.53; N, 1.67.

Synthesis of (pyrPOCOP)RhCO (2.4)

In a nitrogen-filled glovebox a 100-mL round-bottom Schlenk flask was charged with compound **2.1** (0.200 g, 0.501 mmol) and $[\text{Rh}(\text{CO})_2\text{Cl}]_2$ (0.097 g, 0.251 mmol) and a Teflon stir bar. The flask was removed from the glovebox and left open to argon on a Schlenk line as a solution of triethylamine (77.0 μL , 0.056 g, 0.551 mmol) in toluene (10 mL) was added via cannula. The solution was stirred at ambient temperature for 1 h then 40 °C for 24 h. The solution color quickly changed from red to yellow. Colorless solid material precipitated throughout the course of the reaction. The crude reaction mixture was filtered through a thin plug of Celite in a Schlenk filter and the toluene removed under vacuum. The crude solid was eluted through a thin plug of silica gel with THF. Evaporation of solvent followed by

washing with pentane (3 x 5 mL) and further drying under vacuum gave **2.5** (0.259 g, 70%) as a bright yellow powder.

^1H NMR (400 MHz, 23 °C, CD_2Cl_2) δ 7.87 (s, 2H, Ar 2,6-H), 1.35 [vt, $J_{\text{P-H}} = 8.0$ Hz, 36H, 2 x P(*t*Bu) $_2$].

$^{13}\text{C}\{^1\text{H}\}$ NMR (101 MHz, 23 °C, CD_2Cl_2) δ 199.8 (dt, $^1J_{\text{Rh-C}} = 59.6$ Hz, $^2J_{\text{P-C}} = 10.1$ Hz, Rh-CO), 165.6 (t, $^2J_{\text{P-C}} = 9.1$ Hz, C3 and C5), 153.6 (m, C2 and C6), 125.6 (t, $^3J_{\text{P-C}} = 6.1$ Hz, C4), 39.6 [td, vt $^1J_{\text{P-C}} = 8.1$ Hz, $^2J_{\text{Rh-C}} = 3.0$ Hz, 2 x P(*t*Bu) $_2$], 28.1 [vt, $^2J_{\text{P-C}} = 4.0$ Hz, 2 x P(*t*Bu) $_2$].

$^{31}\text{P}\{^1\text{H}\}$ NMR (162 MHz, 23 °C, CD_2Cl_2) δ 220.4 (d, $^1J_{\text{Rh-P}} = 155.5$ Hz).

IR (thin film THF): $\nu(\text{CO}) = 1956\text{ cm}^{-1}$

Elemental Analysis Calculated for $\text{C}_{22}\text{H}_{38}\text{NRhO}_3\text{P}_2$ (529.39): C, 49.91; H, 7.23; N, 2.65. **Found:** C, 48.58; H, 7.19; N, 2.68.

Synthesis of (BCF-pyrPOCOP)RhCO (**2.5**)

In a nitrogen-filled glovebox a 50-mL Schlenk flask was charged with compound **2.2** (0.150 g, 0.165 mmol) and $[\text{Rh}(\text{CO})_2\text{Cl}]_2$ (0.033 g, 0.083 mmol) and a Teflon stir bar and dissolved in 8 mL toluene. The flask was removed from the glovebox and left open to argon on a Schlenk line as the solution was stirred at ambient temperature. The solution color quickly changed from yellow to orange and stirring was continued for 1 h. A small amount of solid material precipitated over the course of the hour. The crude reaction mixture was filtered through a thin plug of Celite and the toluene removed under vacuum. The crude solid was eluted through a thick plug of silica gel

with 5:1 hexane:dichloromethane. Evaporation of solvent followed by washing with pentane (3 x 5 mL) and further drying under vacuum gave analytically pure **2.3** (0.118 g, 69%) as a bright orange powder.

^1H NMR (400 MHz, 23 °C, CD_2Cl_2) δ 7.73 (s, 2H, Ar 2,6-H), 1.34 [t, $^3J_{\text{P-H}} = 8.0$ Hz, 36H, 2 x P(*t*Bu)₂].

$^{13}\text{C}\{^1\text{H}\}$ NMR (101 MHz, 23 °C, CD_2Cl_2) δ 198.6 (m, Rh-CO), 165.7 (m, C3 and C5), 147.9 (dm, $^1J_{\text{C-F}}$, 242.4 Hz, C-F), 137.1 (dm, $^1J_{\text{C-F}} = 262.6$ Hz, C-F), 122.6 (d, $^3J_{\text{P-C}} = 6.1$ Hz, C2 and C6), 121.1 (t, $^3J_{\text{P-C}} = 9.1$ Hz, C4), 40.2 [td, vt $^1J_{\text{P-C}} = 8.1$ Hz, d $^2J_{\text{Rh-C}} = 2.0$ Hz, 2 x P(*t*Bu)₂], 27.9 [vt, $^2J_{\text{P-C}} = 4.0$ Hz, 2 x P(*t*Bu)₂].

$^{31}\text{P}\{^1\text{H}\}$ NMR (162 MHz, 23 °C, CD_2Cl_2) δ 228.3 (d, $^1J_{\text{Rh-P}} = 152.3$ Hz).

$^{19}\text{F}\{^1\text{H}\}$ NMR (376 MHz, 23 °C, CD_2Cl_2) δ -132.1 (d, $^3J_{\text{F-F}}$, 22.6 Hz, *o*-F), -158.75 (t, $^3J_{\text{F-F}}$, 18.8 Hz, *p*-F), -164.7 (t, $^3J_{\text{F-F}}$, 18.8 Hz, *m*-F).

IR (thin film THF): $\nu(\text{CO}) = 1990\text{ cm}^{-1}$

Elemental Analysis Calculated for $\text{C}_{40}\text{H}_{38}\text{NRhBF}_{15}\text{O}_3\text{P}_2$ (1041.37): C, 46.13; H, 3.68; N, 1.35. **Found:** C, 46.23; H, 3.73; N, 1.18.

Synthesis of (BCF-pyrPOCOP)IrHCl (**2.6**)

In a nitrogen-filled glovebox a 100-mL Schlenk tube with a Teflon Kontes stopcock was charged with compound **2.2** (0.300 g, 0.329 mmol) and $[\text{Ir}(\text{COD})\text{Cl}]_2$ (0.111 g, 0.165 mmol) and a Teflon stir bar and dissolved in 12 mL toluene. The flask was sealed, removed from the glovebox and placed in an oil bath heated to 100 °C. The solution color gradually changed from brown to orange and stirring in the oil

bath was continued for 36 h. The crude reaction mixture was filtered through a thick plug of dried neutral alumina and the toluene removed under vacuum. The crude solid was washed with pentane (3 x 6 mL) followed by further drying under vacuum at 60 °C to give **2.6** (0.239 g, 64%) as a bright orange powder.

^1H NMR (400 MHz, 23 °C, CD_2Cl_2) δ 7.65 (s, 2H, Ar 2,6-H), 1.37 [vt, $^3J_{\text{P-H}} = 8.0$ Hz, 36H, 2 x P(*t*Bu) $_2$], -38.9 (t, $^2J_{\text{P-H}} = 12.0$ Hz, 1H, Ir-H).

$^{13}\text{C}\{^1\text{H}\}$ NMR (101 MHz, 23 °C, CD_2Cl_2) δ 165.0 (t, $^2J_{\text{P-C}} = 7.1$ Hz, C3 and C5), 147.9 (dm, $^1J_{\text{C-F}} = 242.4$ Hz, C-F), 147.2 (m, C2 and C6), 139.9 (dm, $^1J_{\text{C-F}} = 255.5$ Hz, C-F), 137.1 (dm, $^1J_{\text{C-F}} = 258.6$ Hz, C-F), 122.7 (t, $^3J_{\text{P-C}} = 5.1$ Hz, C4), 43.6 and 40.2 [vt each, $J_{\text{P-C}} = 10.1$ Hz and 11.1 Hz, 2 x P(*t*Bu) $_2$], 27.1 [m, 2 x P(*t*Bu) $_2$].

$^{31}\text{P}\{^1\text{H}\}$ NMR (162 MHz, 23 °C, CD_2Cl_2) δ 187.1.

$^{19}\text{F}\{^1\text{H}\}$ NMR (376 MHz, 23 °C, CD_2Cl_2) δ -132.2 (d, $^3J_{\text{F-F}} = 18.8$ Hz, *o*-F), -158.5 (t, $^3J_{\text{F-F}} = 18.8$ Hz, *p*-F), -164.6 (t, $^3J_{\text{F-F}} = 18.8$ Hz, *m*-F).

Elemental Analysis Calculated for $\text{C}_{39}\text{H}_{39}\text{NiIrBClF}_{15}\text{O}_2\text{P}_2$ (1139.14): C, 41.12; H, 3.45; N, 1.23. **Found:** C, 41.17; H, 3.49; N, 1.22.

Synthesis of (BCF-pyrPOCOP)NiBr (**2.7**)

In a nitrogen-filled glovebox a 100-mL Schlenk tube with a Teflon Kontes stopcock was charged with compound **2.2** (0.250 g, 0.274 mmol) and $\{(i\text{-PrCN})\text{NiBr}_2\}_n$ (0.079 g, 0.274 mmol) and a Teflon stir bar. The flask was brought out of the glove box and under a flow of argon 15 mL toluene and triethylamine (46.0 μL , 0.033 g, 0.329 mmol). The solution color quickly changed from green to dark

brownish yellow and stirring was continued for 48 h in an oil bath preheated to 100 °C. After this time, the crude reaction mixture was cooled to ambient temperature and then filtered through a thin plug of Celite and the toluene removed under vacuum. The crude solid was eluted through a small column of silica gel with 7:1 hexane:dichloromethane. Evaporation of solvent followed by washing with pentane (3 x 5 mL) and further drying under vacuum gave analytically pure **2.7** (0.217 g, 76%) as a bright yellow powder.

¹H NMR (400 MHz, 23 °C, CD₂Cl₂) δ 7.66 (s, 2H, Ar 2,6-H), 1.52 [vt, ³J_{P-H} = 8.0 Hz, 36H, 2 x P(*t*Bu)₂].

¹³C{¹H} NMR (101 MHz, 23 °C, CD₂Cl₂) δ 166.4 (t, ²J_{P-C} = 10.1 Hz, C3 and C5), 151.9 (t, ³J_{P-C}, 18.2 Hz, C2 and C6), 147.8 (dm, ¹J_{C-F} = 242.4 Hz, C-F), 140.0 (dm, ¹J_{C-F} = 250.5 Hz, C-F), 137.0 (dm, ¹J_{C-F} = 234.3 Hz, C-F), 123.3 (t, ³J_{P-C} = 6.1 Hz, C4), 40.1 [vt, J_{P-C} = 7.1 Hz, 2 x P(*t*Bu)₂], 27.8 [vt, J_{P-C} = 3.0 Hz, 2 x P(*t*Bu)₂].

³¹P{¹H} NMR (162 MHz, 23 °C, CD₂Cl₂) δ 204.9 (s).

¹⁹F{¹H} NMR (376 MHz, 23 °C, CD₂Cl₂) δ -132.13 (d, ³J_{F-F}, 22.6 Hz, *o*-F), -158.27 (t, ³J_{F-F}, 18.8 Hz, *p*-F), -164.42 (t, ³J_{F-F}, 18.8 Hz, *m*-F).

Elemental Analysis Calculated for C₃₉H₃₈NNiBBBrF₁₅O₂P₂ (1049.1): C, 44.65; H, 3.65; N, 1.34. **Found:** C, 44.67; H, 3.45; N, 1.37.

Synthesis of (pyrPOCOP)NiBr (**2.8**)

In a nitrogen-filled glovebox a 20-mL scintillation vial was charged with compound **2.7** (0.064 g, 0.062 mmol), polystyrene-DMAP (0.041 g, 0.123 mmol), 5

mL toluene, and a Teflon stir bar. The flask was capped and heated to 100 °C in an aluminum block for 12 h. After this time, the flask was cooled to ambient temperature, removed from the glovebox and then filtered through a Teflon syringe filter (0.45 µm) the toluene removed under vacuum. The crude solid was added to a 50-mL Schlenk tube which was also charged with potassium bromide (0.366 g, 3.10 mmol), 5 mL dry acetonitrile and 2 mL dry tetrahydrofuran and a Teflon stir bar. The mixture was stirred and heated in an 80 °C oil bath for 8 h. Cooling of the crude reaction mixture followed by filtration through a Teflon syringe filter (0.45 µm) and evaporation of solvent followed by washing with pentane (3 x 5 mL) and further drying under vacuum gave **2.8** (0.027 g, 81%) as a yellow powder.

¹H NMR (400 MHz, 23 °C, CD₂Cl₂) δ 7.74 (s, 2H, Ar 2,6-H), 1.51 [vt, ³J_{P-H} = 8.0 Hz, 36H, 2 x P(*t*Bu)₂].

¹³C{¹H} NMR (101 MHz, 23 °C, CD₂Cl₂) δ 166.5 (t, ²J_{P-C} = 10.1 Hz, C3 and C5), 138.0 (t, ³J_{P-C} = 19.2 Hz, C2 and C6), 126.5 (t, ³J_{P-C} = 5.1 Hz, C4), 40.1 [vt, *J*_{P-C} = 6.1 Hz, 2 x P(*t*Bu)₂], 28.0 [vt, *J*_{P-C} = 3.0 Hz, 2 x P(*t*Bu)₂].

³¹P{¹H} NMR (162 MHz, 23 °C, CD₂Cl₂) δ 195.9 (s).

Elemental Analysis Calculated for C₂₁H₃₈NNiBrO₂P₂ (537.1): C, 46.96; H, 7.13; N, 2.61. **Found:** C, 46.71; H, 7.03; N, 2.49.

Synthesis of (BCF-pyrPOCOP)NiH (**2.9**)

In a nitrogen-filled glovebox a 250-mL Schlenk round-bottom Schlenk flask with was charged with compound **2.7** (0.140 g, 0.133 mmol) and LiAlH₄ (0.076 g, 2.00

mmol) and 20 mL dry toluene. Then a Teflon stir bar was added and the flask was capped with a rubber septum. The flask was brought out of the glove box and placed under a flow of argon. The solution was stirred at ambient temperature for 24 h. After this time, the crude reaction mixture was filtered via cannula through a thin plug of Celite in a coarse-fritted Schlenk filter and the toluene removed under vacuum. The crude solid was washed with pentane (3 x 5 mL) and dried under vacuum to give **2.9** (0.066 g, 51%) as a bright yellow powder.

^1H NMR (400 MHz, 23 °C, C_6D_6) δ 8.16 (s, 2H, Ar 2,6-H), 1.00 [vt, $^3J_{\text{P-H}} = 8.0$ Hz, 36H, 2 x P(*t*Bu)₂], -7.92 (t, $^2J_{\text{P-H}} = 52.0$ Hz, Ni-H).

$^{13}\text{C}\{^1\text{H}\}$ NMR (101 MHz, 23 °C, C_6D_6) δ 165.3 (t, $^2J_{\text{P-C}} = 11.1$ Hz, C3 and C5), 148.1 (dm, $^1J_{\text{C-F}} = 242.4$ Hz, C-F), 139.9 (dm, $^1J_{\text{C-F}} = 257.6$ Hz, C-F), 137.2 (dm, $^1J_{\text{C-F}} = 245.4$ Hz, C-F), 123.1 (t, $^3J_{\text{P-C}} = 5.1$ Hz, C4), 38.2 [vt, $J_{\text{P-C}} = 8.1$ Hz, 2 x P(*t*Bu)₂], 27.5 [m, 2 x P(*t*Bu)₂].

$^{31}\text{P}\{^1\text{H}\}$ NMR (162 MHz, 23 °C, C_6D_6) δ 234.6 (s).

$^{19}\text{F}\{^1\text{H}\}$ NMR (376 MHz, 23 °C, C_6D_6) δ -132.0 (br s, *o*-F), -156.4 (t, $^3J_{\text{F-F}} = 18.8$ Hz, *p*-F), -163.4 (t, $^3J_{\text{F-F}} = 18.8$ Hz, *m*-F).

IR (thin film THF): $\nu(\text{Ni-H}) = 1804\text{ cm}^{-1}$

Synthesis of (pyrPOCOP)NiH (**2.10**) and DMAP:**B**(C₆F₅)₃ mixture

In a nitrogen-filled glovebox a 20-mL Scintillation vial was charged with compound **2.9** (0.050 g, 0.051 mmol) and DMAP (0.006 g, 0.051 mmol) and 5 mL dry toluene. Then a Teflon stir bar was added and the flask was capped and heated

to 50 °C in an aluminum block for 5 h. The flask was then cooled and solvent evaporated to give a mixture of DMAP:B(C₆F₅)₃ and **2.10**.

¹H NMR (400 MHz, 23 °C, C₆D₆) δ 8.05 (s, 2H, Ar 2,6-H), 1.05 [vt, ³J_{P-H} = 8.0 Hz, 36H, 2 x P(*t*Bu)₂], -7.87 (t, ²J_{P-H} = 53.0 Hz, Ni-H)

¹³C{¹H} NMR (101 MHz, 23 °C, C₆D₆) δ 165.3 (t, ²J_{P-C} = 11.1 Hz, C3 and C5), 123.1 (t, ³J_{P-C} = 5.1 Hz, C4), 38.2 [vt, J_{P-C} = 8.1 Hz, 2 x P(*t*Bu)₂], 27.5 [m, 2 x P(*t*Bu)₂].

³¹P{¹H} NMR (162 MHz, 23 °C, C₆D₆) δ 225.1 (s).

IR (thin film THF): ν(Ni-H) = 1772 cm⁻¹

Generation of nickel formate complex **2.11**

An oven-dried J-Young style NMR tube was charged with 0.015 mmol of **2.9** and 0.5 mL C₆D₆. The tube was degassed by five freeze-pump-thaw cycles and placed under 1 atmosphere of CO₂. A -78 °C dry ice/isopropanol trap was used to prevent adventitious water from CO₂ from entering the reaction. The tube was sealed and rotated at rate of 3 revolutions/minute while conversion to the formate complex was monitored by NMR spectroscopy.

Data for (BCF-pyrPOCOP)Ni(OCHO) (**2.11**)

¹H NMR (400 MHz, 23 °C, C₆D₆) δ 7.99 (br, 1H, Ni-OCHO), 7.92 (s, 1H, Ar 2,6-H), 1.13 [vt, ³J_{P-H} = 8.0 Hz, 36H, 2 x P(*t*Bu)₂].

$^{13}\text{C}\{^1\text{H}\}$ NMR (101 MHz, 23 °C, C_6D_6) δ 167.0 (m, C3 and C5), 148.0 (dm, $^1J_{\text{C-F}} = 242.4$ Hz, C-F), 140.1 (dm, $^1J_{\text{C-F}} = 248.6$ Hz, C-F), 137.3 (dm, $^1J_{\text{C-F}} = 242.4$ Hz, C-F), 123.1 (t, $^3J_{\text{P-C}} = 6.1$ Hz, C4), 39.7 [vt, $J_{\text{P-C}} = 5.1$ Hz, 2 x P(*t*Bu) $_2$], 26.7 [m, 2 x P(*t*Bu) $_2$].

$^{31}\text{P}\{^1\text{H}\}$ NMR (162 MHz, 23 °C, C_6D_6) δ 202.6 (s).

$^{19}\text{F}\{^1\text{H}\}$ NMR (376 MHz, 23 °C, C_6D_6) δ -132.1 (br, *o*-F), -155.8 (t, $^3J_{\text{F-F}}$, 22.6 Hz, *p*-F), -163.1 (t, $^3J_{\text{F-F}}$, 15.0 Hz, *m*-F).

IR (thin film C_6D_6): $\nu(\text{CO}) = 1634\text{ cm}^{-1}$

Synthesis of (BCF-POCOP)Ir(C_2H_4) (2.12)

In an argon-filled glove box a 250-mL round-bottomed Schlenk flask was charged with **2.6** (0.200 g, 0.176 mmol) and potassium *tert*-butoxide (0.030 g, 0.263 mmol) and a Teflon stir bar. On a Schlenk manifold the flask was purged with ethylene for 10 minutes before 15 mL toluene was added. Ethylene was bubbled into the solution as stirring was continued for 3 h. After this time the flask was placed under argon and filtered through a thin pad of Celite in a coarse-fritted Schlenk filter and toluene was removed under vacuum. Pentane (8 mL) was added and removed under vacuum three times to volatilize *tert*-butanol. The produce was dried under vacuum to give **2.13** as a scarlet red powder (0.110 g, 56%).

^1H NMR (400 MHz, 23 °C, C_6D_6) δ 8.13 (s, 2H, Ar 2,6-H), 2.86 (br s, 4 H, C_2H_4), 1.01 [vt, $^3J_{\text{P-H}} = 8.0$ Hz, 36H, 2 x P(*t*Bu) $_2$].

$^{13}\text{C}\{^1\text{H}\}$ NMR (101 MHz, 23 °C, C_6D_6) δ 166.5 (t, $^2J_{\text{P-C}} = 10.1$ Hz, C3 and C5), 148.5 (dm, $^1J_{\text{C-F}} = 242.4$ Hz, C-F), 140.1 (dm, $^1J_{\text{C-F}} = 257.6$ Hz, C-F), 137.0 (dm, $^1J_{\text{C-F}} = 252.2$ Hz, C-F), 124.0 (t, $^3J_{\text{P-C}} = 6.1$ Hz, C4), 39.4 [vt, $J_{\text{P-C}} = 8.1$ Hz, 2 x P(*t*Bu)₂], 36.2 (s, C₂H₄), 28.0 [m, 2 x P(*t*Bu)₂].

$^{31}\text{P}\{^1\text{H}\}$ NMR (162 MHz, 23 °C, C_6D_6) δ 199.9 (s).

$^{19}\text{F}\{^1\text{H}\}$ NMR (376 MHz, 23 °C, C_6D_6) δ -131.8 (br, *o*-F), -157.2 (t, $^3J_{\text{F-F}}$, 18.8 Hz, *p*-F), -163.8 (t, $^3J_{\text{F-F}}$, 22.6 Hz, *m*-F).

General Procedure for attempted alkane transfer dehydrogenation:

A 50-mL thick-walled Schlenk tube was charged under argon with an equimolar mixture of alkane and *tert*-butylethylene and the catalyst system of choice in a 3000:1 substrate to catalyst ratio. The tube was closed with a Kontes Teflon stopcock and the flask was degassed via five freeze-pump-thaw cycles, followed by heating in an oil bath at the specified temperature (100-200 °C) for 12-24 h. The contents of the flask were cooled, hexamethylbenzene was added, and the mixture was analyzed by GC.

X-Ray Structure Determination

Compound **2.6** (BCF-pyrPOCOP)IrHCl

Low-temperature diffraction data (ϕ - and ω -scans) were collected on a Bruker AXS D8 VENTURE KAPPA diffractometer coupled to a PHOTON 100 CMOS detector with Mo K_{α} radiation ($\lambda = 0.71073 \text{ \AA}$) from an I μ S micro-source for the structure of compound (**2.6**). The structure was solved by direct methods using SHELXS and refined against F^2 on all data by full-matrix least squares with SHELXL-2014 using established refinement techniques.⁴¹⁻⁴³ All non-hydrogen atoms were refined anisotropically. All hydrogen atoms were included into the model at geometrically calculated positions and refined using a riding model. The isotropic displacement parameters of all hydrogen atoms were fixed to 1.2 times the U value of the atoms they are linked to (1.5 times for methyl groups). All disordered atoms were refined with the help of similarity restraints on the 1,2- and 1,3-distances and displacement parameters as well as rigid bond restraints for anisotropic displacement parameters.

Compound **2.6** crystallizes in the monoclinic space group $P2_1/c$ with two molecules in the asymmetric unit along with two molecules of diethyl ether.

Empirical formula	C ₄₃ H ₄₈ B Cl F ₁₅ Ir N O ₃ P ₂
Formula weight	1212.22
Temperature	100(2) K
Wavelength	0.71073 Å
Crystal system	Monoclinic
Space group	P2 ₁ /c
Unit cell dimensions	
a = 24.5782(19) Å	a = 90°
b = 12.8790(9) Å	b = 95.873(3)°
c = 30.394(2) Å	g = 90°
Volume	9570.6(12) Å ³
Z	8
Density (calculated)	1.683 Mg/m ³
Absorption coefficient	3.011 mm ⁻¹
F(000)	4808
Crystal size	0.260 x 0.220 x 0.160 mm ³
Theta range for data collection	2.247 to 36.355°
Index ranges	-38 ≤ h ≤ 40, -21 ≤ k ≤ 21, -50 ≤ l ≤ 50
Reflections collected	287901
Independent reflections	46373 [R(int) = 0.0584]
Completeness to theta = 25.242°	99.9 %
Absorption correction	Semi-empirical from equivalents
Max. and min. transmission	0.5676 and 0.4399
Refinement method	Full-matrix least-squares on F ²
Data / restraints / parameters	46373 / 0 / 1235
Goodness-of-fit on F ²	1.104
Final R indices [I > 2σ(I)]	R1 = 0.0477, wR2 = 0.0753
R indices (all data)	R1 = 0.0773, wR2 = 0.0816
Extinction coefficient	n/a
Largest diff. peak and hole	2.979 and -5.127 e.Å ⁻³

Table 2. Crystal data and structure refinement for **2.6**

Compound 2.7 (BCF-POCOP)NiBr

Low-temperature diffraction data (ϕ - and ω -scans) were collected on a Bruker AXS D8 VENTURE KAPPA diffractometer coupled to a PHOTON 100 CMOS detector with Mo K_α radiation ($\lambda = 0.71073 \text{ \AA}$) from an I μ S micro-source for the structure of compound **2.7**. The structure was solved by direct methods using SHELXS and refined against F^2 on all data by full-matrix least squares with SHELXL-2016 using established refinement techniques.⁴¹⁻⁴³ All non-hydrogen atoms were refined anisotropically. All hydrogen atoms were included into the model at geometrically calculated positions and refined using a riding model. The isotropic displacement parameters of all hydrogen atoms were fixed to 1.2 times the U value of the atoms they are linked to (1.5 times for methyl groups).

Compound **2.7** crystallizes in the monoclinic space group $P2_1/n$ with one molecule in the asymmetric unit.

Empirical formula	C ₃₉ H ₃₈ B Br F ₁₅ N Ni O ₂ P ₂
Formula weight	1049.07
Temperature	100(2) K
Wavelength	0.71073 Å
Crystal system	Monoclinic
Space group	P2 ₁ /n
Unit cell dimensions	
a=18.331(2) Å	a= 90°.
b = 12.0823(15) Å	b= 99.077(5)°.
c = 19.875(3) Å	g = 90°.
Volume	4346.9(9) Å ³
Z	4
Density (calculated)	1.603 Mg/m ³
Absorption coefficient	1.539 mm ⁻¹
F(000)	2112
Crystal size	0.450 x 0.450 x 0.400 mm ³
Theta range for data collection	2.250 to 36.417°.
Index ranges	-28<= <i>h</i> <=30, -20<= <i>k</i> <=20, -33<= <i>l</i> <=33
Reflections collected	151341
Independent reflections	21162 [R(int) = 0.0554]
Completeness to theta = 25.242°	99.9 %
Absorption correction	Semi-empirical from equivalents
Max. and min. transmission	0.7471 and 0.6178
Refinement method	Full-matrix least-squares on F ²
Data / restraints / parameters	21162 / 0 / 571
Goodness-of-fit on F ²	1.025
Final R indices [I>2sigma(I)]	R1 = 0.0357, wR2 = 0.0693
R indices (all data)	R1 = 0.0611, wR2 = 0.0765
Extinction coefficient	n/a
Largest diff. peak and hole	0.918 and -0.964 e.Å ⁻³

Table 2. Crystal data and structure refinement for complex **2.7**.

References

- (1) Peris, E.; Crabtree, R.H. *Chem. Soc. Rev.* **2018**, *47*, 1959
- (2) Adhikary, A.; Guan, H. *ACS Catal.* **2015**, *5*, 6858.
- (3) Göttker-Schnetmann, I.; White, P.; Brookhart, M. *J. Am. Chem. Soc.* **2004**, *126*, 1804.
- (4) Göttker-Schnetmann, I.; White, P.S.; Brookhart, M. *Organometallics* **2004**, *23*, 1766.
- (5) Morales-Morales, D.; Redon, R.; Yung, C.; Jensen, C. M. *Inorg. Chim. Acta.* **2004**, *357*, 2953.
- (6) Vabre, B.; Linderperg, F.; Zargarian, D. *Green Chem.* **2013**, *15*, 3188.
- (7) Liberman-Martin, A.L.; Bergman, R.G.; Tilley, T.D. *J. Am. Chem. Soc.* **2013**, *135*, 9612.
- (8) Liberman-Martin, A.L.; Levine, D.S.; Liu, W.; Bergman, R.G.; Tilley, T.D. *Organometallics* **2016**, *35*, 1064.
- (9) Johnson, A.M.; Contrella, N.D.; Sampson, J.R.; Zheng, M.; Jordan, R.F. *Organometallics* **2017**, *36*, 4990.
- (10) Horak, K.T.; VanderVelde, D.G.; Agapie, T. *Organometallics* **2015**, *34*, 4753.
- (11) Beringhelli, T.; Donghi, D.; Maggioni, D.; D'Alfonso, G. *Coord. Chem. Rev.* **2008**, *252*, 2292.
- (12) Gerald Lesley, M.J.; Woodward, A.; Taylor, N.J.; Marder, T.B.; Cazenobe, I.; Ledoux, I.; Zyss, J.; Thornton, A.; Bruce, D.W.; Kakkar, A.K. *Chem. Mater.* **1998**, *10*, 1355.
- (13) Zhu, K.; Achord, P.D.; Zhang, X.; Krogh-Jespersen, K.; Goldman, A.S. *J. Am. Chem. Soc.* **2004**, *126*, 13044.
- (14) Kulkin, S.A.; Sheloumov, A.M.; Dolgushin, F.M.; Ezernitskaya, M.G.; Pergudov, A.S.; Petrovskii, P.V.; Koridze, A.A. *Organometallics* **2006**, *25*, 5466.

- (15) Rivada-Wheelaghan, O.; Dauth, A.; Leitus, G.; Diskin-Posner, Y.; Milstein, D. *Inorg. Chem.* **2015**, *54*, 4526.
- (16) Goldberg, J.M.; Wong, G.W.; Brastow, K.E.; Kaminsky, W.; Goldberg, K.I.; Heinekey, D.M. *Organometallics* **2015**, *34*, 753.
- (17) Vabre, B.; Spasyuk, D.M.; Zargarian, D. *Organometallics* **2012**, *31*, 8561.
- (18) Polezhaev, A.Z.; Kuklin, S.A.; Ivanov, D.M.; Petrovskii, P.V.; Dolgushin, F.M.; Ezernitskaya, M.G.; Koridze, A.A. *Russ. Chem. Bull. Int. Ed.* **2009**, *58*, 1847.
- (19) Montag, M.; Efremenko, I.; Cohen, R.; Shimon, L.J.W.; Leitus, G.; Diskin-Posner, Y.; Ben-David, Y.; Salem, H.; Martin, J.M.L.; Milstein, D. *Chem. Eur. J.* **2010**, *16*, 328.
- (20) Cherry, S.D.T.; Kaminsky, W.; Heinekey, D.M. *Organometallics* **2016**, *35*, 2165.
- (21) Brück, A.; Gallego, D.; Wang, W.; Irran, E.; Driess, M.; Hartwig, J.F. *Angew. Chem. Int. Ed.* **2012**, *51*, 11478.
- (22) Jonasson, K.J.; Ahlsten, N.; Wendt, O.F. *Inorg. Chim. Acta.* **2011**, *379*, 76.
- (23) Kovalenko, O.O.; Wendt, O.F. *Dalton Trans.* **2016**, *45*, 15963.
- (24) Vabre, B.; Lambert, M.L.; Petit, A.; Ess, D.H.; Zargarian, D. *Organometallics*. **2012**, *31*, 6041.
- (25) Pandarus, V.; Castonguay, A.; Zargarian, D. *J. Chem. Soc., Dalton Trans.* **2008**, 4756.
- (26) Gossage, R.A.; van de Kuil, L.A.; van Koten, G. *Acc. Chem. Res.* **1998**, *31*, 423.
- (27) Chakraborty, S.; Krause, J.A.; Guan, H. *Organometallics* **2009**, *28*, 582.
- (28) Jude, H.; Bauer, J.A.K.; Connick, W.B. *Inorg. Chem.* **2002**, *41*, 2275.
- (29) Jude, H.; Bauer, J.A.K.; Connick, W.B. *Inorg. Chem.* **2004**, *43*, 725.
- (30) Jude, H.; Bauer, J.A.K.; Connick, W.B. *Inorg. Chem.* **2005**, *44*, 1211.
- (31) Eberhardt, N.A.; Guan, H. *Chem. Rev.* **2016**, *116*, 8373.

- (32) Schmeier, T.J.; Nova, A.; Hazari, N.; Maseras, F. *Chem. Eur. J.* **2012**, *18*, 6915.
- (33) Schmeier, T.J.; Hazari, N.; Incarvito, C.D.; Raskatov, J.A. *Chem. Commun.* **2011**, *47*, 1824.
- (34) Chakraborty, S.; Patel, Y.G.; Krause, J.A.; Guan, H. *Polyhedron* **2012**, *32*, 30.
- (35) Chakraborty, S.; Zhang, J.; Patel, Y.G.; Krause, J.A.; Guan, H. *Inorg. Chem.* **2013**, *52*, 37.
- (36) Chakraborty, S.; Zhang, J.; Krause, J.A.; Guan, H. *J. Am. Chem. Soc.* **2010**, *132*, 8872.
- (37) Hazari, N.; Heimann, J.E. *Inorg. Chem.* **2017**, *56*, 13655.
- (38) Heimann, J.E.; Bernskoetter, W.H.; Guthrie, J.A.; Hazari, N.; Mayer, J.M. *Organometallics* **2018**, *37*, 3649.
- (39) Heimann, J.E.; Bernskoetter, W.H.; Hazari, N.; Mayer, J.M. *Chem. Sci.* **2018**, *9*, 6629.
- (40) Kreye, M.; Freytag M.; Jones, P.G.; Williard, P.G.; Bernskoetter, W.H.; Walter, M.D. *Chem. Commun.* **2015**, *51*, 2946.
- (41) Sheldrick, G.M.; *Acta. Cryst.* **1990**, *A46*, 467.
- (42) Sheldrick, G.M.; *Acta. Cryst.* **2008**, *A64*, 112.
- (43) Müller, P. *Crystallography Reviews* **2009**, *15*, 57.

Chapter 3

Alkoxide-mediated C-X Bond Cleavage with Silanes

Portions of this chapter adapted with permission from:

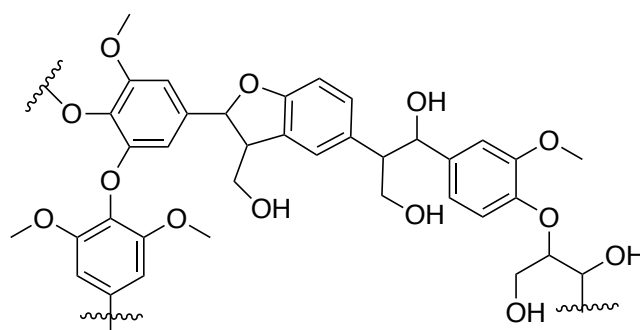
Fedorov, A.; Toutov, A.A.; Swisher, N.A.; Grubbs, R.H. *Chem. Sci.* **2013**, *4*, 1640-1645. Doi: 10.1039/C3SC22256J

Abstract

An unusual cleave of C-O and C-S bonds by silanes in the presence of alkoxide bases is presented. Cleavage of both C(sp²)-O and C(sp³)-O bonds was achieved at high temperatures using excesses of both alkoxide bases and tertiary silanes. The factors affecting selectivity in this transition metal-free method are discussed. A very unusual side reaction of C-H silylation is also presented and discussed. Initial results towards C-S cleavage in benzothiophenes are presented.

Introduction

In the past few decades, the growing demand for energy combined with declining fossil fuel reserves has created a tremendous surge in interest for efficient manufacturing of fuels and bulk chemicals from renewable bioresources.¹ The natural heterobiopolymer lignin has developed into a major target for cost-efficient biomass conversion because the repeating aromatic ether structural units could offer high energy content products and potential access to useful derivatives for fine chemical applications.² However, at present, utilization of lignin is clearly limited since current technology does not allow for efficient decomposition into its constituent building blocks with the desired selectivity.¹ One of the major challenges associated with such a process is the need to reductively cleave the different types of strong aromatic C-O bonds present in lignin,³ which is also a relevant problem for the liquefaction of coal (**Scheme 3.1**).⁴



Scheme 3.1. Structure of hardwood lignin.

Considerable advances in the utilization of aryl alkyl ethers as electrophiles in

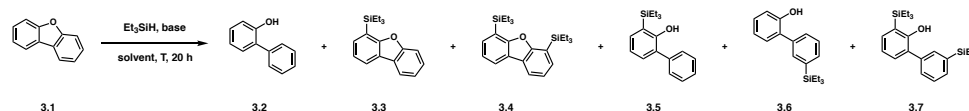
cross-coupling reactions with Ni catalysts⁵ has prompted important recent discoveries of selective reductive deoxygenation transformations involving aryl-oxygen bonds. Specifically, Martin has utilized in situ prepared phosphine-ligated Ni species to cleave the aryl-oxygen bond in aryl alkyl ethers using tertiary silanes as the stoichiometric reductant,⁶ and a similar approach was also reported by Chatani.⁷ Switching to N-heterocyclic carbenes as supporting ligands for Ni allowed Hartwig to selectively cleave diaryl ethers with different reductants including dihydrogen and Et₃SiH, albeit with Ni loadings as high as 5-20%.⁸⁻¹⁰ In a recent contribution by the same group, high catalyst loadings were avoided by employing a heterogeneous Ni catalyst.¹² Furthermore, Lercher and Zhao demonstrated that the use of silica-supported Ni nanoparticles allows for efficient cleavage of aryl ethers with dihydrogen in the aqueous phase.¹³ It would be beneficial to have a general methodology for *aromatic* C-O bond cleavage that does not employ nickel¹⁴ or other transition metal catalysts. The only known alternative approaches for metal free ether cleavage at relatively low temperatures^{2a}, rely on excess alkali metals or electrocatalytic processes¹⁵ that tend to be costly, unsustainable and impractical. In an attempt to overcome these constraints, we have discovered that in the absence of exogenous transition metal species, stoichiometric mixtures of alkoxide or hydride bases with organosilanes form potent regioselective reductive systems for the cleavage of diaryl and aryl alkyl ethers to the corresponding phenolic and aromatic compounds. This approach may serve as a guide for further development of a useful method to obtain aromatic feedstocks from polymeric materials. Additionally, the directed *ortho*-silylation that was

discovered in conjunction with the ether cleavage studies presented herein holds promise for selective and practical introduction of the silyl group into aromatic frameworks for their subsequent functionalization.

Results and Discussion

Our investigation into silane-mediated, aromatic C-O bond reduction began with dibenzofuran (**3.1**) – a model compound for the beta-5 linkage in lignin.^{1b} A survey of potential reductants identified that the combination of potassium *tert*-butoxide, triethylsilane and various transition metal complexes forms a potent and convenient system for the reduction of C_{ar}-O bonds. However, when we performed control experiments in the absence of transition metal species, we observed nearly complete conversion of dibenzofuran. ICP-MS analysis of the reaction mixtures, reactants, and products demonstrated that trace amounts of transition metals did not exceed 10 ppm.¹⁶ Thus, heating of **1** with 5 equiv. of Et₃SiH and 2 equiv. of KO*t*-Bu in a sealed vial in toluene at 100 °C for 20 hours gave 98% conversion of dibenzofuran to a mixture of products including the desired C_{ar}-O cleavage product biphenyl-2-ol (**3.2**, 38%) along with five unexpected silylated products (**3.2-3.7**, **Table 3.1**, **Entry 1**). We speculate that under the reaction conditions, **3.1** is selectively *ortho*-silylated giving dibenzofurans **3.3** and **3.4**, which in turn undergo C-O bond cleavage to biphenyl-2-ols **3.5-3.7**. Furthermore, reactions in toluene and mesitylene (*vide infra*) do give solvent-derived silylated products and in the case of toluene where aromatic regioisomers arise, benzylic C-H silylation prevails. Such reactivity with unactivated substrates is particularly remarkable since transition metals and directing groups¹⁷ or very high temperatures¹⁸ are normally required for related functionalizations. While

this transition-metal-free C-H silylation process has potential applications in organic synthesis¹⁹ and is itself poised for further investigation, we first focused on tuning the selectivity to favour the intended C-O scission. Increasing the amount of base to 5 equivalents resulted in improved 63% yield of **3.2** at the expense of other products (Table 3.1, Entry 2). Switching to 165 °C in mesitylene while keeping equimolar silane-to-base ratio not only allowed for reduced Et₃SiH loading, but also cleanly gave targeted biphenyl-2-ol **3.2** with 85% yield (Entry 3).



Entry	[H] ^c (equiv.)	Base (equiv.)	Solvent	T, °C	Conv. (%)	3.2	3.3	3.4	3.5	3.6	3.7
1	5	KOt-Bu (2)	Toluene	100	98	38	16	10	21	2	7
2	5	KOt-Bu (5)	Toluene	100	97	63	10	2	20	—	2
3	3	KOt-Bu (3)	Mes.	165	100	85 ^d	3	—	5	2	—
4	3	KOEt (3)	Mes.	165	95	77	10	—	6	1	—
5	5	CsOR ^e (3)	Toluene	100	89	75	3	11	—	—	—
6	5	KH (1)	Dioxane	100	49	1	43	5	—	—	—
7	5	KOt-Bu (0.5)	Toluene	100	90	12	48	20	9	—	1
8	5	KOt-Bu (2)	Toluene	80	98	29	18	26	9	—	7
9	5	KOt-Bu (2)	Toluene ^f	100	98	5	28	46	—	—	—
10	3	KOt-Bu (3)	Mes. ^g	165	100	95	—	—	—	—	—

^a GC yields and conversions are reported using tridecane as a standard. ^b No conversion is observed using base alone or Et₃SiH without basic activators.

^c [H] = Et₃SiH. ^d Isolated yield of **2** was 79%. ^eR = 2-ethylhexyl. ^f Reaction conducted open to an Ar line. ^g With 1,4-cyclohexadiene (100 equiv.) as a co-solvent.

Table 3.1. Conditions for dibenzofuran cleavage.

Bases other than KOt-Bu were found to give comparable activity and selectivity for C-O bond cleavage. Thus, at 165 °C potassium ethoxide is somewhat less effective than KOt-Bu (Entry 4), while a cesium alkoxide (Entry 5) gave similar selectivity for the formation of desired **2** when compared to potassium *tert*-butoxide,

albeit at lower yield of the reduced product under identical conditions. Given the latter result, it is interesting to note that Et₃SiH with lithium or sodium *tert*-butoxide provides no conversion of **1** suggesting that the counter ion plays a critical role in the generation of the active reductant species and, possibly, in activation of the substrate ether.²⁰ In order to test this hypothesis we conducted the same reaction with KO*t*-Bu but in the presence of 18-crown-6 as a potassium chelator and indeed observed no conversion. Additionally, our reaction mixtures were EPR active, which is consistent with reactive radicals²¹ that have been documented for homolytic aromatic substitution reactions.²² Since it was reported that addition of 1,10-phenanthroline in conjunction with KO*t*-Bu proved beneficial for those processes,²² we evaluated its effect and found it to be detrimental since no conversion of **3.1** was observed. Based on these initial observations, we propose that the active reductant silicon species may be organosilicates.²³⁻²⁵ In order to test for this possibility, we investigated other hydride donors as possible activators for conversion of **3.1**. Interestingly, upon switching to KH in dioxane we obtained monosilylated **3.3** in excellent selectivity, albeit with diminished conversion, and with no solvent-derived reduced products. This silylation manifold also dominates when sub-stoichiometric amounts of KO*t*-Bu are used or when the reaction temperature is lowered, as presented in entries 7 and 8 (**Table 3.1**). Since GC headspace analysis of sealed reaction mixtures indicated formation of H₂, we conducted the reaction opened to an atmosphere of argon and found a dramatic decrease in reductive cleavage product formation that was offset by increased silylation (Entry 9). This result suggests that dihydrogen might be important to prevent decomposition of the active reducing species.²⁶ In a search to

further modulate the selectivity by shutting down radical pathways we conducted the reaction using 1,4-cyclohexadiene as a non-polar hydrogen donor²⁷ co-solvent and observed exclusive formation of **2** with 95% yield (Entry 10). These results demonstrate our ability to tune the selectivity of the reaction by optimizing the reaction conditions.

$$\text{Ar}_1\text{-O-Ar}_2 \xrightarrow[165\text{ }^\circ\text{C, 20 h, Mes}]{\text{Et}_3\text{SiH (3); KOt-Bu (3)}} \text{Ar}_{1,2}\text{-H} + \text{Ar}_{1,2}\text{-OH}$$

Entry	Diaryl ether	Conv. (%)	Ar ₁ -H Ar ₂ -H	Ar ₁ -OH Ar ₂ -OH
1		96	64	65
2		100	76	98
3		100	52	84
4 ^b		100	50	88
5 ^c	$\text{Ar}_1\text{-O-Ar}_2$ Ar ₁ = phenyl Ar ₂ = 1-naphthyl	100	— 70	91 —
6 ^d	$\text{Ar}_1\text{-O-Ar}_2$ Ar ₁ = 2-naphthyl Ar ₂ = 1-naphthyl 1 : 4	100	57	58 15
7 ^d	 3:1 Ar ₁ = 4-Ph-Ph Ar ₂ = Ph	100	41 19	21 65

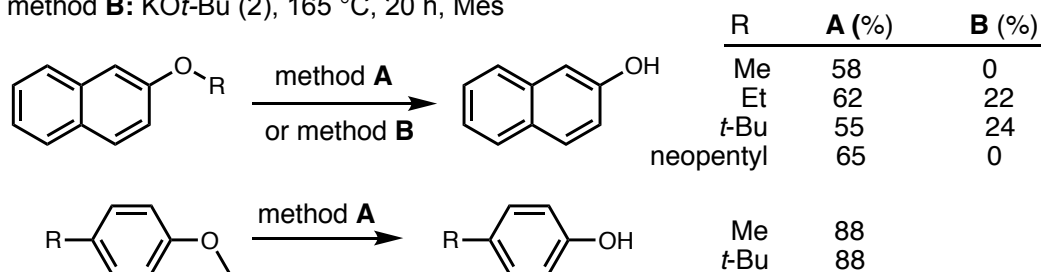
^a GC yields and conversions are reported using tridecane as a standard. ^b Trace amount of 1,2,3,4-tetrahydronaphthalene was detected. ^c Reaction was run at 100 °C for 20 h in toluene with 2 equiv. each of Et₃SiH and KOt-Bu. ^d Reaction was run at 75 °C for 40 h in toluene.

Table 3.2. Conditions for diaryl ether cleavage.

In order to explore the cleavage of aryl ether C-O bonds in unstrained substrates and probe if it proceeds without undesired overreduction of the resulting aromatic fragments, we subjected diphenyl ether to the additives-free optimized reaction conditions described above. This substrate provided benzene and phenol in moderate yields (**Table 2**, Entry 1) with the rest of the mass balance being attributed principally

to silylated as well as other unidentified products. With this result in hand we proceeded to evaluate the reactivity of more complex diaryl ethers. Both symmetrical and unsymmetrical diaryl ethers were shown to be competent substrates and underwent C-O cleavage with good to excellent efficiencies (Entries 2-7). Many of the evaluated diaryl ethers proved more reactive as compared to diphenyl ether and allowed for the use of milder reaction conditions. In the case of 1-naphthyl phenyl ether (Entry 5), bond cleavage occurred regiospecifically at the naphthyl C-O bond to furnish naphthalene and phenol in 70 and 91% yield respectively, with no 1-naphthol or benzene detected. With the unsymmetrical dinaphthyl ether (Entry 5), C-O bond reduction occurred regioselectively to provide 2-naphthol and 1-naphthol in good combined yield with approximately a 4:1 ratio of the two isomers, respectively. The unsymmetrical *para*-phenyl substituted diphenyl ether (Entry 7) reacts with good overall yield and with moderate regioselectivity for reduction of the slightly more electron rich C-O bond²⁸ indicating the apparent influence of electronic effects in site-selectivity of C-O bond cleavage. This factor becomes determining for the selectivity of cleavage of 4-O-5 lignin models that contain strong methoxy donors adjacent to the C-O bond being broken (*vide infra*, **Scheme 3.2**). We also wish to point out that such selectivity is complementary to that reported by Hartwig for Ni catalyzed reduction with dihydrogen wherein unsymmetrical diaryl ethers were preferentially cleaved at the side of the more electron-deficient aryl ring.⁸

method **A**: Et₃SiH (3), KO^t-Bu (3), 165 °C, 20 h, Mes
 method **B**: KO^t-Bu (2), 165 °C, 20 h, Mes



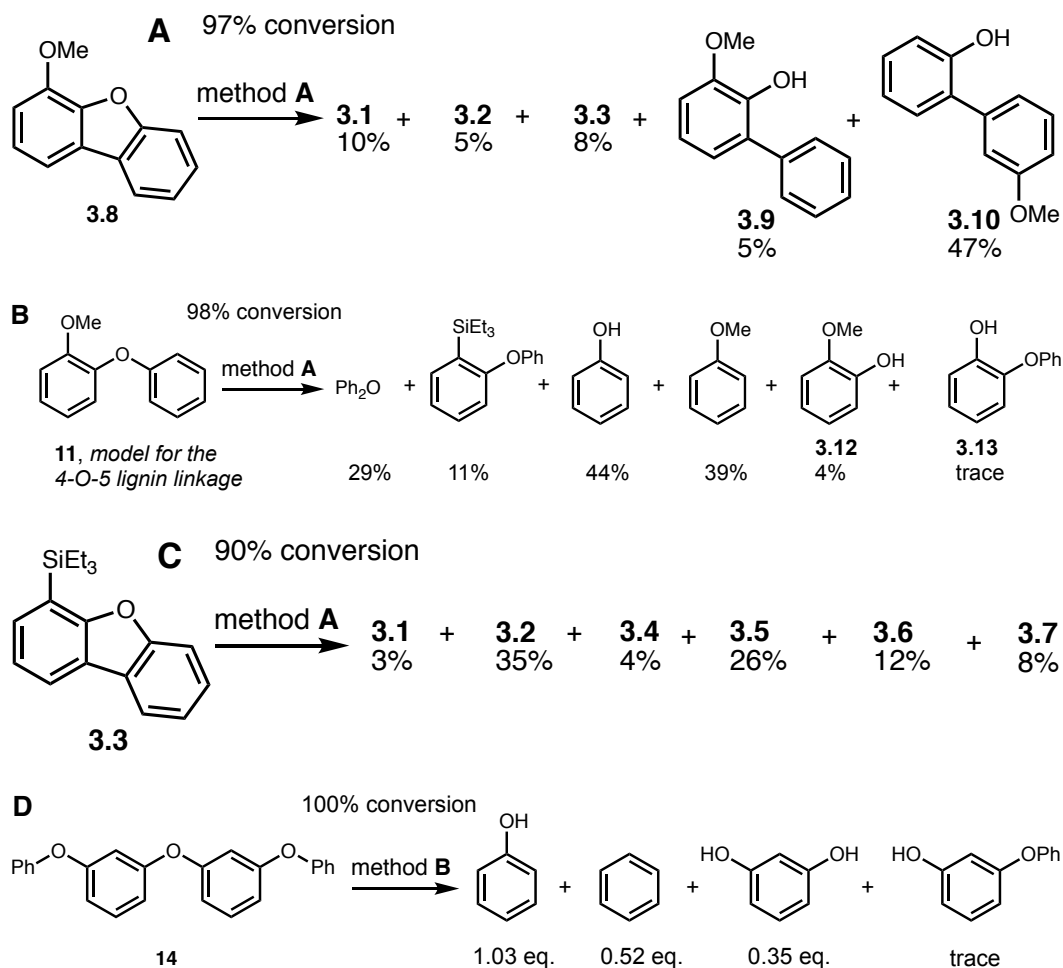
Scheme 3.2. Cleavage of aryl alkyl ethers.

We next investigated the reduction of aryl alkyl ethers under the optimized conditions applied to diaryl ethers to probe the cleavage selectivity of sp² versus sp³ C-O bond.²⁹ The reaction of 2-methoxynaphthalene gave 2-naphthol as the major product in moderate yield (Scheme 1). GC-MS analysis of the crude reaction mixture indicated the presence of trace amounts of naphthalene along with 2-methylnaphthalene and further reduced species, including products of partial aromatic reduction. Compounds presumably derived from 2-naphthol silylation were also detected. Likewise, cleavage of 2-ethoxynaphthalene under the same conditions gave 2-naphthol in slightly higher yield, but with the same or analogous side products. We next chose to investigate sterically bulkier ethers to probe the versatility and possible mechanism of the C-O bond cleavage. Despite the large alkyl substituent adjacent to the ether oxygen, reaction of 2-neopentyloxynaphthalene provided 2-naphthol in approximately the same yield as with the less bulky substrates. Even 2-*tert*-butyloxynaphthalene was cleaved to give the expected naphthol in 55% yield (**Scheme 3.2**). Control experiments performed at identical conditions but without triethylsilane provided 2-naphthol in cases of 2-ethoxy- and 2-*tert*-

butyloxynaphthalene albeit with substantially diminished yields. Since 2-methoxy- and 2-neopentyloxy- substrates remained intact in such silane-free cleavages, a β elimination mechanism is likely to be operative.³⁰

When we attempted to reduce 4-*tert*-butyl and 4-methyl anisoles under the standard conditions, the yields of the corresponding phenols were high, likely because of more challenging silylation of the substituted phenyl ring for the steric reasons (Scheme 2). Overall, the selectivity for *alkyl* C-O bond scission contrasts with that observed in Ni-⁶⁻⁸ and borane²⁶ catalyzed C-O cleavage reactions where *aryl* C-O reduction occurs. It is also notable that under our conditions only trace amounts of naphthalene ring hydrogenation products were observed, which contrasts with the results of silane-based ionic hydrogenations reported in the literature.³¹

method **A**: Et₃SiH (5), KO^t-Bu (2), 100 °C, 20 h, toluene; method **B**: Et₃SiH (3), KO^t-Bu (3), 165 °C, 20 h, mesitylene



Scheme 3.3. Reductive cleavage of lignin model substrates

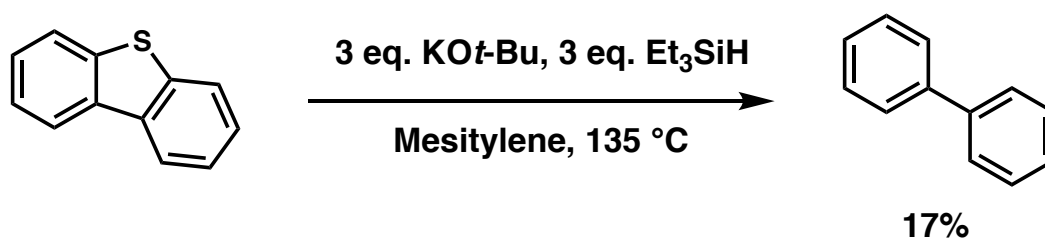
It is instructive to compare the cleavages of methoxy-substituted diaryl ethers **3.8** and **3.11** (Scheme 3.3) with the results presented above. While aryl alkyl ethers show strong preference for the reduction of alkyl oxygen over aryl oxygen bonds, both methoxy substrates in Scheme 3 demonstrate a reversal of regioselectivity, furnishing almost exclusively aryl oxygen bond rupture products. We attribute this effect to the presence of a donor oxygen atom *ortho* to the C-O bond undergoing rupture.

Supporting this inference is the high selectivity of the reductive ring-opening of dibenzofuran derivative **3.8** that mainly leads to **3.10**. Likewise, preferred formation of phenol and anisole is observed with similar selectivity over phenols **3.12** and **3.13** in the cleavage of lignin model **3.11**. We speculate that such an effect can be rationalized by the oxygen atom resonance stabilization of the positive charge build up during electrophilic activation of the C-O bond that is being broken. In order to test this hypothesis, we subjected **3** to our reaction conditions and isolated the ring-opened phenols **3.5** and **3.6** along with the desilylated products **3.1** and **3.2** (**Scheme 3.3**, inset C). In the absence of resonance stabilization, the selectivity of cleavage was reversed in favour of isomer **5**. It is also worth noting that, as formation of **1** and **2** demonstrates, the silylation reaction is thus reversible under the typical reaction conditions.³² After having illustrated the potential for the challenging 4-O-5 lignin models **3.8** and **3.11**, we decided to examine our method with an oligomeric ether **3.14** that contains six C_{ar}-O bonds (**Scheme 3.3**, inset D). Remarkably, at 165 °C in mesitylene quantitative conversion of **14** was achieved and gave phenol, benzene, resorcinol, and other unidentified products with merely 0.5 equiv. of silane per aryl oxygen bond.

As mentioned previously, it appears probable that alkyl organosilicates are the key reactive species involved.³³⁻³⁴ To the best of our knowledge no known variants of organosilicates have been reported to possess such powerful reducing properties that can affect the reductive ruptures described in this work.³⁵

As an extension of the current work, we reacted dibenzothiophene under the conditions used for dibenzofuran cleavage (**Scheme 3.4**). Partial loss of the sulfur

atom was observed as biphenyl was recovered as a primary product. Such desulfurization represents an interesting deviation from the selectivity encountered with furans and warrants further investigation.



Scheme 3.4. Dibenzothiophene reduction with alkoxide and silane.

Experimental

All reactions were carried out in dry glassware under an argon atmosphere using standard Schlenk line techniques or in a Vacuum Atmospheres Glovebox under a nitrogen atmosphere unless specified otherwise. Mesitylene (puriss., $\geq 99.0\%$ (GC)) was degassed by three freeze-pump-thaw cycles prior to use. All other solvents were purified by passage through solvent purification columns and further degassed with argon. NMR solvents for air-sensitive experiments were dried over CaH_2 and vacuum transferred or distilled into a dry Schlenk flask and subsequently degassed with argon. Triethylsilane (99%) was purchased from Sigma-Aldrich and degassed by three freeze-pump-thaw cycles prior to use and other commercially available liquid reagents were treated analogously. Di-4-(methyl)phenyl ether, 1-naphthol, 2-naphthol, 4-*tert*-butyl anisole, 1,3-diphenoxybenzene, 2-methoxynaphthalene, and

1.0M tetrabutylammonium fluoride THF solution were purchased from Sigma-Aldrich and used as received. Sublimed grade KO t -Bu (99.99%) was purchased from Sigma-Aldrich and subjected to vacuum sublimation (30 mTorr, 160 °C) prior to use. 4-(Methoxy)dibenzofuran,³⁶ di-4-(*tert*-butyl)phenyl ether,¹² naphthyl ethers,¹² 4-(phenyl)phenyl phenyl ether¹², 2-ethoxynaphthalene³⁷, 2-neopentyloxynaphthalene³⁷, 2-*tert*-butyloxynaphthalene³⁸ were synthesized according to the literature procedures. Standard NMR spectroscopy experiments were conducted on a Varian Mercury (¹H, 300 MHz) spectrometer, a Varian Inova 400 MHz spectrometer, a Varian 500 MHz spectrometer equipped with an AutoX probe, or a Varian 600 MHz spectrometer equipped with a Triax Probe. Chemical shifts are reported in ppm downfield from Me₄Si by using the residual solvent peak as an internal standard. Spectra were analyzed and processed using MestReNova. GC-FID analyses were obtained on an Agilent 6890N gas chromatograph equipped with a HP-5 (5%-phenyl)-methylpolysiloxane capillary column (Agilent). GC-MS analyses were obtained on an Agilent 6850 gas chromatograph equipped with a HP-5 (5%-phenyl)-methylpolysiloxane capillary column (Agilent). High resolution mass spectra (EI and FAB) were acquired by the California Institute of Technology Mass Spectrometry Facility.

General Procedure

In a glovebox, a 4 mL screw cap vial was loaded with the corresponding substrate (0.1 mmol, 1 equiv.), base (0.5–5 equiv.) and a magnetic stirring bar, followed by syringe addition of the solvent (1 mL) and triethylsilane (1–5 equiv.). The reaction vial was sealed with a Teflon-lined screw cap and heated at a given temperature and

time inside the glovebox (Table S2). After cooling to room temperature, dark red to black reaction mixture was diluted with diethyl ether (3 mL) and carefully quenched with 1 mL of 1 N aqueous HCl. Tridecane (internal standard for GC) was added, the organic layer was separated and the aqueous layer was extracted with ether (3 mL) until TLC controls show no UV-active compounds present in the extracts. The combined organic layers were passed through a short pad of Celite and subjected to GC/FID, GC/MS, and ^1H -NMR analyses. Unless stated otherwise, in preparative experiments only products with the overall yield exceeding 2% were isolated and characterized.

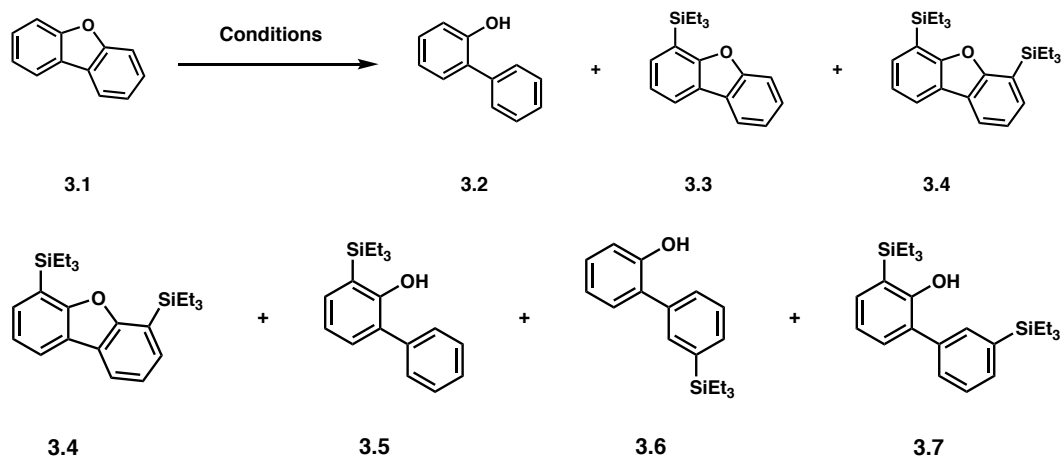
In the case of naphthyl alkyl ethers, a different workup procedure was used. After cooling, the reaction was diluted with dichloromethane (5 mL) and carefully quenched with 2 mL of 1 N aqueous HCl. Tridecane was added, and the mixture was transferred to a separatory funnel. The organic phase was separated, and the aqueous layer was extracted with dichloromethane (3 mL). The combined organic layers were dried over anhydrous MgSO_4 and filtered. For all reactions, the products were identified using GC/MS and GC/FID and NMR by comparison with the authentic samples. Trace soluble side products observed in naphthyl alkyl ether reductions included naphthalene, 1,2,3,4-tetrahydronaphthalene, and 5,6,7,8-tetrahydro-2-naphthol.

ICP-MS analysis was conducted using the California Institute of Technology MS facility with 100 mg samples of dibenzofuran, triethylsilane, mesitylene and potassium tert-butoxide, which were added to 50 mL DigiTUBE digestion tubes (SCP Science) followed by addition of 3.0 mL of Plasma Pure nitric acid (SCP

Science) to each digestion tube and heating to 75 °C for 36 hours. After digestion, each sample was diluted using Nanopure/Milli Q water to 50 mL and sample analysis performed on an HP 4500 ICP-MS spectrometer. Semiquantitative analysis was performed using a 10 ppm solution of lithium, yttrium, cerium, and thallium for calibration. Each sample was analyzed twice and the average measurements are given.

Element	Reagent (unit: ppm)				
	Dibenzofuran	KOt-Bu	Et ₃ SiH	Mesitylene	Reaction Mixture
Fe	0.15	4.92	0.67	0.11	5.80
Ru	0.00	0.07	0.00	0.01	3.13
Os	0.01	0.01	0.01	0.00	0.20
Co	0.00	0.01	0.00	0.00	0.26
Rh	0.00	0.00	0.00	0.00	1.07
Ir	0.00	0.01	0.00	0.09	0.40
Ni	0.12	0.06	0.06	0.38	0.79
Pd	0.00	0.04	0.00	0.01	0.88
Pt	0.00	0.07	0.00	0.01	1.74
Cu	0.03	10.42	0.04	0.09	7.59

Table 3.3 ICP-MS analysis of reagents used.



Entry	EtSiH (equiv.)	Base (equiv.)	Solvent	T, °C	Conv. (%)	3.2	3.3	3.4	3.5	3.6	3.7
1	0	KOt-Bu (2)	Toluene	100	0	—	—	—	—	—	—
2	5	None	Toluene	100	0	—	—	—	—	—	—
3	5	KOt-Bu (2)	Toluene	100	70	34	28	4	—	—	—
4	5	KOt-Bu (2)	Toluene	100	98	38	16	10	21	2	7
5	4	KOt-Bu (2)	Toluene	100	100	41	17	15	12	1	9
6	3	KOt-Bu (2)	Toluene	100	96	42	20	9	13	1	4
7	2	KOt-Bu (2)	Toluene	100	87	34	30	10	6	1	3
8	1	KOt-Bu (2)	Toluene	100	56	19	29	1	2	—	1
9	5	KOt-Bu (0.5)	Toluene	100	89	12	48	20	9	—	1
10	2	KOt-Bu (0.5)	Toluene	100	66	9	43	8	2	—	—
11	5	KOt-Bu (5)	Toluene	100	97	63	10	1	22	—	2
12	5	KH (1)	Dioxane	100	49	1	43	5	—	—	—
13	5	KOt-Bu (2)	Dioxane	100	70	25	28	10	4	1	1
14	—	KOt-Bu (2)	EtSiH	100	99	26	13	25	11	1	21
15	5	KOt-Bu (2)	Toluene	80	98	29	18	26	9	—	7
16	3	KOt-Bu (3)	Mes.	165	100	85	3	—	5	2	—
17	2	KOt-Bu (2)	Mes.	165	100	62	8	1	12	1	—
18	3	KOt-Bu (2)	Mes.	165	97	52	17	5	16	1	2
19	1	KOt-Bu (1)	Mes.	165	57	30	21	—	—	—	—
20	3	KOt-Bu (0.5)	Mes.	165	85	29	35	15	4	—	2
21	5	KOt-Bu (5)	Mes.	165	100	77	3	0	3	8	—
22	3	KH (3)	Mes.	165	100	66	3	0	5	11	—
23	3	KOEt (3)	Mes.	165	100	85	4	0	1	8	—
24	3	KOEt (3)	Toluene	100	40	19	19	2	—	—	—
25	3	KOMe (3)	Mes.	165	64	31	27	2	3	1	—
26	3	NaOt-Bu (3)	Mes.	165	0	—	—	—	—	—	—
27	3	LiOt-Bu (3)	Mes.	165	0	—	—	—	—	—	—
28	3	NaOEt (3)	Mes.	165	0	—	—	—	—	—	—
29	5	CsOR (2)	Toluene	100	89	75	3	11	—	—	—

30	3	KOt-Bu (3)	Benzene	85	96	37	20	13	12	—	9
31	5	KOt-Bu (2)	DMF	100	0	—	—	—	—	—	—
32	5	KOt-Bu (2)	DMA	100	0	—	—	—	—	—	—
33	5	KOt-Bu (2)	Diglyme	100	0	—	—	—	—	—	—
34	5	KOt-Bu (2)	<i>t</i> -BuOH	100	0	—	—	—	—	—	—
35	5	KOt-Bu (2)	Diisopro pyl carbinol	100	0	—	—	—	—	—	—

Table 3.4 Optimization of dibenzofuran cleavage. Mes = mesitylene.

4-(Triethylsilyl)dibenzofuran (**3.3**)

The title compound was prepared by analogy to the protocol for the synthesis of 4-(trimethylsilyl)dibenzofuran by Kelly and co-workers.³⁹ Data for (**3**): Colorless oil. ¹H-NMR (500 MHz, CDCl₃): δ 7.99-7.96 (m, 2H_{ar}), 7.59 (d-like, *J* = 10 Hz, 1H_{ar}), 7.54 (dd, *J* = 2, 5 Hz, 1H_{ar}), 7.48-7.44 (m, 1H_{ar}), 7.37-7.33 (m, 2H_{ar}), 1.03 (m, 15H, 3CH₂CH₃). ¹³C-NMR (126 MHz, CDCl₃): δ 161.30, 156.05, 133.57, 126.92, 122.52, 122.48, 121.58, 120.68, 111.75, 7.63, 3.59. HRMS: [C₁₈H₂₂OSi] calculated 282.1440; measured 282.1444.

4,6-Bis(triethylsilyl)dibenzofuran (**3.4**)

To a solution of dibenzofuran (2.00 g, 11.9 mmol, 1 equiv.) and tetramethylethylenediamine (11.1 mL, 29.7 mmol, 2.5 equiv.) in tetrahydrofuran (50 mL) *t*-butyllithium (17.5 mL of 1.7 M solution in pentane, 29.8 mmol, 2.5 equiv.) was slowly added at -78 °C under argon. The mixture was allowed to reach ambient temperature and stirring was continued for 4 h prior to addition of chlorotriethylsilane (10.1 mL, 60 mmol, 5 equiv.). The resulting mixture was stirred at ambient

temperature for another 16 h. After quenching the reaction with the saturated ammonium chloride solution (40 mL) and extraction with diethyl ether (3x30 mL), the combined organic layers were dried over anhydrous sodium sulfate, filtered and the filtrate concentrated in vacuo. Crude reaction mixture was purified by chromatography on silica (hexanes) and product obtained was recrystallized from a mixture of methanol and isopropanol (1:1) to afford 4,6-bis(triethylsilyl)dibenzofuran (1.28 g, 2.45 mmol, 28%) as colorless needles. Data for (**4**): Colorless needles. M.p. = 59-61 °C. ¹H-NMR (300 MHz, CDCl₃): δ 7.97 (dd, *J* = 3, 9 Hz, 2H_{ar}), 7.54 (dd, *J* = 3, 9 Hz, 2H_{ar}), 7.33 (t, *J* = 9 Hz, 2H_{ar}), 1.07-0.95 (m, 30H, 6CH₂CH₃). ¹³C-NMR (126 MHz, CDCl₃): δ 160.90, 133.48, 122.87, 122.34, 121.57, 120.03, 7.66, 3.52. HRMS: [C₂₄H₃₆OSi₂] calculated 396.2305; measured 396.2321.

3-(Triethylsilyl)biphenyl-2-ol (**3.5**)

The title compound was prepared via cleavage of **3** (*vide infra*).

Data for (**5**): White solid. M.p. = 44-46 °C ¹H-NMR (300 MHz, CDCl₃): δ 7.52-7.40 (m, 5H_{ar}), 7.36 (dd, *J* = 3, 9 Hz, 1H_{ar}), 7.23 (dd, *J* = 3, 6 Hz, 1H_{ar}), 6.98 (t, *J* = 9 Hz, 1H_{ar}), 5.41 (s, 1H, OH), 1.02-0.96 (m, 9H, CH₃), 0.91-0.83 (m, 6H, CH₂). ¹³C-NMR (75 MHz, CDCl₃): δ 157.25, 137.51, 135.97, 131.30, 129.58, 129.39, 128.01, 127.17, 123.04, 120.40, 7.79, 3.69. HRMS: [C₁₈H₂₄OSi] calculated 284.1596; measured 284.1583.

(3'-Triethylsilyl)biphenyl-2-ol (**3.6**)

The title compound was prepared via cleavage of **3** (*vide infra*).

Data for (**6**): Colorless oil. ^1H -NMR (500 MHz, CDCl_3): δ 7.57-7.56 (m, 1H_{ar}), 7.54-7.52 (m, 1H_{ar}), 7.49-7.44 (m, 2H_{ar}), 7.28-7.24 (m, 2H_{ar}), 7.02-6.99 (m, 2H_{ar}), 5.24 (s, 1H, OH), 0.98 (t, J = 10 Hz, 9H, CH₃), 0.82 (q, J = 15 Hz, 6H, CH₂). ^{13}C NMR (126 MHz, CDCl_3): δ 152.44, 139.07, 136.12, 134.71, 133.76, 130.23, 129.36, 129.08, 128.53, 128.44, 120.80, 115.72, 7.43, 3.31. HRMS: [$\text{C}_{18}\text{H}_{24}\text{OSi}$] calculated 284.1596; measured 284.1585.

3,3'-Bis(triethylsilyl)biphenyl-2-ol (**3.7**)

The title compound was prepared according to General Procedure by heating dibenzofuran (**1**, 840 mg, 5.0 mmol, 1 equiv.) with KO t -Bu (1.12 g, 10 mmol, 2 equiv.) and Et₃SiH (4.0 ml, 25 mmol, 5 equiv.) in 20 ml of toluene for 20 hours at 100 °C. After acidic aqueous work up, the crude reaction mixture was purified by chromatography on silica using hexanes and hexanes-ether (10:1) to give, among other isolated products, 20 mg (0.05 mmol, 1%) of **7**. Data for (**7**): oily solid ^1H -NMR (300 MHz, CDCl_3): δ 7.53-7.44 (m, 2H_{ar}), 7.46-7.44 (m, 2H_{ar}), 7.36 (dd, J = 1.5, 7.5 Hz, 1H_{ar}), 7.23 (dd, J = 1.5, 7.5 Hz, 1H_{ar}), 6.98 (t, J = 7 Hz, 1H_{ar}), 5.42 (s, 1H, OH), 1.01-0.96 (m, 18H, 6CH₃) 0.91-0.77 (m, 15H, 6CH₂). ^{13}C NMR (75 MHz, CDCl_3): δ 157.37, 139.45, 136.61, 135.87, 135.09, 133.86, 131.38, 129.57, 128.71, 127.55, 122.97, 120.36, 7.80, 7.57, 3.69, 3.46. HRMS: [$\text{C}_{24}\text{H}_{38}\text{OSi}_2$] calculated 398.2461; measured 396.2470.

References

(1) (a) J. C. Hicks, *J. Phys. Chem. Lett.* **2011**, *2*, 2280; (b) J. Zakzeski, P. C. A. Bruijninx, A. L. Jongerius and B. M. Weckhuysen, *Chem. Rev.* **2010**, *110*, 3552; (c) J. R. Regalbuto, *Science* **2009**, *325*, 822; (d) G. W. Huber, S. Iborra and A. Corma, *Chem. Rev.* **2006**, *106*, 4044.

(2) For selected recent advances, see: (a) V. M. Roberts, V. Stein, T. Reiner, A. Lemonidou, X. Li and J. A. Lercher, *Chem. Eur. J.* **2011**, *17*, 5939; (b) T. D. Matson, K. Barta, A. V. Iretskii and P. C. Ford, *J. Am. Chem. Soc.* **2011**, *133*, 14090; (c) K. Barta, T. D. Matson, M. L. Fettig, S. L. Scott, A. V. Iretskii and P. C. Ford, *Green Chem.* **2010**, *12*, 1640; (d) M. Kleinert and T. Barth, *Energy & Fuels* **2008**, *22*, 1371; (e) T. H. Parsell, B. C. Owen, I. Klein, T. M. Jarrell, C. L. Marcum, L. J. Hauptert, L. M. Amundson, H. I. Kenttämä, F. Ribeiro, J. T. Miller and M. M. Abu-Omar, *Chem. Sci.* **2013**, *4*, 806.

3 (a) R. Parthasarathi, R. A. Romero, A. Redondo and S. Gnanakaran, *J. Phys. Chem. Lett.* **2011**, *2*, 2660; (b) S. Kim, S. C. Chmely, M. R. Nimlos, Y. J. Bomble, T. D. Foust, R. S. Paton and G. T. Beckham, *J. Phys. Chem. Lett.* **2011**, *2*, 2846.

(4) D. G. Levine, R. H. Schlosenberg and B. G. Silbernagel, *Proc. Natl. Acad. Sci. U.S.A.* **1982**, *79*, 3365.

(5) (a) B. M. Rosen, K. W. Quasdorf, D. A. Wilson, N. Zhang, A.-M. Resmerita, N. K. Garg and V. Percec, *Chem. Rev.* **2011**, *111*, 1346; (b) D.-G. Yu, B.-J. Li and Z.-J. Shi, *Acc. Chem. Res.* **2010**, *43*, 1486. (c) M. Tobisu and N. Chatani, *Top. Organomet. Chem.* **2013**, *44*, 35. (d) B.-J. Li, D.-G. Yu, C.-L. Sun and Z.-J. Shi, *Chem. Eur. J.* **2011**, *17*, 1728.

(6) P. Álvarez-Bercedo and R. Martin, *J. Am. Chem. Soc.* **2010**, *132*, 17352.

(7) M. Tobisu, K. Yamakawa, T. Shimasaki and N. Chatani, *Chem. Commun.* **2011**, *47*, 2946.

(8) A. G. Sergeev and J. F. Hartwig, *Science* **2011**, *332*, 439.

(9) Mechanistic details about Ni-catalyzed aryl-oxygen cleavage reported: P. Kelley, S. Lin, G. Edouard, M. W. Day and T. Agapie, *J. Am. Chem. Soc.* **2012**, *134*, 5480.

(10) For examples of other transition metal catalyzed approaches to breaking lignin-related C-O bonds, see: (a) B. Sedai, C. Diaz-Urrutia, R. T. Baker, R. Wu, L. A. P. Silks and S. K. Hanson, *ACS Catal.* **2011**, *1*, 794; (b) J. M. Nichols, L. M. Bishop, R. G. Bergman and J. A. Ellman, *J. Am. Chem. Soc.* **2010**, *132*, 12554; (c) S. Son and F. D. Toste, *Angew. Chem. Int. Ed.* **2010**, *49*, 3791; (d) S. K. Hanson, R. T. Baker, J. C. Gordon, B. L. Scott and D. L. Thorn, *Inorg. Chem.* **2010**, *49*, 5611; (e) C. Crestini, M. Crucianelli, M. Orlandi and R. Saladino, *Catalysis Today* **2010**, *156*, 8; (f) M. S. Kharasch and R. L. Huang, *J. Org. Chem.* **1952**, *17*, 669.

- (11) For Ir-based cleavage of alkyl ethers with Et₃SiH, see: J. Yang, P. S. White and M. Brookhart, *J. Am. Chem. Soc.* **2008**, *130*, 17509.
- (12) A. G. Sergeev, J. D. Webb and J. F. Hartwig, *J. Am. Chem. Soc.* **2012**, *134*, 20226.
- (13) He, J.; Zhao, C.; Lercher, J. A. *J. Am. Chem. Soc.* **2012**, *134*, 20768.
- (14) Allergic reactions caused by nickel were recently reviewed: R. Darlenski, J. Kazandjieva and K. Pramatarov, *Int. J. Dermatol.* **2012**, *51*, 523.
- (15) (a) Z. Grobelny, *Eur. J. Org. Chem.* **2004**, 2973; (b) A. Maercker, *Angew. Chem. Int. Ed.* **1987**, *26*, 972; (c) T. Keumi, C. Murata, Y. Sasaki and H. Kitajima, *Synthesis* **1980**, 634.
- (16) Potassium *tert*-butoxide was sublimed before use.
- (17) F. Kakiuchi, K. Tsuchiya, M. Matsumoto, E. Mizushima and N. Chatani, *J. Am. Chem. Soc.* **2004**, *126*, 12792.
- (18) N. Tsukada and J. F. Hartwig, *J. Am. Chem. Soc.* **2005**, *127*, 5022.
- (19) L. T. Ball, G. C. Lloyd-Jones and C. A. Russell, *Science* **2012**, *337*, 1644.
- (20) Corriu reported that in contrast to potassium, sodium or lithium alkoxides do not give hydridosilicates with trialkoxy or triaryloxysilanes: B. Becker, R. Corriu, C. Guerin and Q. Wang, *J. Organomet. Chem.* **1989**, *359*, C33.
- (21) Radical silylation of arenes is well known. See, for example: (a) W. Du, B. Kaskar, P. Blumbergs, P.-K. Subramanian and D. P. Curran, *Bioorg. Med. Chem.* **2003**, *11*, 451. (b) C. Chatgililoglu, *Chem. Rev.* **1995**, *95*, 1229.
- (22) (a) C.-L. Sun, H. Li, D.-G. Yu, M. Yu, X. Zhou, X.-Y. Lu, K. Huang, S.-F. Zheng, B.-J. Li and Z.-J. Shi, *Nat. Chem.* **2010**, *2*, 1044. Also, see Supporting Information to this article. (b) A. Studer and D. P. Curran, *Angew. Chem. Int. Ed.* **2011**, *50*, 5018.
- 23(a) R. Holmes, *Chem. Rev.* **1996**, *96*, 927; (b) C. Chuit, R. J. P. Corriu, C. Reye and J. C. Young, *Chem. Rev.* **1993**, *93*, 1371; (c) S. E. Denmark and G. L. Beutner, *Angew. Chem. Int. Ed.* **2008**, *47*, 1560; (d) E. P. A. Couzijn, J. C. Slootweg, A. W. Ehlers and K. Lammertsma, *Z. Anorg. Allg. Chem.* **2009**, *635*, 1273.
- (24) (a) P. D. Prince, M. J. Bearpark, G. S. McGrady and J. W. Steed, *Dalton Trans.* **2008**, *0*, 271; (b) M. J. Bearpark, G. S. McGrady, P. D. Prince and J. W. Steed, *J.*

Am. Chem. Soc. **2001**, *123*, 7736; (c) N. Rot, T. Nijbacker, R. Kroon, F. J. J. de Kanter, F. Bickelhaupt, M. Lutz and A. L. Spek, *Organometallics* **2000**, *19*, 1319; (d) R. Corriu, C. Guerin, B. Henner and Q. Wang, *Inorg. Chim. Acta* **1992**, *198-200*, 705; (e) R. Corriu, C. Guerin, B. Henner and Q. Wang, *Organometallics* **1991**, *10*, 3574; (f) R. J. P. Corriu, C. Guerin, B. Henner and Q. Wang, *Organometallics* **1991**, *10*, 2297; (g) R. J. P. Corriu, C. Guerin, B. J. L. Henner and Wang, Q. *J. Organomet. Chem.* **1992**, *439*, C1.

(25) (a) D. J. Hajdaszj, Y. Ho and R. R. Squires, *J. Am. Chem. Soc.* **1994**, *116*, 10751. (b) I. H. Krouse and P. G. Wenthold, *Organometallics* **2004**, *23*, 2573, and references therein.

(26) Hydrogenolysis of arenes and alkyl aryl ethers with H₂ under borane catalysis is preceded: M. Yalpani, T. Lunow and R. Koester, *Chem. Ber.* **1989**, *122*, 687.

(27) A. L. Koner, U. Pischel and W. M. Nau, *Org. Lett.* **2007**, *9*, 2899.

(28) The Hammett parameters for *p*-Ph substituents are -0.18 for σ^+ series and -0.01 for σ , see: C. Hansch, A. Leo and R. W. Taft, *Chem. Rev.* **1991**, *91*, 165.

(29) For alkyl aryl cleavage under Lewis acid catalysis, see: V. Gevorgyan, J.-X. Liu, M. Rubin, S. Benson and Y. Yamamoto, *Tetrahedron Lett.* **1999**, *40*, 8919.

(30) R. L. Letsinger and D. F. Pollart, *J. Am. Chem. Soc.* **2010**, *10*, 12554; also, see ref. 14b.

(31) (a) J. W. Larsen and L. W. Chang, *J. Org. Chem.* **1979**, *44*, 1168. (b) M. Eckert-Maksić and D. Margetić, *Energy & Fuels* **1993**, *7*, 315.

(32) We checked if the qualitative **3.5/3.6** ratio depends on the desilylation rate after dibenzofuran ring opening in **3.3** had occurred by subjecting the two isomers independently to the reaction conditions and found that isomer **3.5** loses the Et₃Si-group faster than **6**, thus supporting our speculations.

(33) GC analysis of a crude reaction mixture obtained after heating of **1** for 20 hours in toluene at 100 °C with 2 equiv. of an isolated silicate K[HSi(OEt)₄] indicates formation of **3.2** among other products

(34) For electron transfer chemistry of hydridosilicates, see: (a) R. Corriu, C. Guerin, B. Henner and Q. Wang, *J. Organomet. Chem.* **1989**, *365*, C7. (b) D. Yang and D. D. Tanner, *J. Org. Chem.* **1986**, *51*, 2267.

- (35) Intermediacy of putative fluoride-activated silicates in the reductions of imides was recently proposed: S. Das, D. Addis, L. R. Knöpke, U. Bentrup, K. Junge, A. Brückner and M. Beller, *Angew. Chem. Int. Ed.* **2011**, *50*, 9180.
- (36) Shultz, D. A.; Sloop, J. C.; Washington, G. *J. Org. Chem.* **2006**, *71*, 9104.
- (37) Cazorla, C.; Pfordt, E.; Duclos, M.; Metay, E.; Lemaire, M. *Green Chem.* **2011**, *13*, 2482.
- (38) Bartoli, G.; Bosco, M.; Locatelli, M.; Marcantoni, E.; Melchiorre, P.; Sambri, L. *Org. Lett.* **2005**, *7*, 427.
- (39) Bekele, H.; Nesloney, C. L.; McWilliams, K. W.; Zacharias, N. M.; Chitnumsub, P.; Kelly, J. W. *J. Org. Chem.* **1997**, *62*, 2259.
- (40) Lian, Y.; Wulff, W. D. *J. Am. Chem. Soc.* **2005**, *127*, 17162.
- (41) Wei, Y.; Yoshikai, N. *Org. Lett.* **2011**, *13*, 5504.
- (42) Rychnovsky, S. D.; Huckins, J. R. *J. Org. Chem.* **2003**, *68*, 10135.